

**Studies on the ATP-Hydrolysis Cycle of Myosin II at  
the Ensemble and Single Molecule Level using Total  
Internal Reflection Fluorescence Microscopy**

von der Naturwissenschaftlichen Fakultät  
der Gottfried Wilhelm Leibniz Universität Hannover

zur Erlangung des Grades  
Doktorin der Naturwissenschaften  
Dr. rer. nat.

genehmigte Dissertation

**M. Sc. Mamta Amrute-Nayak**

geboren am 10.01.1979 in Dongar Yawli, Amaravati, Indien

Hannover 2006

**Name of referees**

Prof. Dr. W. Müller

Prof. Dr. B. Otto

Prof. Dr. B. Brenner

**Chairperson**

Prof. Dr. M. Kalesse

**Date of disputation:** 24.8.06

Arnab  
&  
My family

---

## Acknowledgements

First of all, I would like to thank my supervisor, Professor Dr. Bernhard Brenner for the excellent guidance, for being available at a short notice for discussions, encouragement and support throughout my PhD.

I would like to thank my Doctorfather Prof. Dr. W. Müller for being helpful and available for answering all kinds of questions that were put to him.

In Particular I would like to thank the following people:

Dr. Tim Scholz for providing all the useful information, scientific discussions and help with the experiments.

Dr. Massimo Antognozzi for helping me with the programming for data analysis and TIRF microscope setting that helped in improving the data acquisition and data quality.

Mr. David Luckhaus for being very helpful, in experiments and scientific discussions.

Ms. Birgit Piep and Mrs. Petra Uta for all the technical support and the biological starting materials provided for the experiments.

Mr. Torsten Beier for the technical assistance in setting up the microscope.

Mr. Ante Radocaj for all the help, discussions, assistance with translating texts and most of all for keeping the atmosphere lively.

Ms. Snigdha Tripathi particularly, for all the moral support through ups and downs during the course of my PhD.

I would like to give special thanks to all my lab members for the open and friendly environment and providing very good working experience.

This project was funded by Deutsche Forschungsgemeinschaft (DFG), Germany.

Most of all I would like to thank my father, Mr. Krishnarao Amrute, my mother Mrs. Usha Amrute and rest of my family for their endless love, encouragement and support throughout my studies without which it would not be possible to reach this level.

Finally, I would like to give special thanks to my husband, Arnab for all his love and support. I dedicate this thesis to my parents and especially to Arnab with all my love.

---

**Keywords:** TIRF microscopy, *in vitro* motility assay, Dwell time assay, Myosin II, Actin

**Schlüsselwörter:** TIRF mikroskopie, In-Vitro Motilität assay, Verweilzeit assay, Myosin II, Aktin

---

## Zusammenfassung

Muskelkontraktion beinhaltet das Gleiten von Aktinfilamenten (A) relativ zu Myosinfilamenten (B). Das Gleiten wird durch die zyklische Wechselwirkung zwischen den Aktinfilamenten und den globulären Myosinköpfen bewirkt und durch Hydrolyse von ATP angetrieben. Bei jedem ATPase-Zyklus des Myosinmoleküls wird die chemische Energie der ATP-Hydrolyse in mechanische Arbeit umgewandelt. Dies erfolgt in Form einer Serie von Strukturumlagerungen des Aktomyosinkomplexes, des sogenannten Kraftschlags, der die Aktinfilamente relativ zu den Myosinfilamenten bewegt. Während dem Kraftschlag werden die Produkte der ATP-Hydrolyse, ADP und  $P_i$  (anorganisches Phosphat), von ihren aktiven Bindungsstellen am Myosin abgetrennt. Die Abtrennung von Phosphat vom M.ADP. $P_i$ -Komplex ist ein entscheidender Schritt im Querbrückenzyklus. Frühere Muskelfaserstudien zeigten auf, daß bei einer Zunahme der  $P_i$ -Konzentration die isometrische Kraft abfällt, wobei nur wenig oder kein Effekt bei der maximalen Verkürzungsgeschwindigkeit festzustellen ist. Die Verringerung der isometrischen Kraft bei Erhöhung der  $P_i$ -Konzentration wurde gedeutet als Umkehr der Reaktionsrichtung vom stark bindenden, krafterzeugenden Zustand (AM.ADP) zum schwach bindenden, nicht krafterzeugenden Zustand (AM.ADP. $P_i$ ), welcher in einem schnellen Gleichgewicht mit von Aktin getrennten Zuständen (z.B. M.ADP. $P_i$ ) steht.

Unter Anwendung von TIRF-Mikroskopie (total internal reflection fluorescence microscopy) wurde der Einfluß von anorganischem Phosphat ( $P_i$ ) auf die Gleitgeschwindigkeit des Aktins in In-Vitro-Motility-Assays gemessen. In Einzelmolekülassays wurde die Verweilzeit, d.h. der Zeitraum, während dem das Nukleotid in der Nukleotidbindungstasche verweilt, gemessen. An ein immobilisiertes Myosinmolekül gebundenes fluoreszenzmarkiertes ATP (Cy3-EDA-ATP) wird als ein diskreter fluoreszierender Punkt registriert, der nach der Abtrennung von ADP verschwindet. Demnach wird das Erscheinen und Verschwinden von fluoreszierenden Punkten mit der Assoziation und Dissoziation des Nukleotids in Korrelation gebracht.

Die Verweilzeiten wurden gemessen um denjenigen Zwischenzustand zu finden, der durch die erhöhte  $P_i$ -Konzentration beeinflusst wird. Neben den Verweilzeiten wurde auch die Anzahl der Myosinmoleküle mit gebundenem Cy3-EDA-ATP durch die Aufzeichnung von Fluoreszenzevents zu bestimmten Zeitpunkten bestimmt. Es

---

wurde gefunden, daß  $P_i$  die Gleitgeschwindigkeit von Aktinfilamenten bei niedrigen ATP-Konzentrationen reduziert. Dieser Effekt ist bei höheren ATP-Konzentrationen weniger ausgeprägt. In den Verweilzeit-Assays für Einzelmoleküle hatte das Vorhandensein von  $P_i$  keinen Einfluß auf die durchschnittliche Verweilzeit, jedoch wurde die Anzahl der Moleküle mit Cy3-EDA-ATP in der Nukleotidbindungstasche reduziert. Dies suggeriert, daß die Anzahl der für Cy3-EDA-ATP zur Verfügung stehenden Myosinmoleküle in Anwesenheit von  $P_i$  verringert wurde.

Die aus den Motility-Assays und Verweilzeitmessungen erhaltenen Daten sind mit dem Konzept konsistent, daß  $P_i$  auch an eine leere Nukleotidbindungstasche binden kann und dabei ein stark bindenden Zwischenzustand ( $AM.P_i$ ) erzeugt.  $P_i$  konkurriert folglich mit ATP um die Bindungsstelle.

Weiterhin wurden auch für individuelle Myosinmoleküle Verweilzeiten fluoreszierender Signale von der Cy3-EDA-ATP-Bindung gemessen. In den meisten Arbeiten werden kinetische Daten von biochemischen Prozessen aus Verweilzeitmessungen an einer großen Anzahl von Molekülen errechnet. Die Durchschnittsbildung in diesem experimentellen Ansatz erschwert jedoch die Unterscheidung zwischen dynamischen Fluktuationen (zeitliche Veränderungen einzelner Moleküle) und statischer Uneinheitlichkeit (Moleküle in verschiedenen Zuständen), wobei dynamische Parameter der Interkonversion (Wechsel zwischen verschiedenen Konformationen des Myosinkopfs) nicht ausreichend bestimmt werden können. Die Auswertung der bei Einzelmolekülen gemessenen Verweilzeiten zeigte zwei unterschiedliche Populationen auf, die sich bei der Zeitkonstante um den Faktor fünf unterscheiden. Den zwei Verweilzeitpopulationen wurden zwei unterschiedlichen Zeitkonstanten des kompletten ATPase-Zyklus zugeordnet, die aus dem Wechsel zwischen zwei unterschiedlichen stabilen Konformationen des Motorproteins resultieren können. Diese postulierten Konformationen werden durch die Zeitkonstanten der Reaktionsschritte charakterisiert, die Verweilzeit der fluoreszierenden Nukleotide bestimmen. Aufgrund dessen schließen wir auf das Bestehen einer dynamischen Fluktuation der enzymatischen Aktivität der Myosin-II-Einzelmoleküle.

---

## Summary (Abstract)

Muscle contraction involves the sliding of actin (A) filaments relative to myosin (M). This sliding is due to the cyclic interaction between actin filaments and the globular myosin heads, and is powered by ATP hydrolysis. During each ATPase cycle of myosin, chemical energy of ATP hydrolysis is transduced into mechanical work by a series of structural changes of the actin-myosin complex, the power-stroke, that drives actin filaments past the myosin filaments. The power-stroke is accompanied with the release of ATP hydrolysis products ADP and  $P_i$  (inorganic phosphate) from the active site of myosin. Release of phosphate from the M.ADP. $P_i$  complex is a crucial step in crossbridge cycle. Previous studies on muscle fibers showed that an increase in  $P_i$  decreases isometric force with little or no effect on maximum shortening velocity. This decrease in isometric tension by  $P_i$  was interpreted to result from the reversal of the strong binding, force exerting state (AM.ADP) to a weak binding non-force generating state (AM.ADP. $P_i$ ) in rapid equilibrium with detached states (e.g. M.ADP. $P_i$ ).

Using TIRF (Total Internal Reflection Fluorescence) microscopy the effect of inorganic phosphate ( $P_i$ ) on the actin filament gliding velocity was determined in *in vitro* motility assays. In a single molecule assays 'dwell time' were measured, i.e., the time during which nucleotide remains in the nucleotide-binding pocket. Binding of fluorescently labeled ATP (Cy3-EDA-ATP) to an immobilized myosin molecule appeared as a discrete fluorescent spot that disappeared with the ADP release. Thus, appearance and disappearance of fluorescent spots were correlated with association and disassociation of the nucleotide, respectively. Dwell time measurements were done to find the intermediate state affected by increased  $P_i$  concentration. In addition to dwell times, the number of myosin molecules having Cy3-EDA-ATP bound was determined by measuring the number of the fluorescent events at any one moment in the field of view.  $P_i$  was found to reduce the sliding velocity of actin filaments at low ATP concentrations, and this inhibitory effect was diminished with increasing [ATP]. In the single molecule dwell time assays,  $P_i$  did not affect the average dwell time but the number of molecules with Cy3-EDA-ATP in the nucleotide-binding pocket was reduced, suggesting that the number of myosin molecules available for Cy3-EDA-ATP binding was reduced in the presence of  $P_i$ . The motility and dwell time data are consistent with the idea that  **$P_i$  can also bind to the empty nucleotide-binding**



---

**pocket yielding a strong binding intermediate (AM.P<sub>i</sub>), i.e. P<sub>i</sub> competes with ATP for binding to the empty active site.**

Secondly, dwell times of fluorescent signals from binding of Cy3-EDA-ATP for individual myosin molecules was studied. Usually kinetics of biochemical processes is derived from measurements on large ensemble of molecules. Such ensemble-averaged experiments have their limitations in that they can barely distinguish dynamical fluctuations (single molecule changes with time) and static heterogeneity (molecules are statically different); also, it is difficult to extract the interconversion dynamics (switching between the different conformations). Analysis of dwell times observed from individual molecules revealed two distinct populations of dwell times, one with a short, and another with an about 5 fold longer time constant. The possibility of different reaction rates was addressed, which is difficult to resolve in ensemble measurements. The two populations of dwell times seen even for individual molecules were attributed to **fluctuations in the rate constant of ATPase cycle due to switching between two different stable conformations of the motor protein.** The two postulated conformations are characterized by distinct rate constants for the reaction steps that determine the dwell time of fluorescent nucleotide. We, therefore, **proposed dynamic fluctuation** in the enzymatic activity of individual myosin II molecules.

---

## TABLE OF CONTENTS

<b>1 ABBREVIATIONS</b>	<b>3</b>
<b>2 INTRODUCTION</b>	<b>5</b>
<b>2.1 MOLECULAR MOTORS</b>	<b>5</b>
<b>2.2 MUSCLE CONTRACTION</b>	<b>6</b>
2.2.1 STRUCTURE OF MUSCLE	6
2.2.3 ACTIN	10
2.2.4 MYOSIN	11
<b>2.3 ACTO-MYOSIN CROSS-BRIDGE CYCLE</b>	<b>14</b>
2.3.1 STRUCTURAL STUDIES	14
2.3.2 KINETIC STUDIES	16
<b>2.4 IN VITRO MOTILITY ASSAY AND SINGLE MOLECULE DETECTION TECHNIQUE</b>	<b>18</b>
<b>2.5 THEORY OF TIRF MICROSCOPY</b>	<b>19</b>
<b>PART I</b>	<b>21</b>
<b>2.6 QUESTIONS</b>	<b>21</b>
2.6.1 AIM	24
<b>3 MATERIALS &amp; METHODS:</b>	<b>25</b>
<b>3.1 BUFFERS</b>	<b>25</b>
<b>3.2 PROTEINS</b>	<b>27</b>
3.2.1 EXTRACTION OF MUSCLE MYOSIN II	27
3.2.2 PREPARATION OF FLUORESCENTLY LABELLED F-ACTIN	28
3.2.3 PREPARATION OF MYOSIN DECORATED ACTIN FILAMENTS	28
<b>3.3 TIRF MICROSCOPY</b>	<b>29</b>
<b>3.4 IN VITRO MOTILITY ASSAY ON BSA COATED SURFACE</b>	<b>31</b>
3.4.1 IN VITRO MOTILITY ASSAY ON PROTEIN G COATED SURFACE	32
<b>3.5 DWELL TIME ASSAY</b>	<b>33</b>
<b>3.6 SINGLE MOLECULE DWELL TIME MEASUREMENTS</b>	<b>34</b>
3.6.1 ON BSA COATED SURFACE	34
3.6.2 ON PROTEIN G COATED SURFACE	34
<b>3.7 CONSTRUCTION OF FLOW CHAMBERS FOR MOTILITY AND DWELL TIME ASSAYS</b>	<b>35</b>
<b>3.8 DATA ANALYSIS</b>	<b>36</b>
3.8.1 ACTIN FILAMENT MOTILITY ANALYSIS SOFTWARE	36
3.8.2 DWELL TIME ANALYSIS	37
<b>4 RESULTS</b>	<b>38</b>
<b>4.1 IN VITRO MOTILITY ASSAY</b>	<b>38</b>
4.1.1 EFFECT OF INORGANIC PHOSPHATE ON ACTIN FILAMENT GLIDING VELOCITY	38
4.1.2 FRAGMENTATION OF ACTIN FILAMENTS IN THE PRESENCE OF P <sub>1</sub> AT LOW ATP CONCENTRATION	40
4.1.3 EFFECT OF THE PHOSPHATE ANALOG ALF <sub>4</sub> <sup>-</sup> ON GLIDING VELOCITY	42
<b>4.2 SINGLE MOLECULE DETECTION MEASUREMENT</b>	<b>43</b>

4.2.1 DWELL TIME OF CY3-EDA-ATP	44
4.2.2 EFFECT OF INORGANIC PHOSPHATE ON DWELL TIME OF CY3-EDA-ATP	47
4.2.3 EFFECT OF $AlF_4^-$ ON DWELL TIMES	48
<b>4.3 MEASUREMENT OF DENSITY OF EVENTS</b>	<b>51</b>
4.3.1 DENSITY OF EVENTS EVENTS IN FIELD OF VIEW IN THE PRESENCE OF $P_i$	51
4.3.2 DENSITY OF EVENTS IN THE PRESENCE OF $AlF_4^-$	51
4.3.3 CONTROL EXPERIMENTS	53
<b>5 DISCUSSION</b>	<b>55</b>
<b>PART II</b>	<b>62</b>
<b>6 INTRODUCTION</b>	<b>63</b>
<b>7 RESULTS</b>	<b>64</b>
<b>7.1 ENSEMBLE DWELL TIME MEASUREMENTS FROM SKELETAL MUSCLE MYOSIN II</b>	<b>64</b>
<b>7.2 INDIVIDUAL MOLECULE DWELL TIME MEASUREMENTS</b>	<b>67</b>
7.2.1 DWELL TIME MEASUREMENTS FROM INDIVIDUAL MUSCLE MYOSIN II	67
<b>7.3 ACTIN SLIDING ON A SURFACE COATED WITH SINGLE HEADED DICTYOSTELIUM MYOSIN</b>	<b>70</b>
7.3.1 DWELL TIME MEASUREMENTS WITH PURE CY3-EDA-ATP ISOFORM (ENSEMBLE MEASUREMENT)	70
7.3.2 DWELL TIME MEASUREMENTS ON INDIVIDUAL DICTYOSTELIUM MYOSIN MOLECULE IMMOBILIZED ON A BSA COATED SURFACE	71
7.3.4 MEASUREMENT ON PROTEIN G COATED SURFACE	72
7.3.5 'OFF TIME' MEASUREMENT	75
7.3.6 DISTRIBUTION OF EVENTS THROUGHOUT THE RECORDED PERIOD	76
<b>8 DISCUSSION</b>	<b>78</b>
<b>9 CONCLUSION</b>	<b>82</b>
<b>10 FUTURE PROSPECTS</b>	<b>83</b>
<i>10.1 EFFECTS OF <math>P_i</math> IN THE PRESENCE OF REGULATORY PROTEINS.</i>	<b>83</b>
<i>10.2 INDIVIDUAL MOLECULE STUDIES TO CHECK THE CONFORMATIONS OF ACTIVE SITE</i>	<b>84</b>
<b>REFERENCE LIST</b>	<b>85</b>
<b>OWN PUBLICATIONS</b>	<b>93</b>
<b>ERKLÄRUNG ZUR DISSERTATION</b>	<b>94</b>
<b>CURRICULUM VITAE</b>	<b>95</b>

# 1 Abbreviations

A	Actin
AB	Assay Buffer
ADP	Adenosine 5' diphosphate
AlF <sub>4</sub>	Aluminium fluoride
Al(NO <sub>3</sub> ) <sub>3</sub>	Aluminium Nitrate
AEBSF	4-(2-Aminoethyl)-benzylsultonylflurid
ATP	Adenosin-5'-Triphosphate
ATPase	Adenosine-5'-Triphosphatase
BSA	Bovine serum albumin
CCD	Charge coupled device
Cy3	Sulfoindocyanine dyes
DTT	DL-Dithiothreitol
E64	N-(trans-Epoxy succinyl-L-Leucin-4-Guanidinobutylamide)
EDA-ATP	2'(3')-O- [N(2-aminoethyl)carbamoyl]ATP
EDTA	Ethylene diamine-N, N, N', N' tetra acetic acid
EGTA	Ethylene glycol-bis(-Aminoethyether)-N,N,N',N'-Tetraacetic acid
G-actin	Globular actin (monomer)
GSH	Glutathione
HEPES	4-(2-hydroxyethyl)-1-piperazine ethanesulfonic acid
HPLC	High performance liquid chromatography
HMM	Heavy Meromyosin
KCl	Potassium chloride
KDa	Kilodalton
M	Myosin
ml	Milliliter
mM	Milimole
MgCl <sub>2</sub>	Magnesium chloride
μm	Micrometer (1μm = 10 <sup>-6</sup> m)
Na <sub>2</sub> ATP	Disodium ATP
NaCl	Sodium chloride

NaF	Sodium Fluoride
NaH <sub>2</sub> PO <sub>4</sub>	Sodium dihydrogen phosphate
Na <sub>2</sub> HPO <sub>4</sub>	Disodium hydrogen phosphate
NaN <sub>3</sub>	Sodium azide
NaOH	Sodium hydroxide
nm	Nanometer (1nm = 10 <sup>-9</sup> m)
P <sub>i</sub>	Inorganic phosphate
pH	negative logarithm of H ion concentration
PP <sub>i</sub>	Pyrophosphate
Rh-Ph	Rhodamine phalloidin
RT	Room temperature
S1	Subfragment 1
T	Temperature
TIRF	Total internal Reflection fluorescence
Triton X-100	Octylphenolpoly (ethyleneglycolether)
TRITC	Tetramethylrhodamine-β- isothiocyanate
U	Unit

## **2 Introduction**

### **2.1 Molecular Motors**

All living cells contain a large number of motor proteins and tracks on which the biomotors move, forming complex ‘highway’ system in a cell. These motors and their tracks (actin filaments and microtubules) are involved in innumerable processes in each individual cell. These nanomachines serve as cargo carriers, transporting for example vesicles, proteins and mRNAs. They are also involved in cell division, movement of whole cells and muscle contraction. The network of tracks on the other hand, forms the cytoskeleton of the cell, gives mechanical support and maintains the cell shape. Molecular motors use the energy derived from ATP hydrolysis for mechanical work, and serve structural, transport and motility purposes for the cell. These motors include microfilament or actin-based motors like myosins, and the microtubule-based motors like kinesin and dynein.

This work is primarily concerned with Myosin II, the molecular motor of skeletal and heart muscle, also termed ‘conventional’ myosin that drives muscle contraction.

## 2.2 Muscle contraction

### 2.2.1 Structure of muscle

Skeletal muscles are made up of fiber bundles (50-300  $\mu\text{m}$  in diameter), each of which can contain hundreds of myofibrils constituting 85 % volume of a muscle fiber. Myofibril is a single multinucleated cell that can extend the length of the muscle. Myofibril is further made up of repeating functional and structural subunits called sarcomere. Sarcomere consists of thick (Myosin) and thin (Actin) filaments between the Z discs. The basic structure of muscle fibers obtained in light microscopy (Figure 2.1) shows bands of striations with alternating light/ *I bands* containing thin filaments and dark/ *A bands* formed due to the higher density of thick filaments. Near the center of the sarcomere thin and thick filaments overlap. A thick filament of the *A band* is bipolar, with myosin heads lying at the distal tips of the filament and tails at the center. The bare zone of thick filament forms the M line. The cross-section of the sarcomere shows the hexagonal lattice arrangement of filaments with one thick filament surrounded by six thin filaments allowing the interaction of myosin and actin.

It was observed that during muscle contraction thick and thin filaments do not change length but the sarcomere shortened. This observation was explained as thick and thin filaments sliding during contraction (Huxley & Niedergerke, 1954; Huxley & Hanson, 1954), and a ‘sliding filament model’ was proposed. The central idea of this model is an ATP dependent interaction between thick and thin filaments generating a force, which causes thin filaments to slide past thick filaments. From high resolution electron micrographs, the structures responsible for force production were later revealed that showed regularly spaced arrays of cross bridges between thick and thin filaments (Huxley, 1963). Myosin cross- bridges were believed to be the motor elements generating force for sliding the filaments. Later studies showed the presence of flexible links at the base of globular myosin heads (Huxley, 1969) and a ‘swinging cross-bridge’ theory was proposed. More recently, the crystal structure of myosin head was resolved that led to further refinement of the previous model as ‘swinging lever arm’ model (Rayment, 1993). According to this model, the light chain-binding

domain of myosin acts as a lever arm that amplifies the small conformational changes in the head domain.

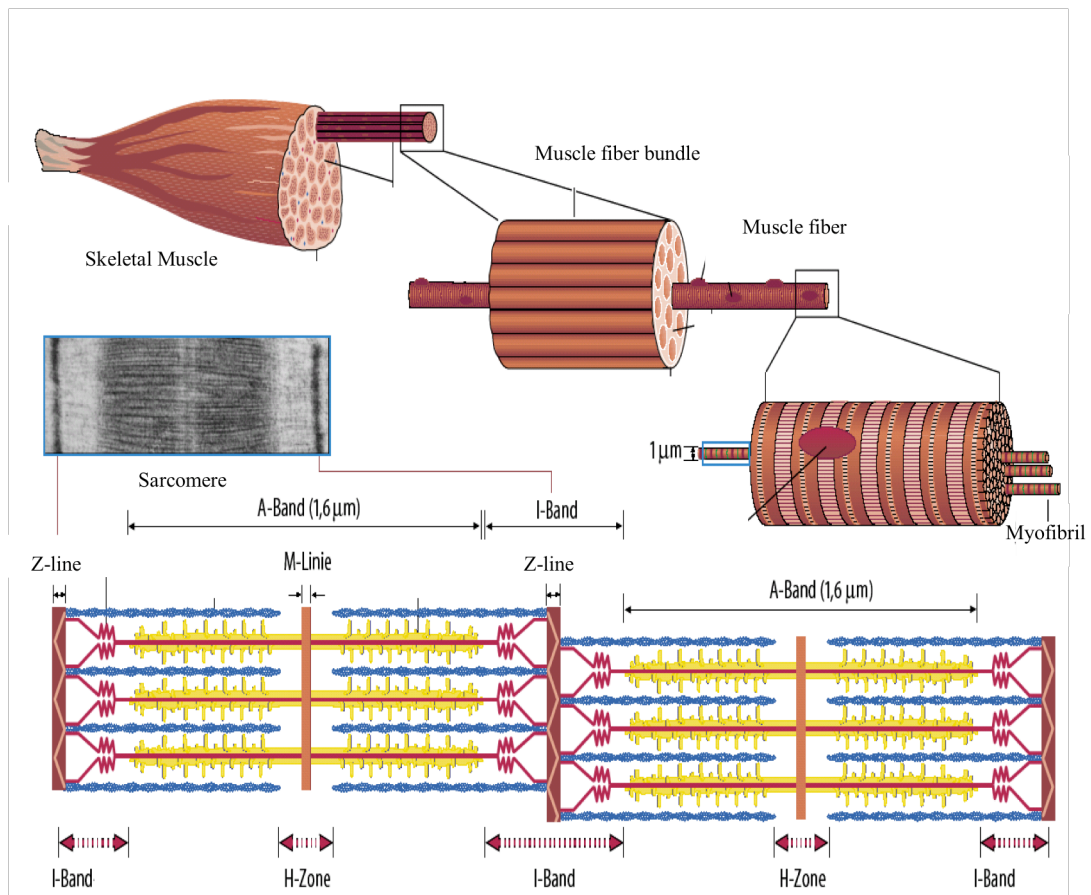


**Figure 2.1: Structure of skeletal muscle.** The arrangement of thick and thin filaments in the sarcomere gives the striated appearance comprising A-band (dark bands) and I-bands (light bands). (Figure from textbook *Physiologie des Menschen*, Schmidt.Lang.Thews, 29<sup>th</sup> edition)



## 2.2.2 Ca<sup>2+</sup> regulation of muscle contraction

The fundamental process of muscle contraction is regulated by the tropomyosin-troponin Ca<sup>2+</sup> system. Increase in Ca<sup>2+</sup> concentration activates actomyosin interaction. In skeletal muscle, contraction is regulated by four accessory proteins closely associated with actin filament, tropomyosin (TM), troponin (TN) (Figure 2.2). Tropomyosin, a rope like protein forms a chain along actin filament. In the resting muscle, tropomyosin blocks access to the high affinity myosin binding sites on actin. Associated with tropomyosin is troponin, a complex of the 3 proteins TN-T, TN-I and TN-C. TN-T is an elongated protein that links TN-C and TN-I to TM. TN-C is the receptor for Ca<sup>2+</sup> that triggers activation of contraction and TN-I is involved in inhibition of actin-myosin interaction. Ca<sup>2+</sup> binding to TN-C modulates the interaction of TN-C with TN-I. Ca<sup>2+</sup> induced movement of TN-I, result in the movement of tropomyosin on the surface of actin filament making the high affinity myosin-binding site on actin accessible for the strong actin-myosin interaction (Chalovich & Eisenberg, 1982; Brenner et al., 1982; Lehman et. al., 1995)

In a myofibril, sarcoplasmic reticulum (SR), a network of membranous tubules acts as a 'storehouse' for Ca<sup>2+</sup>. Under relaxing condition Ca<sup>2+</sup> concentration in muscle cell is kept below 0.1 μM by the transfer of Ca<sup>2+</sup> from the cytosol into the SR. To respond quickly a signaling pathway has evolved in a muscle cell. Transverse tubules (T tubules), which are invaginations of plasma membrane into the cytosol enter at the Z disk, where they come in close contact with the SR. This system is developed to bring the depolarization signal to SR, which in response, release the Ca<sup>2+</sup> into the cytosol, resulting in an increase in cytosolic Ca<sup>2+</sup>. Muscle contraction is initiated with the increase in Ca<sup>2+</sup> in cytosol, whereas it stops contracting or reaches a relaxation state when Ca<sup>2+</sup> is pumped back to the SR. Figure 2.3 shows the activation and relaxation of muscle fiber in response to high and low Ca<sup>2+</sup> concentration, respectively.

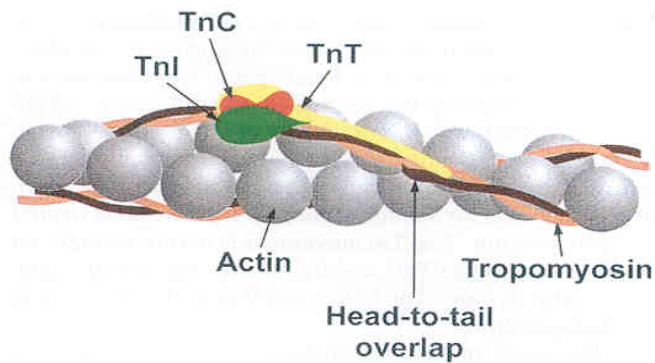


**Figure 2.2:** Actin filament associated with regulatory proteins Tropomyosin and Troponin (TN-T, TN-C and TN-T).  $\text{Ca}^{2+}$  regulates muscle contraction through these proteins that makes high affinity binding sites on actin accessible for the myosin head domain. (Gordon et al., 2000)

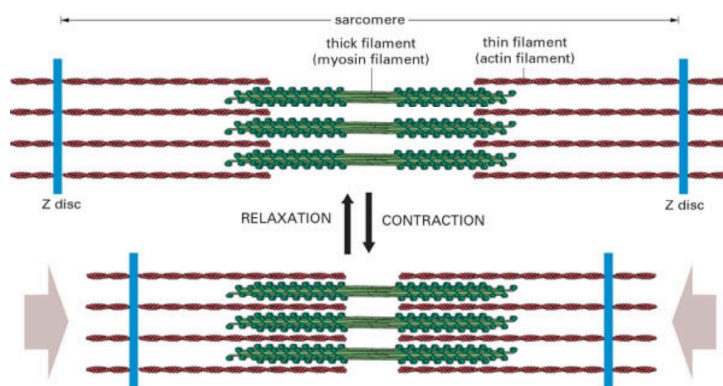


**Figure 2.3:** Schematic representation of muscle contraction. Actin and myosin filaments of a sarcomere overlap on either side of midline. Actin filaments are anchored to the Z disc through their + end whereas bipolar myosin filaments are tethered by titin to the Z disc. Following the activation by  $\text{Ca}^{2+}$ , sliding of actin and myosin filaments causes contraction without shortening. Relaxation is brought about by outflux of  $\text{Ca}^{2+}$  to the sarcoplasmic reticulum. (Figure from text book Molecular Biology of Cell, Alberts & Walter 1998)

### 2.2.3 Actin

Thin filament or F-actin is a helically arranged polymer of the monomeric G-actin (42 kDa). G-actin is associated with ATP, which is hydrolyzed during polymerization process (Szent-Gyorgi, 1968). The structure of G-actin shows actin to consist of 4 similar domains with a cleft in the center (Figure 2.4). This cleft is a nucleotide (ATP/ADP) binding site together with  $Mg^{2+}$  or  $Ca^{2+}$  (Kabsch *et al.*, 1990; Lorenz *et al.*, 1993). Each of the domains carries a subdomain; one involved in actin-actin interaction and the other forming the top of the nucleotide-binding pocket. Actin filaments have polarity with + or barbed end and – or pointed end shown with the characteristic arrowhead appearance in HMM decorated actin filaments in EM studies (Reedy *et al.*, 1965). Actin filaments may undergo *treadmilling*, in which the filament length remains constant while actin monomers add at one end (Barbed / + end) and dissociate from the other end (pointed / – end). Capping proteins bind at the ends of actin filaments. Depending on the ends they bind + / – end, they may stabilize or disassemble F-actins.

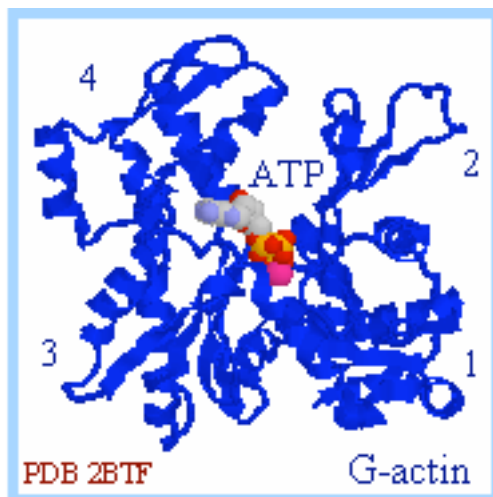


**Figure 2.4:** Structure of G-actin monomer. The subdomains are designated 1-4 separated by nucleotide binding cleft. (Figure modified from Kabsch *et. al.* 1990)

## 2.2.4 Myosin

Myosin is an ATPase that converts chemical energy into directed movement. Over 18 classes (Hodge & Cope, 2000; Mermall et al., 1998; Sellers et al., 2000) of myosin have been identified so far based on sequence homology (Cope et al., 1996). The common feature of all these myosin molecules is a motor domain with actin binding and ATPase properties.

The myosin II molecule is highly asymmetric, consisting of two globular heads attached to a long tail. Myosin has 6 subdomains with total molecular weight of 520 kDa. The two heavy chains weigh 220 kDa each and 4 light chains termed as regulatory and essential light chains each of 20 kDa. Each globular head is composed of approximately 850 amino acid residues having 1 heavy chain associated with 2 light chains. The globular heads contain the nucleotide-binding site and actin-binding site, whereas the long tail of myosin forms the backbone of the thick filament. The myosin heads can be cleaved from the rest of the molecule by proteolysis yielding subfragment-1 (S1), which are very soluble components (Figure 2.5).

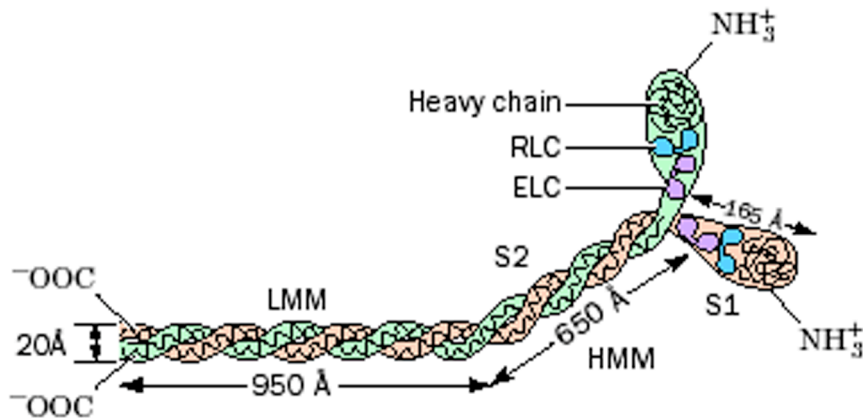


**Figure 2.5:** Schematic diagram of myosin molecule.

Light meromyosin (LMM) forms the core of thick filament attached to the myosin head via subfragment 2 (S2). Heavy meromyosin (HMM) comprising S1 & S2 can be cleaved to subfragment 1, which is a functional myosin head having both ATP and actin binding sites. (Figure from textbook of Biochemistry, Voet & Voet, 1995)

The structure of skeletal muscle myosin S1 revealed that the myosin head is itself very asymmetric. It has a length of over 16.5 nm, approximately 6.5 nm wide and 4 nm deep. This molecular fragment can be further divided into 2 parts: a globular component formed exclusively from the heavy chain and an extended motif that forms an  $\alpha$ -helix around which essential and regulatory chains are bound. The light chain domain is also referred to as the regulatory domain. These structures suggest that one of the roles of the light chains is to stabilize the conformation of the helix and it may serve to transduce and amplify the effects of conformational change in the head domain. The head domain contains 3 distinct regions the 25 kDa N terminal domain, the 50 kDa central domain and the 20 kDa converter domain named after their molecular weights. A prominent cleft that splits the myosin head into 2 major domains i.e., the upper and lower 50 kDa domains is termed as the 50 kDa cleft.

The nucleotide-binding pocket is located between the upper 50 kDa and 25 kDa domains, whereas the actin-binding site lies between the upper 50 kDa domain and 20 kDa converter domain. Within the catalytic domain actin and ATP binding sites are on opposite sides of the molecule 3.5 nm apart (Rayment et al., 1993a,b). As kinetic data indicate, the binding affinity of S1 for actin changes with ATP binding and the product release from the active site is induced by binding of actin to S1. It was hypothesized that this communication may occur through the  $\beta$  sheet structure present in the narrow 50 kDa cleft, that runs directly under the nucleotide-binding pocket and is assumed to be a communication route between ATP and actin binding sites (Figure 2.6 a)

Molecular modeling (Yount et al., 1995) of ATP into the chicken skeletal S1 crystal structure (Rayment et al., 1993b) showed that the adenine ring of the ATP projected out of the protein, whereas the triphosphate moiety, on the opposite end of the molecule was tightly bound in a tube-like structure, termed the phosphate tube (Figure 2.6 b). The phosphate tube pointed into the interior of the protein, and was formed by three structurally conserved elements, the P-loop, switch 1 and switch 2. The rear opening of the phosphate tube was located at the apex of the large 50 kDa cleft. This opening appeared to be a likely approach route for the water molecule that attacks the  $\gamma$ -phosphate of ATP during hydrolysis.

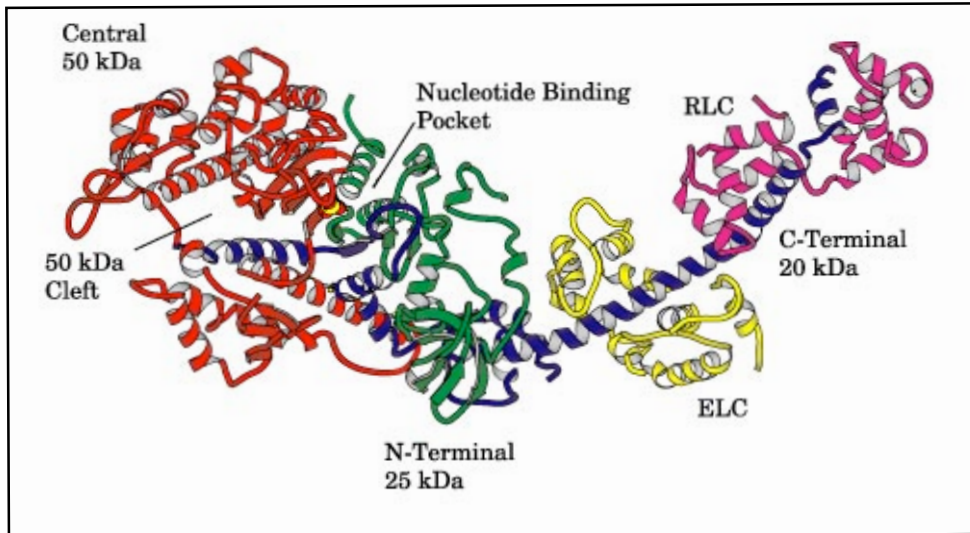
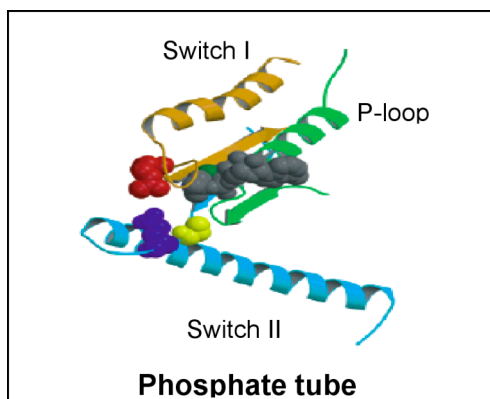


**Figure 2.6:** a) Ribbon representation of chicken skeletal muscle myosin Subfragment-1 showing major domains.

The subdomains are; the 50 kDa central domain (Red), 25 kDa N-terminal domain (Green) and 20 kDa C-terminal domain (Blue). The lever arm extending from C-terminal domain associated with essential light chain (ELC, yellow) and regulatory light chain (RLC, Pink) (Rayment, 1996)



b) Ribbon representation of nucleotide binding pocket. Backbone atoms of residues from P-loop, switch-I and switch-II are shown in green, orange and light blue, respectively. Bound nucleotide is shown in grey and  $Mg^{2+}$  in dark green. (Onishi & Morales, 2004).

## 2.3 ActoMyosin cross-bridge cycle

### 2.3.1 Structural studies

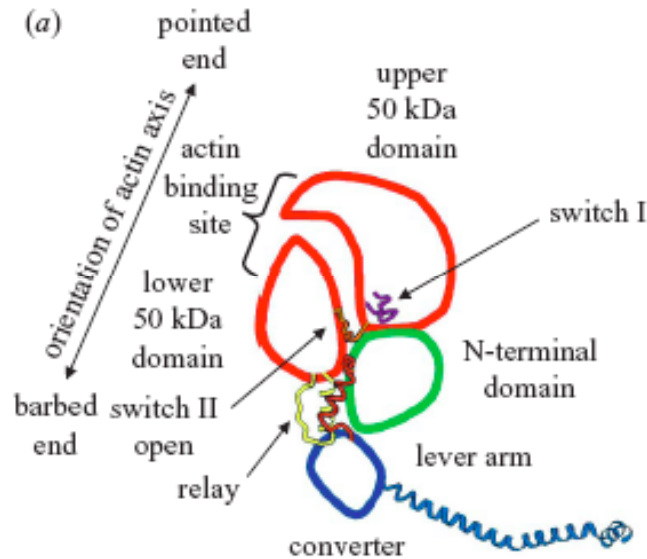
Muscle contraction involves relative sliding of actin filaments (A) to myosin filaments (M) (Huxley & Hanson, 1954; Huxley & Niedergerke, 1954). This sliding is driven by the cyclic interaction between actin filaments and the head domains of myosin molecules, and is powered by ATP hydrolysis. An approximate model for the actomyosin complex was obtained through a combination of structures of chicken skeletal muscle S1 with the earlier structure of actin (Holmes & Kabsch 1990) and an image reconstruction of the actomyosin complex was obtained by electron microscopy (Miligan & Flicker 1987, Miligan & Safer 1990). This structure was used as the basis of a structural hypothesis for how myosin converts chemical energy into direct movement. According to this, domain movements in myosin, induced by the binding of ATP to actin bound myosin state, generates a cyclic series of conformational changes that reduce the affinity of myosin for actin and place the myosin in a state in which it can hydrolyze the nucleotide. Central to this hypothesis was the suggestion that myosin interacts with actin in a stereospecific manner.

Crystallographic studies on truncated *Dictyostelium* myosin show two distinct structural states for myosin S1 (Rayment 1993a,b):

‘Open’ or ‘end’ conformation characterized by nucleotide free or rigor state (Figure 2.7).

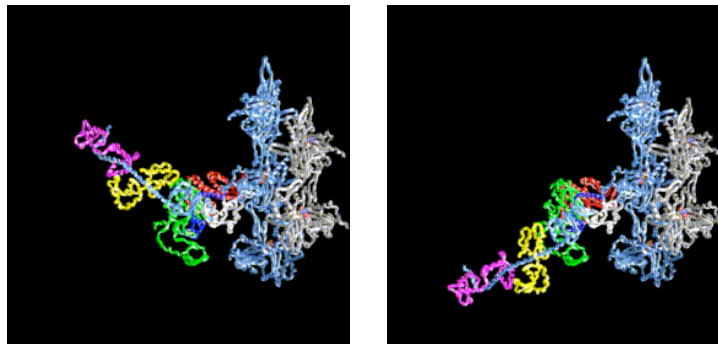
‘Closed’ or ‘beginning’ conformation favored by ATP or ADP.P<sub>i</sub> complex.

Myosin drives actin by switching between these 2 states. ‘Open’ and ‘Closed’ refer to the status of the ATP binding site that lies between 50 kDa upper domain and N-terminal domain. ‘Open’ and ‘Closed’ also refers to the switch II loop, which is open in AM bound state and closed when ATP is in nucleotide binding pocket. The switching is believed to be responsible for the rotation of the C-terminal lever arm. In the ‘Closed’ form the lever arm is at the beginning of the powerstroke (post-powerstroke) whereas in the ‘Open’ form it is at the end of the powerstroke (pre-powerstroke conformation) (Figure 2.8). The ‘Closed’ state is required for ATP hydrolysis.



### Post-powerstroke

**Figure 2.7: Schematic representation of myosin heads in the near rigor state (Rayment, 1993).** Subdomains in the motor domain are shown as compact globular elements connected by joints. The light chains are removed from lever arm for clarity. (Houdusse et. al. 2000)



### Pre-powerstroke

### Post-powerstroke

**Figure 2.8: The end state or pre-powerstroke:** Subunits showed in blue and white on right side are from F-actin. Modeled from the Dictyostelium myosin motor domain truncated at residue 761 and complexed with ADP.BeFx (Fisher et al. 1995). The lever arm has been modeled from the chicken S1 data by superimposing the converter domain.

**The beginning state or post-powerstroke:** Reconstructed from the crystallographic data on Dictyostelium construct complexed with ADP.vanadate. The 70° rotation of the lever arm moves between the two states (pre and postpowerstroke states).



### 2.3.2 Kinetic studies

Solution kinetic studies provided a molecular mechanism and a quantitative model for the events, which were assumed to take place in muscle contraction. Using quench flow to monitor the change in the reaction intermediates and products in real time, Lymn and Taylor (1971) proposed a simple kinetic model for the actomyosin interaction (Figure 2.9). They observed that in the presence of actin the steady state ATP hydrolysis rate was much faster. The rate of actomyosin dissociation after binding ATP was too fast to be measured in stopped-flow apparatus. The structural change that causes sliding of actin and myosin filament is accompanied with the release of ATP hydrolysis products ADP and  $P_i$  from active site. Later work showed that although the actin affinity towards myosin is reduced by a factor of  $10^3$ , ATP binding does not necessarily lead to dissociation of actin from myosin (Stein, 1979). This led to a model of 2 attached states (Eisenberg & Green, 1980); a weakly bound and strongly bound. This model proposed that detached states (M.T & M.D.P) are in rapid equilibrium with attached states (A.M.T & A.M.D.P), where T = ATP, M = Myosin, A= Actin, D = ADP and P =  $P_i$ .

Later studies showed that, during each ATPase cycle, chemical energy of ATP hydrolysis is transformed into mechanical work by a multi-step power-stroke that drives actin filaments several nanometers past the myosin filaments. Release of phosphate from the AM.ADP. $P_i$  complex is a crucial step in crossbridge cycle. It is believed that  $P_i$  release is closely related to the initiation of power-stroke (Hibberd & Goldman, 1985.)

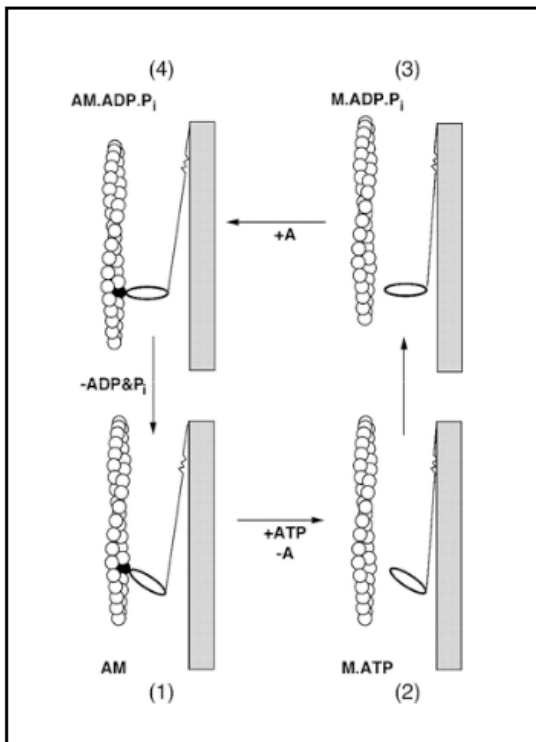


**Figure 2.9:** The Lymn-Taylor cycle. The myosin cross-bridge is bound to actin in the rigor (state 1). ATP binding causes fast dissociation of myosin from actin (state 2). The hydrolysis of ATP to ADP and P<sub>i</sub> leads to rebinding to actin (state 4). This leads to the release of the products and return of myosin to state 1. In the last transition, actin is "rowed" past myosin. (Figure from Geeves & Holmes, 1999)

## **2.4 *In vitro* motility assay and single molecule detection technique**

The development of *in vitro* motility assay was an important step in the early 1980's that paved the way for single molecule mechanics. Fluorescently labeled actin filaments were visualized moving over a bed of immobilized myosin molecules on the glass surface in the presence of MgATP (Kron & Spudich, 1986).

Further advances in technology made it possible to visualize single fluorescent dye molecules under a fluorescence microscope leading to the development of Single Molecule Detection Technique. Real time imaging of single fluorophores in aqueous solution (Funatsu & Yanagida, 1995) was achieved using TIRF microscopy. This powerful optical technique was used to study single molecule enzyme kinetics, where single ATP hydrolysis (ATP binding, hydrolysis up to the ADP release) by immobilized myosin molecules were measured using fluorescently labelled ATP.

## 2.5 Theory of TIRF microscopy

TIRF (Total Internal Reflection Fluorescence) microscopy utilizes the unique property of an induced evanescent field. It allows selective illumination and excitation of fluorophores in a limited specimen region immediately adjacent to a glass-water interface. An excitation light beam is allowed to travel at an incident angle greater than critical angle through the solid glass coverslip. Refractive index (RI) differences between the glass (high RI) and water (low RI) phases regulate how light is reflected or refracted at the interface as a function of incident angle. At a specific critical angle, the beam of light is totally internally reflected from the glass/water interface. The reflection generates a very thin electromagnetic field in the aqueous medium. This field called the evanescent wave undergoes exponential intensity decay with increasing distance from the surface.

The preferred depth of the evanescent wave intensity can be obtained by adjusting the angle of incident beam for illumination, wavelength and refractive index difference between media on each side of the interface. The evanescent field can selectively excite fluorophores located near the glass liquid interface by using the incident beam of suitable wavelength. Fluorophores away from the surface or in the solution are not excited due to the decreased evanescent field intensity. This results in the reduction of background fluorescence. Thus this technique enables production of images with a significant increase in signal to background ratio.

The concept of TIRFM is schematically presented in Figure 2.10.

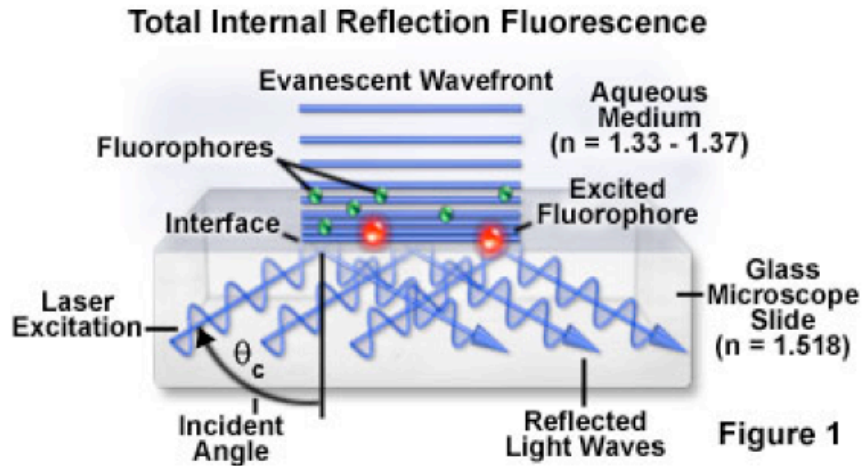
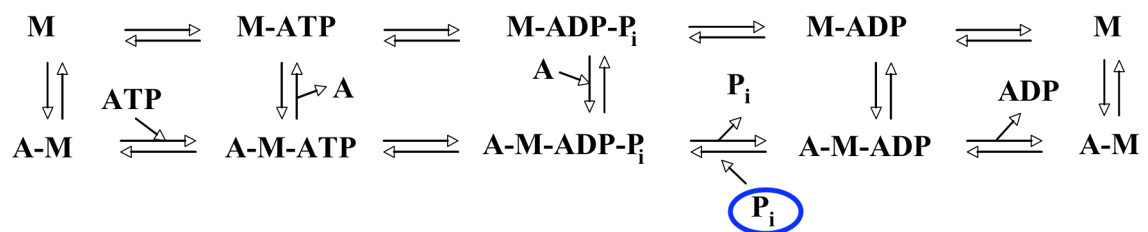


**Figure 2.10. TIRF microscopy scheme.** The incident beam with high incident angle is allowed to pass through the glass slide with high refractive index (RI) of **1.5** into the aqueous medium of low RI of 1.33. The evanescent wave formed due to the total internal reflection of incident beam is showed as blue horizontal lines extended in the aqueous medium. Red circles show excited fluorophores that are close to the surface and green fluorophores that are away from the surface are not excited. (Scheme from Nikon microscopy webpage).

## Part I

### 2.6 Questions

Myosin ATPase uses chemical free energy for the production of force and work in contracting muscle by hydrolysis of ATP to products ADP and  $P_i$ . However the relationship between the intermediate biochemical states in the contractile cycle and mechanical properties remains unresolved. Scheme 1 describes the basic mechanism of ATP hydrolysis during actomyosin crossbridge cycle, based on solution studies.



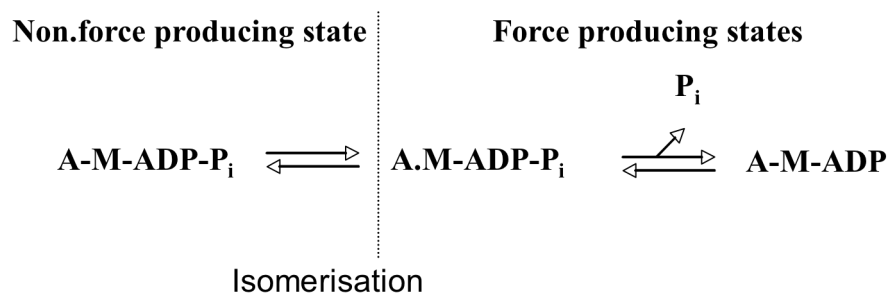
**SCHEME 1**

Scheme 1 is shown for the ATPase cycle in the absence (Upper row) and presence (lower row) of Actin. A = Actin, M = Myosin.

$P_i$  is believed to be the first hydrolysis product to be released from the actomyosin complex (Trentham, 1972; Taylor 1979; Cooke, 1985). The release of inorganic phosphate from the quaternary complex AM.ADP. $P_i$  has been associated with force and work production in muscles. The phosphate release believed to proceed through a 'back door' mechanism (Geeves & Holmes, 1999), is associated with large free energy change. In solution experiments with the isolated proteins, the product release steps liberate more than half of the energy available from net ATPase reaction. Most of this free energy change corresponds to  $P_i$  release (White & Taylor, 1976; Siemankowski, 1985). These observations made  $P_i$  the likely candidate for the main step in actomyosin ATPase cycle for chemo-mechanical coupling.

$P_i$  release is a reversible step, however the cellular concentration of  $P_i$  is in millimolar range and the dissociation constant for  $P_i$  binding to AM.ADP is  $10^3$  M (White & Taylor 1976), so  $P_i$  dissociation from AM.ADP is almost irreversible (Sleep & Hutton, 1980).

A pivotal role of  $P_i$  in the generation of force producing states has been studied extensively in muscle fibers and solution. Effects of  $P_i$  and its analogs on contracting muscle fibers have been used to develop an understanding of the central relevance of  $P_i$  release for force generation. For instance, effects of  $P_i$  were examined at steady state parameters like isometric force and unloaded shortening velocity as well as on pre-steady state kinetic properties by using release of  $P_i$  from caged  $P_i$ . Photolysis of caged  $P_i$  within an actively contracting muscle fiber causes a decline of force (Millar & Homsher 1990; Dantzig et al., 1992; Walker et al., 1992). Oxygen isotope exchange experiments between water and  $P_i$  provided the direct evidence that  $P_i$  in the medium can bind to the ATPase catalytic site in activated isometric fibers (Webb & Trentham, 1986). As a result of these steady state and pre-steady state kinetic studies it was proposed that a reduction of the overall free energy of ATP hydrolysis occurs at a high concentration of  $P_i$ . Upon binding of  $P_i$  to the M.ADP or A.M.ADP intermediates, occupancy of strong binding, force generating state is shifted toward a weak-binding or no force producing AM.ADP. $P_i$  in rapid equilibrium with the detached M.ADP. $P_i$  state (Eisenberg, 1980). Thus  $P_i$  rebinding marks the transition from myosin states with low affinity for actin (M.ATP & M.ADP. $P_i$ ) to states with high actin affinity (M.ADP & M) (Hibberd & Trentham, 1986; Brenner, 1990). Shortening velocity and MgATPase would not be much affected by  $P_i$  in conditions where  $P_i$  release does not contribute to the rate-limiting step of the overall cross-bridge cycle. To fully account for the observed pre-steady state and steady state kinetic data it was proposed that a strong binding AM.ADP. $P_i$  must exist in the path toward force generation (Dantzig et al., 1992; Miller & Homsher, 1990; Takagi et al., 2004). Thus two-step mechanism for  $P_i$  release was proposed, with a force generating isomerisation of AM.ADP. $P_i$  preceding the release of  $P_i$ .



SCHEME 2

Some results, however were not explained by this concept. At low ATP concentrations, an increase in  $P_i$  concentration to 50 mM caused a significant decrease in unloaded shortening velocity (Pate and Cooke, 1989). Secondly, when fiber stiffness of isometrically contracting fibers was measured for different speeds of stretch, the resulting stiffness speed relations were shifted to slower stretch velocities in the presence of 6-10 mM  $P_i$ . This implies that in the presence of  $P_i$  cross bridges in actively contracting fibers accumulate more in the strong binding cross-bridge states than in the absence of  $P_i$  (Brenner, 1993).

It was pointed out that the kinetics of the biochemical steps in a muscle fiber might not be the same as in solution. The concern was that the procedure required to isolate and fragment the proteins for transient biochemistry might alter them. Also the solution conditions are different particularly the ionic strength and the mechanical stress and strain present in the muscle filament lattice that might affect the equilibrium constants of any energy transducing steps (Goldman & Brenner 1987). Studying the effects of  $P_i$  on force generation in skinned muscle fibers is also complicated because of the diffusion barriers. And also during active contraction, the ATP hydrolysis rate is too high to control over substrate and product concentrations inside the myofilament, so one has to compromise with the temperature conditions to be able to capture the fast kinetics.



### 2.6.1 Aim

To overcome these problems with solution and muscle fiber studies, and provide the better understanding of chemo-mechanical coupling in muscle contraction, it is necessary to study it in a system where it is possible to maintain the physiological conditions without affecting the properties of the molecules.

- ✚ My first goal was to study the actomyosin system with isolated proteins to minimize the contribution from other proteins in muscle fibers, using native myosin (full length myosin) but maintaining physiological conditions.
- ✚ Secondly I wanted to study the effect of increased  $P_i$  concentration on actin filament gliding velocity on myosin coated surface in *in vitro* motility assays, which mimics the measurements of unloaded shortening velocity in intact muscle fibers.
- ✚ All available experimental data, biochemical, mechanical and structural, were the result of the action of large ensemble of molecules, from which we had to extrapolate the properties of individual molecules. To gain insight into the response of individual molecules to different conditions, along with the ensemble measurements, I also wanted to investigate the effect of  $P_i$  on actomyosin ATPase at single molecule level. Studying the effect of  $P_i$  on the actomyosin ATPase at single molecule might provide additional information about the affected intermediate state in ATPase cycle. It may not be possible to extract this information from ensemble measurements.
- ✚ Finally, I wanted to compare and correlate the ensemble and single molecule data to better understand the chemistry of how the individual molecules work in isolated and grouped conditions in a coordinated manner.

## 3 Materials & Methods

### 3.1 Buffers

Skinning solution contained 50 mM phosphocreatine, 10 mM glutathione, 8 mM  $\text{NaN}_3$ , 5 mM EGTA, 5 mM magnesium acetate, 5 mM  $\text{KH}_2\text{PO}_4$ , 5 mM DTT, 3 mM  $\text{Na}_2\text{ATP}$ , 0.5% Triton X-100. For inhibition of proteases, 0.01 mM Leupeptin, 0.001 mg/ml Aprotinin, 0.01 mM Antipain, 0.01 mM E64, 0.01 mM Pepstatin and 1 mM AEBSF were added.

Myosin extraction buffer contained 500 mM NaCl, 10 mM HEPES, 5 mM  $\text{MgCl}_2$ , 2.5 mM magnesium adenosine-5'-triphosphate (MgATP) and 30 mM dithiothreitol (DTT), pH 7. Actin polymerisation buffer was composed of 100 mM KCl and 10 mM HEPES, pH 7. Assay buffer (AB) contained 25 mM imidazole hydrochloride, 25 mM NaCl, 4 mM  $\text{MgCl}_2$ , 1 mM EGTA, 10 mM DTT. Assay buffer with BSA (AB.BSA) was prepared from fatty acid free BSA (Sigma, A6003-5G) with final concentration of 0.5 mg/ml. Motility Buffer (AB.BSA.ATP) was prepared by addition of 50 mM stock solution of MgATP to AB.BSA. The final concentration was 2 mM MgATP. Motility buffer was accompanied by oxygen scavenging system to avoid bleaching. The oxygen scavenging system contained 18  $\mu\text{g/ml}$  catalase, 0.1 mg/ml glucose oxidase, 3 mg/ml D-glucose, 10 mM DTT. Assay buffers were always used with 10 mM DTT.

For experiments in which ligands were tested (i.e. 30  $\mu\text{M}$  - 5 mM MgATP with 5 mM inorganic phosphate or 5 mM  $\text{AlF}_4^-$ ), the basic buffer composition was equivalent to the AB buffer. The ionic strength of buffers was maintained at 55 mM by adjusting NaCl concentration in the AB buffer, accordingly. Phosphate buffer was prepared from monobasic  $\text{NaH}_2\text{PO}_4$  and dibasic  $\text{Na}_2\text{HPO}_4$  salts. To remove contaminant pyrophosphate ( $\text{PP}_i$ ) from 100 mM  $\text{H}_2\text{P}_0_4^{-3}$  buffer stock solution, the pH was set to 9.0 and the stock solution was autoclaved at 121°C for 15 minutes (Gyimesi et al., 2005a). The pH was adjusted to 7 before use.  $\text{AlF}_4^-$  was prepared from a stock solution of 500 mM  $\text{Al}(\text{NO}_3)_3$  and 100 mM NaF. To avoid precipitation, the working dilutions were made immediately before use by mixing the required quantities of  $\text{Al}(\text{NO}_3)_3$  and NaF (molar ratio 1: 5). The pH was adjusted to 7.0 with 0.1 M NaOH.

A 50 mM stock solution pyrophosphate buffer was prepared from Tetrasodium diphosphate ( $\text{Na}_4\text{P}_2\text{O}_7 \cdot 10\text{H}_2\text{O}$  from Merck). The pH was adjusted to 7.4 with 5 M HCl.

The Cy3-EDA-ATP used was the mixture of the 2' and 3' Cy3-EDA-ATP isoforms, and was provided by Dr. Kazuhiro Owia. The purity of Cy3-EDA-ATP was greater than 99% as determined by HPLC using the Nova-Pak  $\text{C}_{18}$  column. Pure 2'-O-Cy3-EDA-ATP and 3'-O-Cy3-EDA-ATP isoforms were also obtained. Separation of two Cy3-EDA-ATP isoforms was done by using the same column, and had different peak retention time demonstrated by the spectras shown below. The purity was 100% for 2'Cy3-EDA-ATP and 97 % for 3'Cy3-EDA-ATP (Owia et al., 2000).

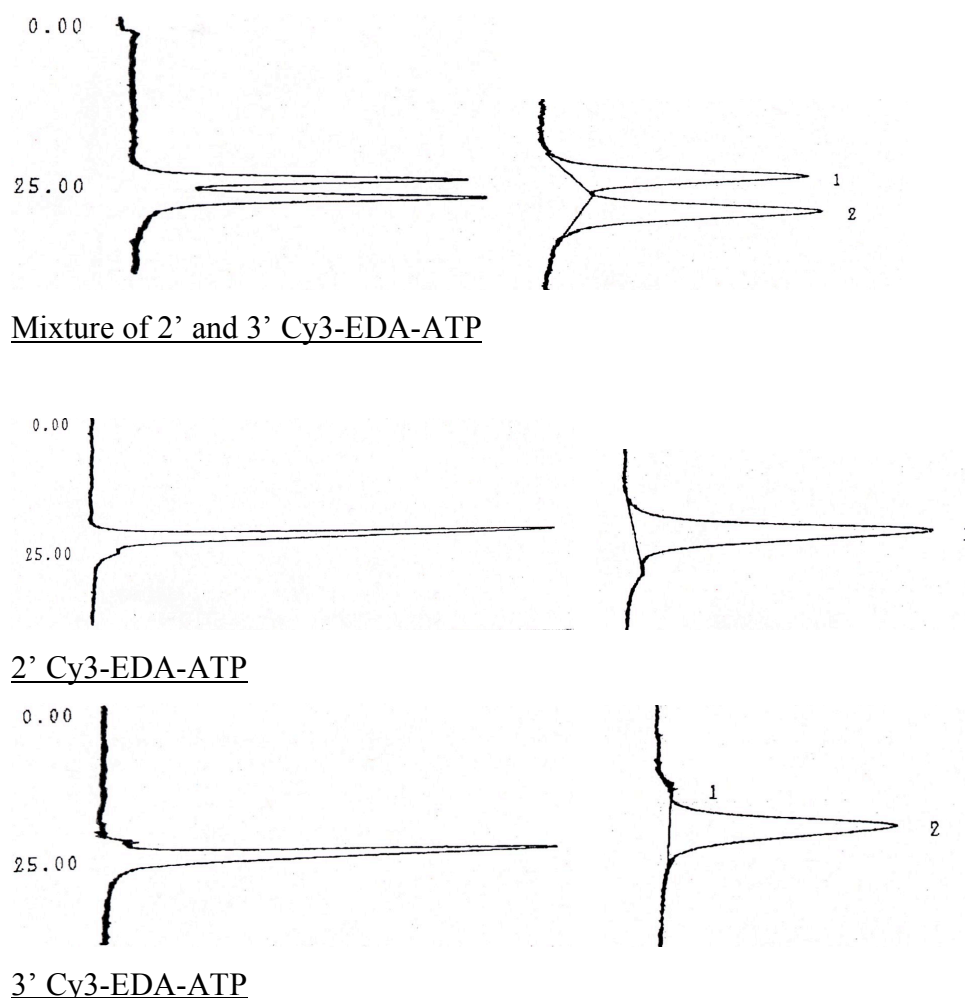


**Figure 3.1: Spectras obtained for the Fluorescently labelled ATP (Cy3-EDA-ATP)** The two isomers shown as a doublet, is a mixture of 2' and 3' Cy3-EDA-ATP. The pure, separated Cy3-EDA-ATP isoforms were evident from single peaks.

## 3.2 Proteins

### 3.2.1 Extraction of muscle myosin II

Fast skeletal muscle myosin II was extracted from skinned rabbit psoas muscle fibers as described previously (Thedinga, E. 1999). First, muscle fiber bundles were isolated from the psoas muscle and prepared for long time storage in liquid nitrogen. The muscle fiber bundles were first kept in skinning solution with Triton X-100 for 30 min and then transferred through a series of the skinning solutions without Triton but increasing concentrations of sucrose (0.5 M, 1 M, 1.5 M and 2 M). Fiber bundles were kept at each sucrose concentration for 30 min. After 30 min in 2 mM sucrose, the fiber bundles were frozen in liquid propane and then stored in liquid nitrogen (Kraft et al., 1995a, b). For extraction of myosin, fiber bundles were thawed in skinning solution without sucrose and allowed to equilibrate for 1 hr. Single muscle fibers of 1–1.5 cm in length and about 100  $\mu\text{m}$  in diameter were isolated according to Yu and Brenner (1989). For *in vitro* motility assays myosin was extracted from a single fiber by incubation in 5  $\mu\text{l}$  of myosin extraction buffer at 1–2°C for 30 min. For dwell time assays, incubation in 5  $\mu\text{l}$  myosin extraction buffer was done for 10 min and for 30 sec for some experiments. Myosin extraction for the motility assays was done for longer time since a high concentration of myosin was required. For the dwell time assays, however, the purity of myosin was the prime concern and also low concentration of myosin was required, so extraction time was shorter. A longer extraction of myosin from muscle fiber results in a contamination with other sarcomeric proteins like i.e., actin, troponin and tropomyosin. To avoid denaturation of myosin due to storage, myosin was extracted from fibers isolated from freshly thawed bundles. The myosin was used within 8 hours of extraction from a fiber.

Single headed Dictyostelium myosin II was provided by Dr. Georgios Tsiavaliaris. This myosin II was an engineered protein, called M765-2R, created by fusing motor domain of Dictyostelium myosin to an artificial lever arm and expressed in *Dictyostelium discoideum*. The first 765 amino acids from the Dictyostelium motor domain were fused to 2  $\alpha$ -actinin subunits that form the rigid lever arm with the 8x His tag at the C-terminal.

### 3.2.2 Preparation of fluorescently labelled F-actin

Actin was purified from rabbit back muscle by the method described by Pardee and Spudich (1982). Tetramethylrhodamine B isothiocyanate (TRITC-C) labelled F-actin was produced by polymerizing G-actin in the presence of TRITC-phalloidin. For polymerization 0.5  $\mu\text{M}$  G-actin and 1  $\mu\text{M}$  TRITC-phalloidin were added to actin polymerisation buffer and incubated for 20 min at room temperature (Harada et al., 1990). Unlabelled actin filaments were generated by mixing polymerisation buffer, 1  $\mu\text{M}$  phalloidin and 0.5  $\mu\text{M}$  G-actin. Polymerisation was allowed for 20 min at room temperature.

### 3.2.3 Preparation of myosin decorated actin filaments

Myosin decorated actin filaments were formed by adding a mixture of myosin and Alexa 488-phalloidin labelled F-actin. 10 mM EDTA was added to chelate all  $\text{Mg}^{2+}$  transferred from the myosin extraction buffer to allow actomyosin rigor complex formation by taking out MgATP. The amount of added F-actin was adjusted to obtain an approximately 20:1 molar ratio of actin monomers to myosin molecules, which on average separates the myosin molecules by  $\approx 100$  nm. By this procedure free myosin was kept to a minimum (Toyoshima et al., 1989). After 30 min of incubation at  $0^\circ\text{C}$ , the solution was diluted approximately 150 fold with AB buffer to obtain suitable concentration of decorated actin filaments. This final solution was then applied to the flow cell.

### 3.3 TIRF Microscopy

An objective type total internal reflection fluorescence (TIRF) microscope was set up on a vibration free table around a 60x oil immersion objective with high numerical aperture (NA 1.45; Olympus Plan Apo 100) in an inverted configuration.

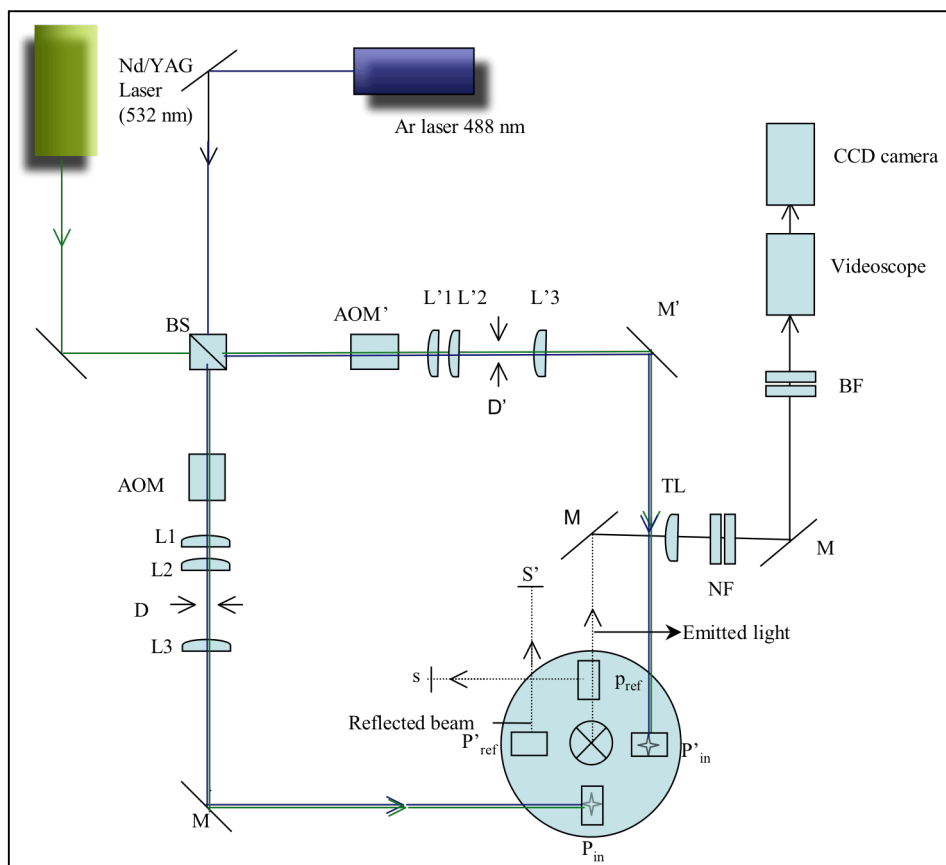
The beams of a green laser (diode pumped frequency doubled Nd : YAG laser, DPSS 532-400, Coherent, CA, USA) and of an air-cooled Ar-ion laser (Type 532-AP-AO1, Melles Griot, CA, USA) were superimposed by a beam splitting cube. Two acousto-optic modulators (Polychromatic Acousto-optic Modulator, Model: N48062-2.5-.55; RF-Driver Module, Model no. N64040-75-1-4CH-5-M, Neos Technologies, FL, USA) allowed to regulate the intensities of the two beams separately. The linearly polarized beams, set perpendicular to each other were focused by achromatic doublets (L3 & L'3 in fig.3.2a) into the back focal plane of the objective lens. Each beam was moved away from the optical axis by mirror M and M' (Fig.3.2a) such that the polarized beam exiting the objective lens was tilted relative to the optical axis. Once the tilted beam exceeds the critical angle, total internal reflection occurs at the coverslip-water interface forming an evanescent wave with exponentially decaying intensity in the aqueous medium adjacent to the coverslip surface. Incoming and reflected beams were projected into and out of the objective lens by 2 pairs of silver coated prisms ( $P_{in}$  and  $P_{ref}$ ). Diaphragms (D and D') were used to control the area of illumination in the object plane. The lens system L1/ L2 and L'1/L'2 were used to expand the laser beams. Two perpendicular beams were used to ensure equal excitation of fluorophores independent on the orientation of the absorption dipoles in the x-y plane. Light emitted by fluorophores was collected by the objective and focused by the tubus lens (TL) to form an image in the plane of the photocathode of the image intensifier (Video Scope VS4-1845, VA, USA). The notch filters (NF) were put in front of the tubus lens to block scattered light of the exciting laser light. Band pass filters (BF) were used to select a suitable wavelength according to the emission spectra of the fluorophores (520F40 for Alexa 488 and 570DF30 for Cy3). The image intensifier formed an intensified image on the action area of a CCD camera (Hamamatsu C2400-87, Osaka, Japan). For camera control and data acquisition the simple PCI software was used. For individual molecule fluorescence lifetime

measurements an Andor iXon CCD camera (Andor technologies, USA) was used which allowed us to further improve the signal to noise ratio, data acquisition time and frame rate. This camera was accompanied by iXon software for data acquisition.

Figure 3.2a is a schematic representation of the TIRF microscope viewed from the top. Figure 3.2b shows a side view of the objective to demonstrate the path of incident and reflected beam and the evanescent field formation.

Cy3-EDA ATP or Cy3-EDA-ADP were observed with the TIRF microscope using the green laser whereas the Ar laser was used to observe the Alexa 488 phalloidin labeled F-actin.

a.



b.

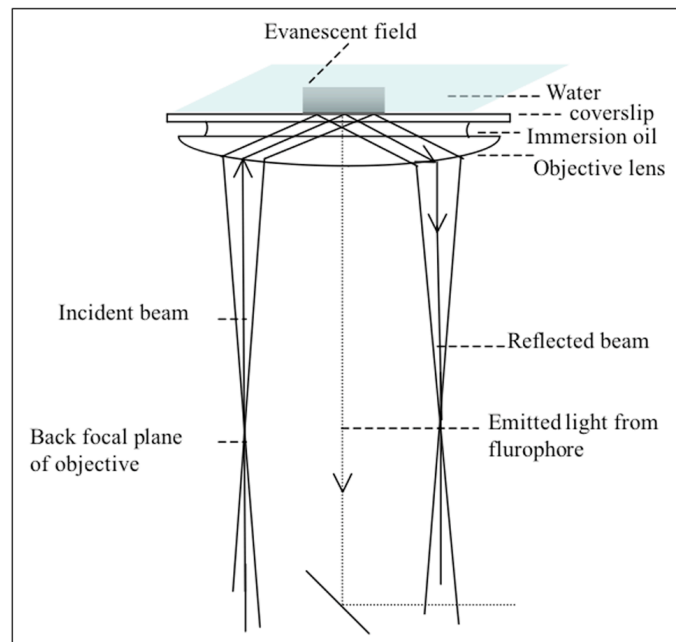


**Figure 3.2: a) Schematic drawing of the TIRF microscope.** Two lasers with wavelength of 532 nm (Nd/YAG) and 488 nm (Ar laser) were used to excite 2 different fluorophores. BS = beam splitting cube; AOM = acousto-optic modulators; M = mirrors; L1, L2 & L3 = convex lenses; TL = tubus lens; D = diaphragm;  $P_{in}$  &  $P_{ref}$  = prisms for incident and reflected beams respectively; S & S' = beam stops; NF = notch filters and BF = band pass filters.

**b) Objective of TIRF system in inverted configuration with incoming and totally reflected beam, as well as evanescent field formation by total internal reflection at the glass-water interface**

### 3.4 *In vitro* motility assay on BSA coated surface

The *in vitro* motility assay was modified from the assay described by Kron S.J. (1991). The flow cell was built using cleaned coverslips by placing double sided sticky tape between 2 coverslips. Glass coverslips were cleaned with 0.2% Helmenex, washed thoroughly with distilled water in a sonicator, and dried in a oven at 55°C overnight. Flow cell volume was 5 - 7  $\mu$ l. Proteins were added to the flow chamber in the following sequence:

- i) The glass surface of the flow cell was coated with BSA by filling the flow cell with AB buffer containing 0.5 mg/ml BSA. ii) After 5 min of incubation with the BSA containing AB buffer, 5  $\mu$ l of the myosin extraction solution was infused. Adsorption of myosin to the BSA-coated glass surface was allowed for 30 sec and stopped by



infusion of 10  $\mu$ l (two cell volumes) of AB buffer; iii) 5  $\mu$ l of solution with non fluorescently labelled F-actin was introduced to block denatured myosin. This was followed by incubation with AB buffer containing 2 mM MgATP to allow dissociation of the unlabelled actin from native myosin heads. iv) Wash with 10  $\mu$ l AB buffer (two cell volumes) to remove MgATP. v) 0.5  $\mu$ l of a solution containing 0.25  $\mu$ M TRITC-phalloidin labelled F-actin was introduced into the flow cell. This was immediately followed by application of 20  $\mu$ l (4 cell volumes) of AB buffer to remove free TRITC-phalloidin. vi) Translocation of the actin filaments was initiated by application of AB buffer containing various concentrations of MgATP and 0.5 mg/ml BSA (ionic strength 55 mM).  $P_i$  and  $AlF_4^-$  were added to the AB buffer according to the requirement.

The flow cell was then placed on the TIRF microscope. Images were acquired at a rate of 10 frames per second (time resolution 100 ms). Gliding velocity was calculated over 50 - 300 frames using Mathematica software.

### 3.4.1 *in vitro* motility assay on protein G coated surface

The actin filament gliding velocity was performed on the protein G and Antibody coated surface to check whether the single headed Dictyostelium myosin II molecules were in the proper orientation to support the motility.

The glass surface of the flow cell was coated with protein G (2 mg/ml). After 1 hr of incubation at room temperature, 10  $\mu$ l of fluorescently labeled Penta anti-His Antibody (1:5 dilution in AB) was infused and binding of the antibody to protein G was allowed for 1 hr at 4°C and stopped by infusion of 10  $\mu$ l (two cell volumes) of AB buffer. 10  $\mu$ l AB solution with 1mg/ml of the single headed Dictyostelium myosin II construct was infused and incubated for 1 hr at 4°C. This was followed by washing with 10  $\mu$ l AB buffer (two cell volumes) to remove unbound myosin. 10  $\mu$ l of unlabelled F-actin were added to block denatured myosin construct molecules followed by washing with AB.BSA containing 2 mM MgATP. 5  $\mu$ l of a solution containing 0.25  $\mu$ M TRITC-phalloidin labelled F-actin was introduced into the flow cell. This was immediately followed by application of 20  $\mu$ l of AB buffer to remove free TRITC-phalloidin. Actin filament motility was initiated by application of AB buffer containing 2 mM MgATP and 0.5 mg/ml BSA (ionic strength 55 mM). Images

were acquired with a time resolution of 160 ms. Actin filament-gliding velocity was calculated using Mathematica software

### **3.5 Dwell time Assay**

Cy3-EDA-ATP, a fluorescent ATP analog in which the ribose is labeled at 2' or 3' position, is a good substrate for myosin as determined by the ATPase activity and actin motility (Conibear et al., 1996; Eccleston et al., 1996; Tokunaga et al., 1997; Owia et al., 2000).

The glass coverslips cleaned with 30% nitric acid and ethanol were used for these assays. Cleaning with 30 % nitric acid and ethanol was done to remove the particles attached to the surface of the coverslip that otherwise would appear as spots of nonspecific fluorescence in the single molecule assays.

The surface of a flow cell was coated with AB buffer containing BSA (0.5 mg/ml) for 5 min. Myosin extraction buffer or myosin decorated actin filaments were injected in the chamber. After 1 min, excess or unbound protein was washed out with AB buffer. Finally, 5 nM Cy3-EDA-ATP in AB buffer, including the oxygen scavenging system, was added. Fluorescent signals of Cy3-EDA-ATP (or Cy3-EDA-ADP) were observed as discrete spots in the TIRF microscope when Cy3-EDA-ATP or Cy3-EDA-ADP bound to myosin. Cy3-nucleotides were excited at 532 nm. Final concentrations of myosin and actin in the flow cell were 100 pM and 2 nM respectively. Individual, immobilized fluorescently labelled actin filaments were located using the Ar laser at 488 nm. By switching to the green laser, binding of individual Cy3-EDA-ATP molecules to myosin could be observed. Dwell times were recorded for myosin alone or for myosin bound to actin filaments (decorated actin filaments). All the experiments were carried out at room temp. (22 - 25°C).

### **3.6 Individual molecule dwell time measurements**

#### **3.6.1 On BSA coated surface**

The flow cell was coated with 0.5 mg/ml BSA in AB buffer, incubated for 4 min and then washed with 2 cell volumes AB buffer. 10  $\mu$ l solution of 30 pM skeletal psoas muscle myosin II in myosin extraction buffer or 100 pM Dictyostelium myosin II in AB buffer was added (Note that dilution of myosin in AB buffer was made right before addition to the flow cell). Incubation was allowed for 1 min and washed with AB buffer. 30 nM 3'Cy3-EDA-ATP was added to flow cell and events were recorded over 20,000 frames with the time resolution of 100 ms.

#### **3.6.2 On protein G coated surface**

A protein G coated surface was generated by infusing 10  $\mu$ l Protein G (Pierce) 2 mg/ml in a flow chamber. The binding of protein G to the surface was allowed for 1 hr at room temperature in humidified condition. It was flushed with 2 chamber volumes AB buffer. Alexa488 labeled Penta Anti-His tag antibody (Mouse IgG1, Qiagen) with a starting concentration of 200  $\mu$ g/ml was infused at a dilution of 1:20,000 and incubated for 1 hr at 4°C for binding to the protein G. It was washed with 3 chamber volumes AB buffer. Then a mixture of 1 nM 6-His peptide (Covance Research product) and 100 pM Dictyostelium myosin was added, and incubated at 4°C for 1 hr. This was done to ensure that at most one antigen binding site of the antibody was blocked by the His peptide, such that formation of duplexes by binding of 2 molecules of the single headed myosin construct to the 2 antigen binding sites of antibody was prevented. The cell was washed with 3 cell volumes of the AB buffer to remove unbound protein. 30 nM 3' Cy3-EDA-ATP was infused in the flow cell. The flow cell was then placed on the TIRF microscope and the fluorescent signal appearance observed in real time. The position of myosin molecules was located by exciting the Alexa 488 labelled Anti-his tag antibody. Then excitation was switched to the green laser to acquire fluorescent signals of 3' Cy3-EDA-ATP upon binding to the myosin construct, which had been located in the first step. Images were acquired

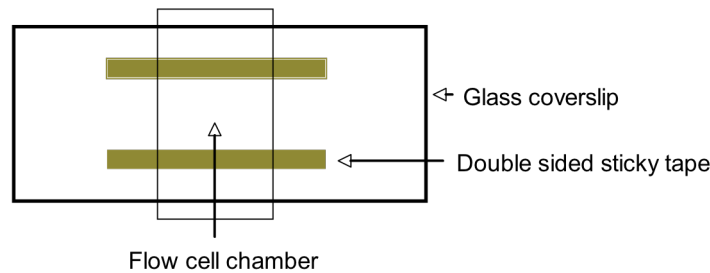
with a time resolution of 100 ms with an Andor iXon CCD camera (Andor technologies, UK)

This arrangement of protein G and antibody-coated surface was done to avoid the artifacts from the orientation of the myosin molecule on the surface. Data analysis was done with Mathematica software.

### 3.7 Construction of flow chambers for motility and dwell time assays

Glass coverslips (24 x 32 mm and 10 x 20 mm) were used to construct a flow chamber for motility assays. Cleaned glass coverslips (Helmenex cleaned for motility and Nitric acid, KOH, and ethanol cleaned for dwell time assays) were used. A 10 x 20 glass coverslip was attached on a 24 x 32 coverslip by two strips of double-sided sticky tape as shown in figure 3.3. The two strips were separated by approximately 5-10 mm, depending on the required chamber volume. The internal chamber volume was approximately 10  $\mu$ l for dwell time assays and 5-7  $\mu$ l for motility assays.

Nitrocellulose coated coverslips were prepared by spreading 0.1% nitrocellulose solution on the glass surface, to be used in motility assays for attaching *Dictyostelium* myosin II to the surface.



#### 3.3: Flow chamber constructed for motility and dwell time assays.

## 3.8 Data Analysis

### 3.8.1 Actin filament motility analysis software

A software routine was developed with Mathematica (Wolfram Research, Inc., USA), in our laboratory by Dr. Massimo Antognozzi, for the analysis of actin filament gliding velocities in *in vitro* motility assays. The basic principle of the software is as follows:

Motility data was recorded using a digital video camera in combination with the TIRF microscope. The video recording produced a series of frames where bright fluorescent filaments slide on a darker background. The purpose of the software was to detect, for each frame, the position of the two ends of the filament and calculate their velocity. If a filament slides smoothly on the surface, then the front end of the filament will progressively occupy new areas, the rear end of the filament will move away from some areas and the part of the filament in between will appear still. The areas of variation (AV) at the leading and trailing edge of the filament can be used to locate the two ends of the filament.

The first step in the automated routine was to threshold the frame sequence and to convert the grey scale produced by the digital camera in a black and white scale. In this way the background noise was eliminated and the contour of the filaments is clearly defined. The value of the each pixel occupied by the filament was set to '1' and the value of background pixels was set to '0'. As a next step, a rolling average was applied to the frame sequence to generate a smoother sequence. In this way any fluctuation in the shape and position of the filament was reduced. Next, for each frame  $F_i$  a new frame  $F_i'$  was generated that represented the changes in filament position using the following formula:

$$F_i' = F_{i+\Delta i} - F_i; \quad (1)$$

The new frame highlighted the AV of the filament. More specifically, pixels with positive values (+1), pixels with negative values (-1) and background pixels (0) correspond to areas where the front end of the filament moves in, areas left by the rear end and background areas, respectively. In equation (1)  $\Delta i$  is an important parameter because it determines the size of the AV locating the two ends of the filament (Figure

3.4). Due to the fluctuations in the speed of filament sliding,  $\Delta i$  has to be adjusted from frame to frame in order to maintain these areas constant for the all frame  $F_i$ ' of an analysed sequence. Finally, the centroid of the AV is calculated to locate the positions of the two ends of the filament.

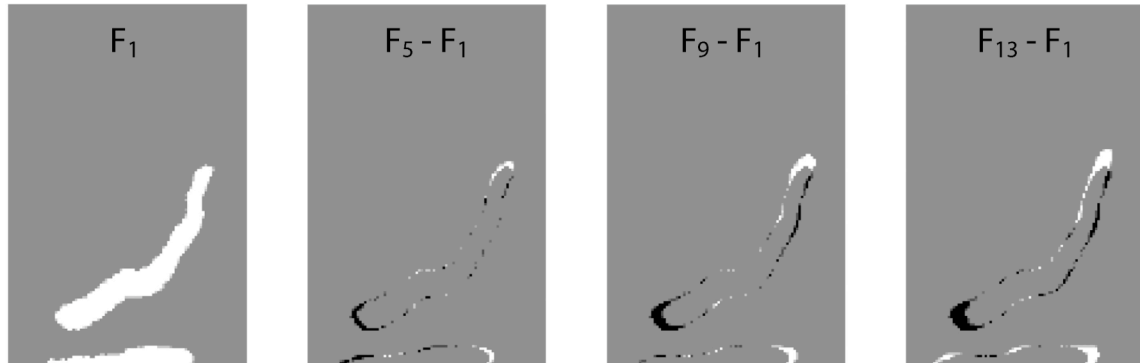


**Figure 3.4:** Effect of the interval  $\Delta i$  on the areas of variation located at the two ends of the filament.

### 3.8.2 Dwell time analysis

A second software routine was created with Mathematica by Dr. Massimo Antognozzi in our laboratory for the analysis of Cy3-EDA-ATP dwell times (fluorescence lifetime) recordings. During the experimental procedure, the binding and dissociation of fluorescently labeled ATP or ADP molecules was recorded on a digital camera and saved in a sequence of frames. At any time, the recorded field of view shows several simultaneous but asynchronous events, starting and ending at definite points in time. The aim of the software is to track each individual event. The basic principle of the software is as follows:

The first step was to search through the entire sequence of frames for the event that appear during the recording period. In the second step, the position of the individual events was identified and defined as an area of interest. Subsequently, the integrated intensity of each area of interest was calculated, frame by frame, for the entire frame sequence and plotted as a time series. These time series were finally analysed to measure the duration of fluorescent spot, i.e., the dwell time, from the one step increase of intensity above threshold until the one step drop in intensity back to the background level, a pre-selected threshold intensity. This dwell time was interpreted as the time spent by a Cy3-EDA-ATP or Cy3-EDA-ADP molecule bound to an immobilized myosin molecule.

## 4 Results

### 4.1 *in vitro* motility assay

The myosin molecules extracted from single psoas muscle fibers in myosin extraction buffer were immobilized on the BSA coated surface. The fluorescently labelled actin filaments were added to the flow cell. With the introduction of 2 mM MgATP the movement of Rh-phalloidin labelled actin filaments was observed under the TIRF microscope. Figure 4.1 shows images of 1 actin filament moving downwards in the field of view.

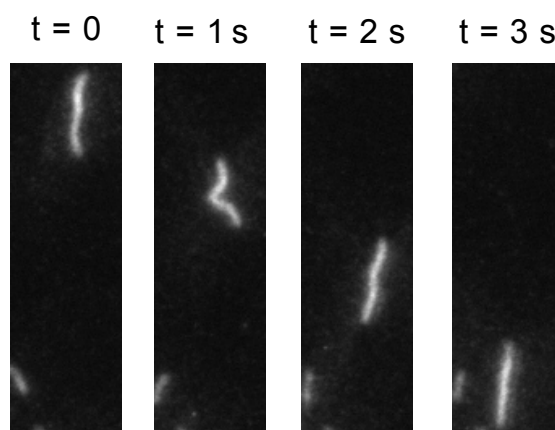


**Figure 4.1 Actin filament gliding over a myosin coated surface in the presence of MgATP.**

The pictures were taken consecutively after every second. Concentration of MgATP = 2 mM; T = 22° C, and ionic strength = 55 mM.

#### 4.1.1 Effect of inorganic phosphate on actin filament gliding velocity

To study possible effects of inorganic phosphate, the gliding velocity of actin filaments on a myosin-coated surface was measured in the presence (5 mM) and absence of phosphate at different MgATP concentrations ranging from 30  $\mu$ M to 5 mM.

Figure 4.2 a & b shows that actin filament gliding velocity increased with increasing MgATP concentration, approaching a plateau around 2 mM MgATP. In the presence

of 5 mM inorganic phosphate the gliding velocity was reduced at low MgATP concentration but became independent of  $P_i$  at MgATP concentrations  $> 0.5 - 1$  mM.

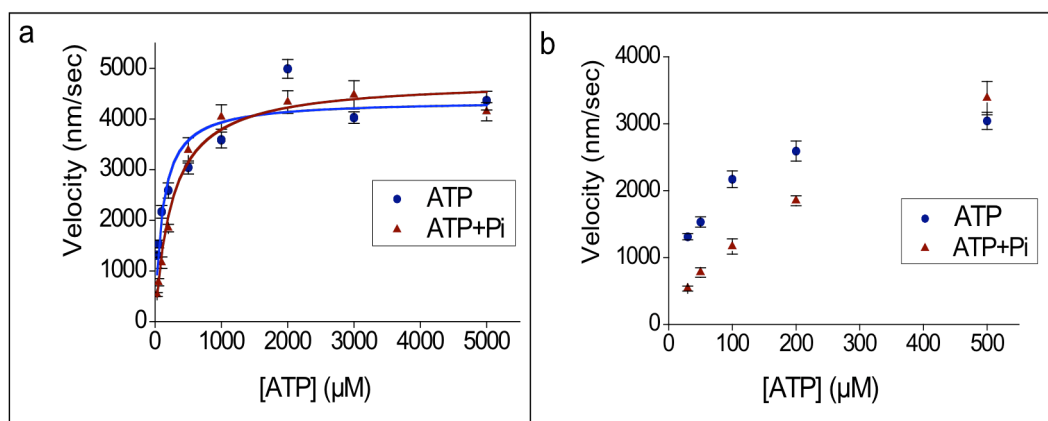


**Figure 4.2: a) Actin gliding velocity** at various MgATP concentrations in the absence (Filled circles) and presence of 5 mM phosphate (Filled triangles), at 22°C and 55 mM ionic strength. Data points are means  $\pm$  SEM. Each data point is an average of 30-40 filaments. MgATP concentration was varied between 30  $\mu$ M and 5 mM. Solid lines are least-squares fit to the hyperbolic function yielding a gliding velocity at infinite MgATP concentration of  $4.3 \pm 0.2$   $\mu$ m/sec and  $4.7 \pm 0.2$   $\mu$ m/sec in the absence and presence of phosphate, respectively. Half maximal gliding velocity is obtained at  $110 \pm 24$   $\mu$ M (0 mM  $P_i$ ) and  $256 \pm 58$   $\mu$ M (5 mM  $P_i$ ).

**b)** The same data is expanded to better illustrate the effect of inorganic phosphate at low MgATP concentrations. The reduction in the gliding velocity was significant ( $P < 0.001$ ) at 30  $\mu$ M, 50  $\mu$ M, 100  $\mu$ M and 200  $\mu$ M MgATP.

Each point in the figure represents the mean  $\pm$  SEM for 30-40 filaments from at least 3 individual motility assays. To estimate gliding velocity expected for infinite [MgATP], data were fitted by a hyperbolic function. The actin filament gliding velocity extrapolated to infinite [MgATP] was slightly increased in the presence of inorganic phosphate from  $4.3 \pm 0.2$   $\mu$ m/sec to  $4.7 \pm 0.2$   $\mu$ m/sec.

This increase in extrapolated gliding velocity in the presence of  $P_i$  is statistically not significant as previously reported for maximum shortening velocity in fibers (Pate & Cooke, 1985). At 30  $\mu$ M ATP, however, gliding velocity in the presence of 5 mM  $P_i$ , decreased by approximately 60% (Fig. 4.2b). Gliding velocity in the presence of  $P_i$  decreased by 50%, 45% and 28% at 50  $\mu$ M, 100  $\mu$ M and 200  $\mu$ M MgATP respectively. This difference becomes insignificant when MgATP concentration was raised to the range within 0.5 mM - 5 mM.



Thus, at low substrate concentrations, the effect of phosphate on gliding velocity was quite prominent. This effect was reversible and gradually diminished with increase in the MgATP concentration.

#### **4.1.2 Fragmentation of actin filaments in the presence of $P_i$ at low ATP concentration**

Fragmentation of the actin filaments was observed at low MgATP concentration in the presence of  $P_i$ . This effect was not so prominent in the absence of  $P_i$  at low MgATP concentration. The fragmentation of the actin filaments was not observed in the presence of  $P_i$  at higher MgATP concentrations. In figure 4.3 upper panel shows the fluorescently labelled images of actin filaments acquired at the beginning and at the end of the recordings for 25 sec, in the absence of  $P_i$ . At 30  $\mu$ M MgATP concentration after 25 sec the length of the filaments did not change. Lower panel shows the images acquired at 30  $\mu$ M ATP concentration in the presence of  $P_i$ . In the presence of  $P_i$  at 30  $\mu$ M MgATP concentrations after 25 sec, however, there was marked increase in the number of filaments with shorter lengths. In figure 4.3 a, b and c, the number of actin filaments and their lengths are plotted. Fig. 4.3a shows the length distribution of actin filaments at 30  $\mu$ M [MgATP] before and after 25sec. The length distribution did not change, but there was slight increase in the number of filaments. In figure 4.3b, at 30  $\mu$ M MgATP and 5 mM  $P_i$ , large difference in the number of filaments and length distribution after 25sec was prominent. Figure 4.3c illustrates the length distribution at 2 mM MgATP and 5 mM  $P_i$ . In this case also the length distribution did not change markedly, but there is small increase in the number of filaments. It should be noted that, at any given recording time, there is in-flow and out-flow of the actin filaments in the field of view. At 30  $\mu$ M MgATP the filaments were faster than in the presence of  $P_i$  (Fig 4.2). Assuming that the exchange of actin filaments is more in the absence of  $P_i$ , the small increase in the number of actin filaments at 30  $\mu$ M ATP could be explained as in-flow of the filaments. At 2 mM MgATP concentration, presence of 5 mM  $P_i$  did not affect the velocity. So, the increase in filament number would be due to the imbalanced in-flow and out-flow of the filament. The reason why we believe that the increase in number of filaments and evident change in the length distribution was due to  $P_i$  at low [MgATP], because there was minimal exchange of filaments in and from the field of view, in the presence of  $P_i$

at low [MgATP] due to very low velocity. Moreover, the longer recordings (upto 60 sec) showed very small actin filaments in this case.

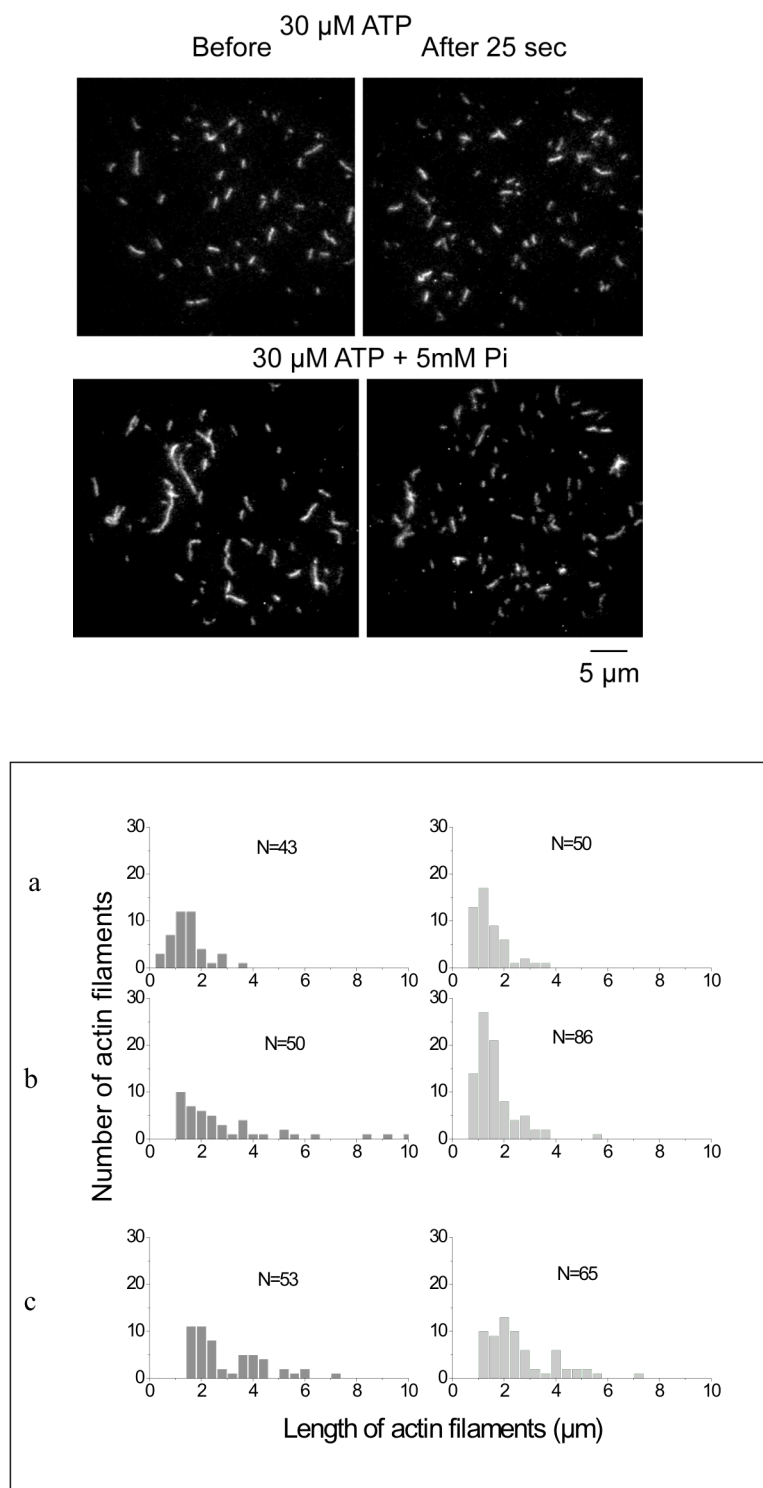


**Figure 4.3: Fragmentation of filaments.** Top panel shows fragmentation of actin filaments in the presence of  $P_i$  (5 mM) at low [MgATP]. The frames were selected from the recording immediately after the addition of 30  $\mu$ M MgATP with and without 5 mM  $P_i$  and 25 sec later.

**Bottom Panel a.** Number of filaments is plotted against the length of filaments in the presence of 30  $\mu\text{M}$  MgATP before and after 25sec of recording. N = Total number of actin filaments.

**b.** In the presence of 30  $\mu\text{M}$  MgATP and 5 mM  $\text{P}_i$

**c.** In the presence of 2 mM MgATP and 5 mM  $\text{P}_i$ .

#### 4.1.3 Effect of the phosphate analog $\text{AlF}_4^-$ on gliding velocity

$\text{AlF}_4^-$ , a structural analog of  $\text{P}_i$ , is known to bind at the active site of myosin at M.ADP state forming M-ADP- $\text{AlF}_4^-$  stable complex (Maruta et al., 1993). This state was considered to be similar to the ATP hydrolysis transition state AM.ADP. $\text{P}_i$  (Post-hydrolysis step) as described from X-ray crystallographic studies (Fisher et al., 1995). It is also known to affect the steady state isometric tension in activated muscle fibers (Chase et al., 1993; Wilson et al., 1995), similar to the effect of  $\text{P}_i$ . Therefore, effect of  $\text{AlF}_4^-$  on gliding velocity was studied to test whether it has similar effect as inorganic phosphate.

Again gliding velocity was measured at various concentration of ATP from 30  $\mu\text{M}$  to 5 mM in the presence of 5 mM  $\text{AlF}_4^-$ . Figure 4.4a shows that  $\text{AlF}_4^-$  has similar effect on gliding velocity as  $\text{P}_i$ . An inhibitory effect was observed at only low MgATP concentration. Maximum observed gliding velocity was  $5.37 \pm 0.336 \mu\text{m}/\text{sec}$  and  $4.3 \pm 0.2 \mu\text{m}/\text{sec}$  in the presence and absence of  $\text{AlF}_4^-$  respectively. In Figure 4.4b, the part at low ATP concentration of Figure 4.4a is expanded to show the inhibitory effect more clearly. The gliding velocities were decreased in the presence of  $\text{AlF}_4^-$  (5 mM) by 32 %, 29 % and 8 % at 30  $\mu\text{M}$ , 50  $\mu\text{M}$  and 100  $\mu\text{M}$  MgATP, respectively. With further increase in MgATP concentration the effect was reversed. Thus although  $\text{AlF}_4^-$  showed a qualitatively similar inhibitory effect it was a weaker inhibitor compare to  $\text{P}_i$ . Since  $\text{AlF}_4^-$  tends to precipitate quickly at higher concentrations,  $\text{AlF}_4^-$  above the concentration of 5 mM could not be used.

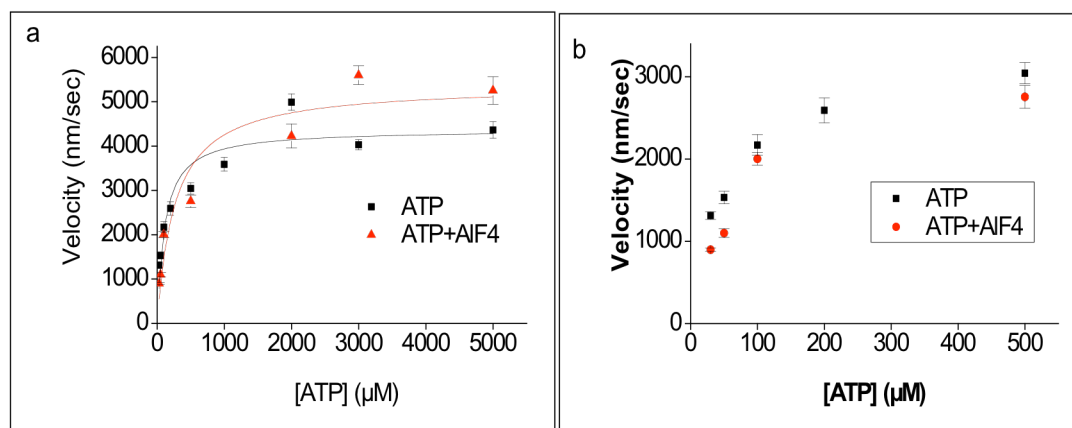


**Figure 4.4: Effect of  $\text{AlF}_4^-$  on actin filament gliding velocity;** a) Black squares represent the gliding velocity measured over a range of 30  $\mu\text{M}$  to 5 mM MgATP concentration whereas, red triangles represent gliding velocity measured in the presence of MgATP and 5 mM  $\text{AlF}_4^-$ . Data was fitted to hyperbolic function. The maximum velocity increased to  $5.3 \pm 336 \mu\text{m}/\text{sec}$  and the ATP concentration at half maximum velocity increased to  $265 \pm 78 \mu\text{M}$  in the presence of 5 mM  $\text{AlF}_4^-$ . b) Expanded scale to compare the  $\text{AlF}_4^-$  affected velocities at low [MgATP]. The error bars are SEM. Measurements were done at ionic strength 55 mM and room temperature (22-25°C).

## 4.2 Single molecule detection measurement

The inhibitory effects of  $\text{P}_i$  and  $\text{AlF}_4^-$  on the gliding velocity were unexpected. To identify the intermediate states to which  $\text{P}_i$  or  $\text{AlF}_4^-$  can bind, single molecule detection technique was used by using fluorescently labeled nucleotides (Cy3-EDA-ATP or Cy3-EDA-ADP). After infusion of fluorescently labeled ATP (Cy3-EDA-ATP) into a flow cell with immobilized myosin, discrete fluorescent spots appear and disappear randomly within the field of view.

We assumed that if  $\text{P}_i$  binds to AM.ADP state and that shifts the equilibrium backwards to weak binding states, we should expect longer lifetime events, whereas if it binds at the end of ‘powerstroke’ (AM state), it should not affect the dwell time but the frequency of the event appearance should decrease. We therefore i) determine the dwell time of these fluorescently labeled nucleotides and ii) the density of fluorescent signals in the field of view both in the absence and presence of  $\text{P}_i$  or  $\text{AlF}_4^-$ .

### 4.2.1 Dwell time of Cy3-EDA-ATP

Appearance of discrete spots was interpreted as binding of Cy3-EDA-ATP to the myosin molecule. After the cleavage of ATP,  $P_i$  leaves the active site first followed by Cy3-EDA-ADP. Thus the fluorescent spots are expected to disappear with the release of Cy3-EDA-ADP. The time during which the fluorescent spot is visible is termed 'dwell time' and is assumed to correspond with the period for which the fluorescently labeled nucleotide remains bound to myosin as Cy3-EDA-ATP or Cy3-EDA-ADP.

For the dwell time measurements data was recorded with 100 milliseconds time resolution for approximately 3-4 minutes. The observation period was limited to 3-4 min to avoid increase in the Cy3-EDA-ADP concentration due to splitting of Cy3-EDA-ATP by the immobilized myosin. Otherwise more and more dwell time signals had been caused by binding or dissociation of Cy3-EDA-ADP. Free Cy3 labelled nucleotides cannot be detected as discrete spots due to their rapid thermal motion. Unbound Cy3 labelled nucleotide will therefore contribute to background which increases in proportion to the Cy3-EDA-ATP concentration. To ensure sufficiently bright spots above the background fluorescence from free Cy3-EDA-ATP, the concentration of Cy3-EDA-ATP was limited to 5 nM.

To maximize the likelihood that events were collected only from Cy3-EDA-ATP bound to myosin molecules, i) we used myosin decorated actin filaments and, ii) analyzed only those fluorescent spots, which colocalised with the actin filaments (Figure 4.5). The positions of the Alexa 488 labelled actin filaments were marked when excited by the Ar laser. To minimize superimposition of fluorescent signals from myosin molecules too close to each other to be resolved as individual locations, firstly a low concentration of myosin was used, so that fluorescent signals were sparsely distributed within the field of view. Secondly, if the intensity arising from a single molecule is defined, intensity profile of the individual fluorescent spots gives an idea whether the signal has appeared from the single molecule or multiple. Figure 4.6 A & B shows the time course of fluorescent signals with one step increase in the intensity, presumably upon binding of Cy3 nucleotide to the myosin until the fluorescent signal decays in one single step most likely upon dissociation of Cy3-EDA-ADP. The intensity profile is expected to show 2 step or multiple step intensity rise or decay if intensities from Cy3-EDA-ATP binding to myosin molecules superimposed due to close proximity of individual myosin molecules.

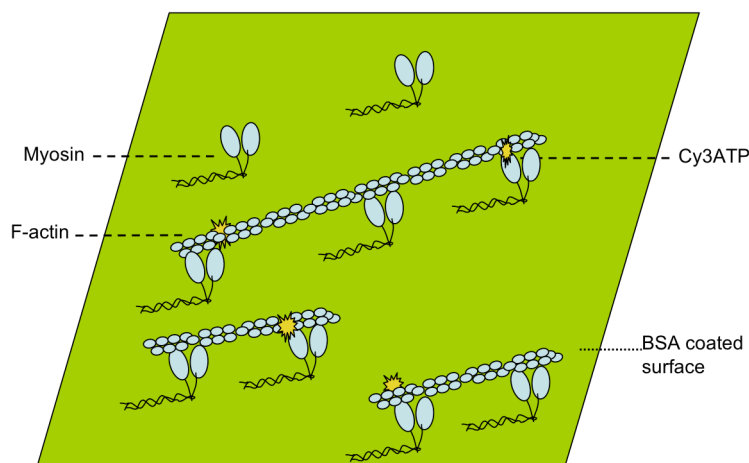
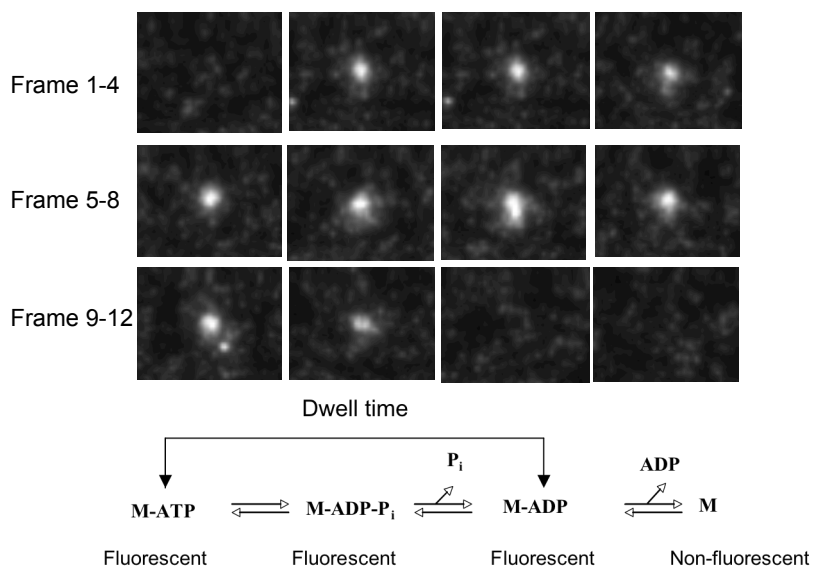


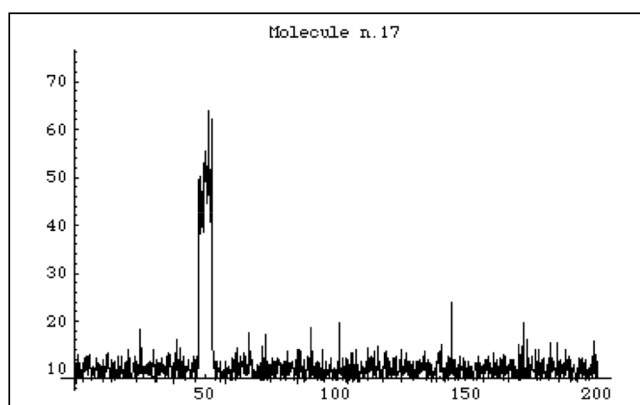
**Figure 4.5: Schematic drawing for colocalisation** of myosin decorated actin filaments (Alexa-488 phalloidin labeled), and signals of Cy3-EDA-ATP bound to myosin molecules attached to actin filaments. Myosin molecules were immobilized on BSA coated surface.

**A**



**Scheme 4.1**

**Figure 4.6: A) Fluorescent lifetime of event.** Frames 1 to 12 illustrate the images where, in frame 2 fluorescent signal appeared and disappeared in frame 11. The dwell time was measured from the appearance of signal until the disappearance. Dwell time is also illustrated in scheme 4.1. Each frame was separated by 100 ms from one another.



**B) Intensity time course of a fluorescent spot.** Binding of Cy3-EDA-ATP to the myosin molecule was observed as one step increase in the fluorescence intensity, and the disappearance of a signal in a single step as dissociation of nucleotide. The time between appearance- disappearance of fluorescent spot was measured as dwell time.

Myosin decorated actin filaments were immobilized on the BSA coated surface in the flow chamber and 5 nM Cy3-EDA-ATP was infused. Fluorescent signals were recorded over 2000 frames (200 sec) and the time trace was analysed by the software described in the method section. The dwell time was obtained by this protocol revealed a wide distribution. To characterize the distribution of the observed dwell time, dwell time histogram was plotted. This distribution was also described by plotting total number of events and events left after certain dwell time (0.2 s bin in this case). The advantage of these plots is that they overcome the problems associated with changing the bin size in histograms.

Figure 4.7a shows the dwell time histogram, i.e., the distribution of events vs dwell time in the presence of Cy3-EDA-ATP. Data could not be fitted well to the single exponential function. Note that the systematic deviation from the single exponential was observed. Same data is plotted as the integrated number of events vs time (Figure 4.7b semilog plot) fitted to triple exponential function. This plot gave a clearer idea regarding different populations having different lifetimes ( $\tau_1$ - $\tau_3$ ).

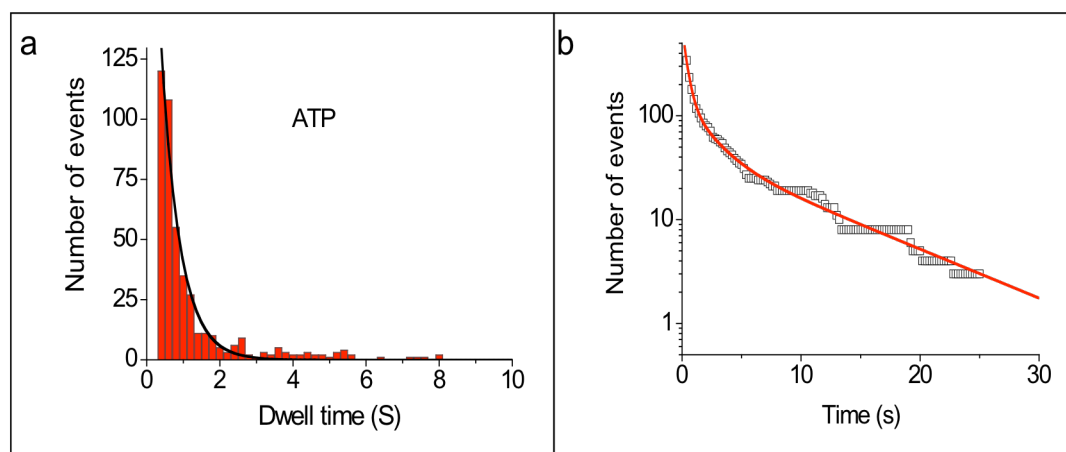


**Figure 4.7: Dwell times in the presence of 5 nM Cy3-EDA-ATP from actomyosin complexes.**

**a)** Histogram of number of observed events vs dwell time, 0.2 seconds binning. Solid line is exponential fit fitted to exponential function,  $N = N_1 * e^{-(t)/\tau_1}$ .  $N$  = Total number of events,  $N_1$  = Number of events with dwell time < 0.2 sec resulting from fitting of single exponential fits,  $t$  = Time (s),  $\tau_1$  = Time constant.

**b)** Number of events on logarithmic scale vs time, with 0.2 sec binning. Solid line is triple exponential function fitted to data points. Time constants of the three exponential terms were 0.39 s, 1.95 s and small population with time constant of 9.19 s respectively. Amplitudes of the three terms were 78 %, 15 %, and 6 % respectively for 3 populations. Data was collected from 9 different sets of experiments at ionic strength 55 mM and room temperature (22-25°C).

#### 4.2.2 Effect of inorganic phosphate on dwell time of Cy3-EDA-ATP

From the interpretation of previous work, it is expected that in the presence of  $P_i$  the dwell time should increase. We therefore assessed the effect of inorganic phosphate on the average lifetime of the event, by adding mixture of 5 nM Cy3-EDA-ATP and 5 mM  $P_i$  in AB.BSA buffer to chambers containing sparsely myosin decorated actin filaments immobilized on the BSA coated surface. These conditions were chosen to clearly separate the lifetime of the events affected by  $P_i$  addition. 5 mM of  $P_i$  were selected, to make the probability of  $P_i$  binding to the AM.ADP complex comparable to the probability of ADP release.



Figure 4.8 a shows the dwell time data plotted as a dwell time histogram. The histogram again was not well fit by a single exponential function (solid line) as seen for Cy3-EDA-ATP alone (Fig 4.7) implying different populations of dwell times. However, the time constant of the best-fit single exponential was similar to the one seen with Cy3-EDA-ATP alone (Fig 4.7). Figure 4.8 b again shows the total number of events and its decay over time in a semi logarithmic plot. This plot again implies the presence of different dwell time populations. The solid line is a fit of a triple exponential function, the minimum required for fitting without systematic deviation of data points from the solid line. Data plotted here is from an individual experiment. However 8 sets of experiments under the same condition also showed no detectable effect of  $P_i$  on the dwell time distribution compared to the data in the presence of Cy3-EDA-ATP alone.

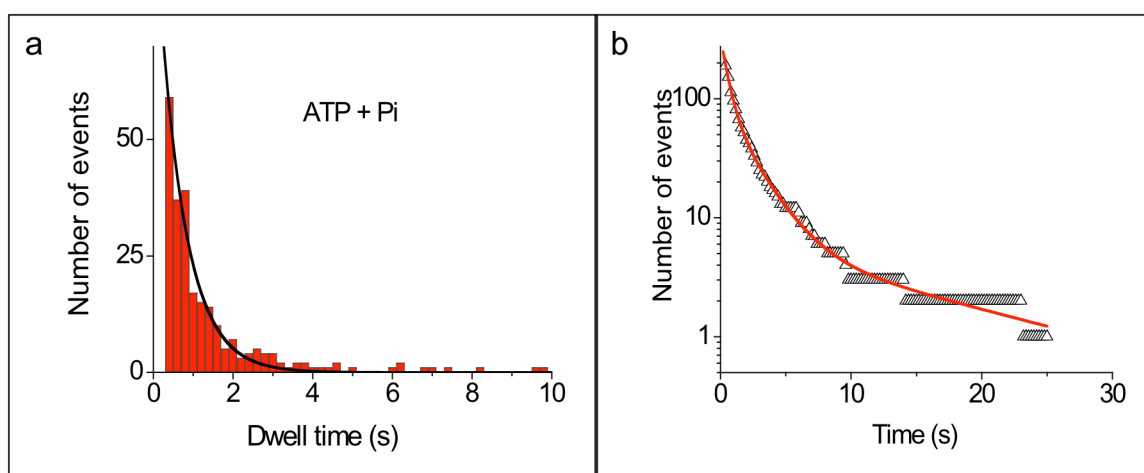


**Figure 4.8: Effect of  $P_i$  on dwell times.** **a)** Plot of the number of events vs dwell time, 0.2 seconds binning, and solid line is a single exponential fit. **b)** Total number of events (logarithmic scale) Vs time, 0.2 sec binning. Solid line is fit to a triple exponential function with time constants 0.52 s, 2.06 s and 15.34 s. The amplitudes of 3 populations were 71 %, 26 %, and 1.8 % respectively. Plots presented here are from an individual experiment. Similar data was collected for 8 different set of experiments at ionic strength = 55 mM and  $T= 22^\circ\text{C}$ .

### 4.2.3 Effect of $\text{AlF}_4^-$ on dwell times

Similar to the studies on effect of  $\text{AlF}_4^-$  on gliding velocity, its effect on average dwell time was checked. As suggested from the fiber studies,  $\text{AlF}_4^-$  can trap myosin in

AM.ADP.AIF<sub>4</sub><sup>-</sup> state upon binding to an AM.ADP intermediate. This AIF<sub>4</sub><sup>-</sup> bound state was found to last for hours in muscle fibers and also in solution studies (Maruta et al., 1993, Werber et al., 1992), meaning slow dissociation of AIF<sub>4</sub><sup>-</sup> from active site of myosin. More recently, two AIF<sub>4</sub><sup>-</sup> bound AM.ADP states have been identified designated as AIF<sub>4</sub><sup>-</sup> I and AIF<sub>4</sub><sup>-</sup> II state (Kraft, et al., 2005) showed distinctive characteristics. In our studies we expect to trap AM.ADP.AIF<sub>4</sub><sup>-</sup> I state. So we expected the longer dwell times.

5 mM AIF<sub>4</sub><sup>-</sup> was applied together with 5 nM Cy3-EDA-ATP to the chamber containing immobilized myosin decorated actin filaments. Figure 4.9 a & b shows the dwell time histogram and the plot of total number of signals vs time in the presence of AIF<sub>4</sub><sup>-</sup>. It was observed that the time constant of the lifetime distribution was increased in the presence of 5 mM AIF<sub>4</sub><sup>-</sup>. This could be explained by trapping of ADP in the nucleotide-binding pocket of myosin by AIF<sub>4</sub><sup>-</sup>. But this trapping appeared to last only for shorter time than suggested by fiber studies, which implied trapping over hours.

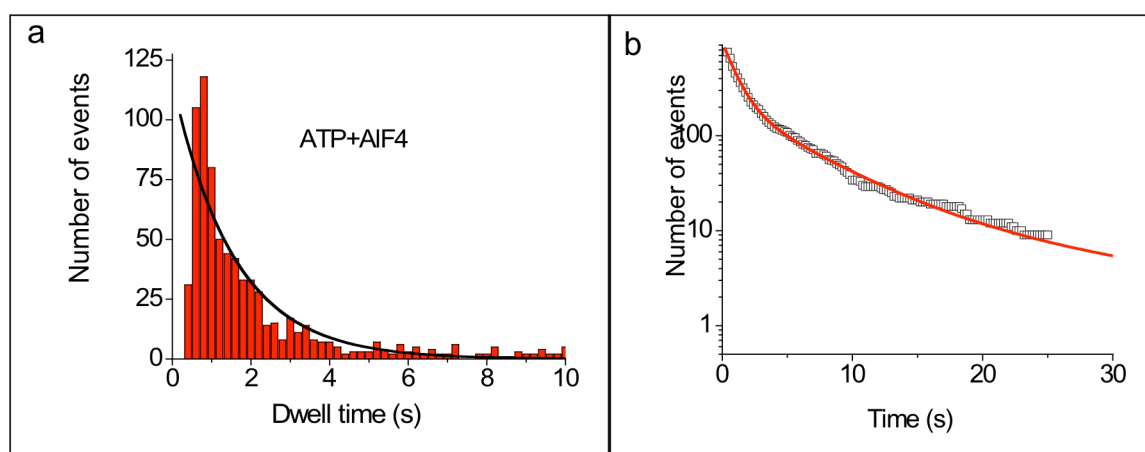


**Figure 4.9: Effect of AIF<sub>4</sub><sup>-</sup> (5 mM) on nucleotide dwell time;** Data obtained in individual experiments with decorated actin filaments (actomyosin complex) in the presence of 5 nM Cy3-EDA-ATP + 5 mM AIF<sub>4</sub><sup>-</sup>.

**a)** Dwell time histogram, 0.2 sec bins. Solid line is single exponential function fit to the dwell time histogram to determine the time constants of the dwell time distribution. Data could not be fitted well to the single exponential function (note systematic deviation).

**b)** Number of events on logarithmic scale against time in sec, 0.2 sec time bin. Solid line is triple exponential fit to the data points. Time constants were longer in the presence of AIF<sub>4</sub><sup>-</sup> compared to time constants in the presence of Cy3-EDA-ATP alone. Time constants of 1 s, 5.18 s and 22 s obtained for 3 distinct populations with amplitudes of 76 %, 21 %, and 1.7 %, respectively in the presence of 5 mM AIF<sub>4</sub><sup>-</sup>. Data were acquired for the 9 experiments that

have shown the same effect of  $\text{AlF}_4^-$  on dwell time at same ionic strength (55 mM) as in other experiments at room temperature (22-25°C).

Time constants from histograms and triple exponential fits to the dwell times in the presence and absence of  $\text{P}_i$  and  $\text{AlF}_4^-$  are listed in the table 1.

<b>Cy3-EDA-ATP (5 nM)</b>	<b>Cy3-EDA-ATP (5 nM) + <math>\text{P}_i</math> (5 mM)</b>	<b>Cy3-EDA-ATP (5 nM) + <math>\text{AlF}_4^-</math> (5 mM)</b>
$\tau = 0.81 \pm 0.214$	$\tau = 0.85 \pm 0.282$	$\tau = 1.338 \pm 0.42$
$\tau_1 = 0.53 \pm 0.02$	$\tau_1 = 0.50 \pm 0.017$	$\tau_1 = 0.88 \pm 0.07$
$\tau_2 = 2.77 \pm 1.17$	$\tau_2 = 2.26 \pm 1.38$	$\tau_2 = 4.06 \pm 1.11$

**Table 4.1. Time constants** values obtained from the histograms and from the plot where the numbers of events are summed up are listed. These values are averaged from 8-9 individual experiments with  $\pm$  SD.  $\tau$  is the time constant of the single exponential fit in dwell time histogram.  $\tau_1$  &  $\tau_2$  are obtained from the plot fitted to triple exponential function. Since the population that produced 3<sup>rd</sup> time constant was very small, it is not listed in the table. Note that the contribution (amplitude) of the 3<sup>rd</sup> population was very small (1.7- 6% of the total population, mentioned in fig legend 4.7, 4.8 and 4.9)

### 4.3 Measurement of density of events

The number of fluorescent signals in the field of view is a measure for number of myosin molecules with Cy3-EDA-ATP bound to the active site. This number depends on the dwell time of the events, concentration of Cy3-EDA-ATP and the density of myosin molecules on the surface. Concentration of Cy3-EDA-ATP and density of myosin molecules (acto-myosin complex) was kept constant in all experiments.

#### 4.3.1 Density of events events in field of view in the presence of $P_i$

Addition of 5 mM  $P_i$  with 5 nM Cy3-EDA-ATP reduced the number of fluorescent signals significantly to approximately 50% of the number than with Cy3-EDA-ATP alone. This implies that the number of myosin molecules with bound Cy3-EDA-ATP has reduced in the presence of  $P_i$  (Figure 4.10)

#### 4.3.2 Density of events in the presence of $AlF_4^-$

The number of the fluorescent signals in the presence of  $AlF_4^-$  in addition to 5 nM Cy3-EDA-ATP increased about two fold in the field of view. This implies that number of myosin molecules with bound nucleotide increased by approximately 2 folds in defined area. This is consistent with the extended lifetime seen in the dwell time assays. Top panel in Figure 4.10 shows the density of events for Cy3-EDA-ATP in the presence of  $P_i$  or  $AlF_4^-$ . The bottom panel summarizes the number of events observed from 4 different data sets. Nonspecific binding of Cy3 nucleotide to the BSA coated surface was tested in the absence of myosin. 2-3 events were detected over 10 frames sequence in the presence and absence of  $P_i$  or  $AlF_4^-$

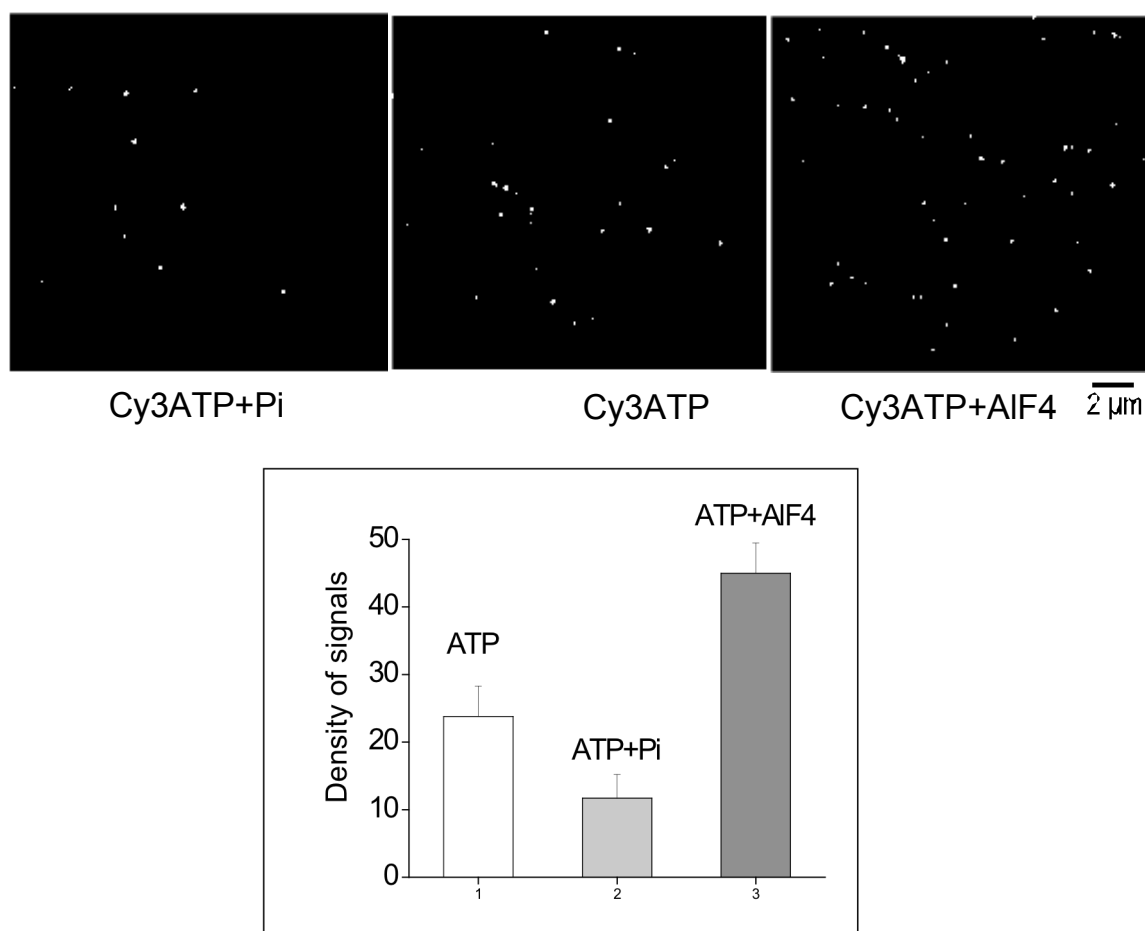


**Figure 4.10: Effect of  $P_i$  and  $AlF_4^-$  on the number of signals** observed within the field of view upon addition of Cy3-EDA-ATP to a chamber with immobilized decorated actin filaments. In upper panel, each image demonstrates the number of events seen over 10 consecutive frames in the presence of 5 nM Cy3-EDA-ATP + 5 mM  $P_i$ , 5 nM Cy3-EDA-ATP and 5 nM Cy3-EDA-ATP + 5 mM  $AlF_4^-$ . Bar diagram in lower panel summarizes data of 4 experiments. Addition of 5 mM  $P_i$  approximately halves the number of signals, while addition of 5 mM  $AlF_4^-$  approximately doubled the number of signals than in the presence of 5 nM Cy3-EDA-ATP alone. Data was collected at the same experimental conditions of ionic strength (55 mM) and temperature (22-25°C).

### 4.3.3 Control Experiments

#### 4.3.3.1 Effect of Pyrophosphate (PP<sub>i</sub>) on the density of events

Previous studies have shown that a phosphate buffer may contain contaminant pyrophosphate in low concentrations (Gyimesi et al., 2005a). MgPP<sub>i</sub> is shown to bind to the nucleotide-binding site of myosin (Yount et al., 1971). Therefore, the effect of PP<sub>i</sub> was examined on the density of fluorescent signals to test whether the observed effect of P<sub>i</sub> on the number of observed signal per field of view was genuinely from P<sub>i</sub> or due to the contaminant PP<sub>i</sub> in the phosphate buffer. 100 nM or 1 μM MgPP<sub>i</sub> concentrations were used for this test, as this was expected to be the contamination range in 5 mM phosphate buffer.

100 nM or 1 μM MgPP<sub>i</sub> together with 5 nM Cy3-EDA-ATP was applied in the flow cell containing myosin decorated actin filaments. No decrease in the density of signals was observed in the presence of 100 nM or 1 μM PP<sub>i</sub> at 5 nM Cy3-EDA-ATP. However, when mixture of 5 mM P<sub>i</sub> and 100 nM PP<sub>i</sub> added, there was still a 50 % reduction in the density of signals. Note that P<sub>i</sub> buffer used in all the experiments was additionally treated to minimize contaminant pyrophosphate concentration (mentioned in method section). Figure 4.11 shows summarized data on the density of signals. This data shows that in the presence of P<sub>i</sub> addition of PP<sub>i</sub> has no further effect. The density of myosin molecules on the BSA coated surface was kept constant for the above tested conditions.

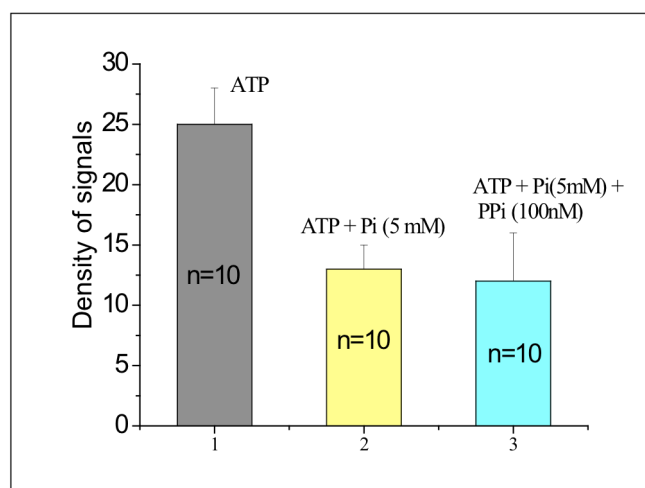


**Figure 4.11: Effect of pyrophosphate on the density of signals.** Data was collected at 22°C and 55 mM ionic strength. Number of events was obtained from 10 consecutive frame sequences at different time points over a recording period of 20 s. The error bars are  $\pm$  SD. 2-3 signals appeared as nonspecific binding of Cy3 nucleotide to myosin free surface in the presence and absence of  $PP_i$ .

#### 4.3.3.2 Nonspecific binding of fluorphores to the surface

To check the binding of Cy3 nucleotides to the BSA coated surface, we first measured the number of signals from Cy3 nucleotide on BSA coated surface in the absence of myosin and then in the presence of myosin. Approximately 10 % of the signals appeared as non-specific binding of Cy3 nucleotides to the BSA coated surface. Use of myosin decorated actin filaments, and analysis of the events those appeared directly from the actin filaments further decreased the chance of nonspecific events in our measurements. The possibility of the ATP binding and dissociating from the myosin head prior to hydrolysis was negligible because of the high binding constant of ATP to myosin active site. Also, it was less probable that the Cy3 labeled nucleotides photo bleached before dissociating, as for the settings (low intensity of the incident light to excite the fluorphores) used for the experiments, the fluorescent dye appeared to be photo-stable.

## 5 Discussion

We used a combination of the techniques to study the effect of  $P_i$  on actomyosin interaction, at the ensemble and single molecule level.

We investigated the effects of inorganic phosphate and its structural analogue  $AlF_4^-$  on actin filament gliding velocity and average dwell time on the fast skeletal muscle myosin II. We conclude that  $P_i$  competes with ATP for nucleotide-binding site at low  $[MgATP]$  and inhibits the actin filament gliding velocity. The actin filament gliding velocity remained unaffected in the presence of  $P_i$  at saturating  $[MgATP]$ , whereas the effect of  $P_i$  on gliding velocity at low  $[MgATP]$  was unexpected. Increased  $[P_i]$  did not affect the dwell time.  $AlF_4^-$  had effect on both gliding velocity and dwell time. Previous studies were interpreted that  $P_i$  binds to myosin in an AM.ADP state. We conclude that  $P_i$  may also bind to the empty nucleotide-binding pocket at low  $[ATP]$  forming an AM. $P_i$  strong binding state.

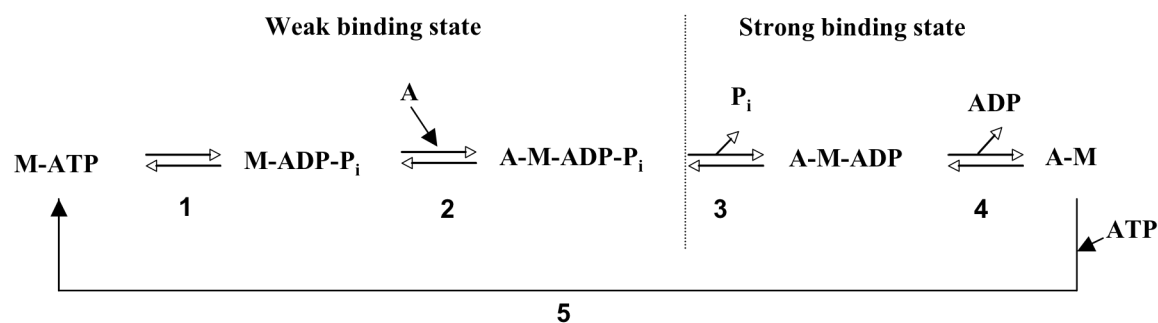
It is well established that inorganic phosphate decreases isometric tension in muscle fibers (Brandt, 1982; Cooke & pate 1985; Kawai, 1987; Tesi & Pogessi 2002) whereas the unloaded shortening velocity and MgATPase rates remain unaltered (Altringham & Johnston, 1985; Chase & Kushmerick, 1988). This was interpreted that inorganic phosphate accumulates myosin heads in a non-force generating A-M.ADP. $P_i$  state by shifting the steady state distribution of myosin heads from strong binding to weakly bound state in the cross-bridge cycle (Eisenberg, 1980; Hibberd & Trentham, 1986). The reversibility of phosphate release was also concluded from oxygen exchange experiments (Webb & Trentham 1986). Using the stable isotopes of oxygen, mass spectrometric analysis showed that an actively contracting muscle fibre could catalyse the exchange of the oxygen atoms of  $P_i$  with that of the solvent. Thus medium  $P_i$  exchange occurred only in activated, but not relaxed muscle fibers implying that the state capable of binding of  $P_i$  is an AM.ADP state.

So, as the ratio of force generating to non-force generating myosin heads goes down it affects the isometric tension that decreases on the log  $[P_i]$ . As the  $[P_i]$  decreases, the number of strong AM.ADP crossbridge increases causing increase in the isometric tension. This is due to the increased free energy available from the ATP hydrolysis, which results in a longer powerstroke length, and thus increasing fraction



of highly strained cross-bridges attached at the beginning of the powerstroke (Pate & Cooke, 1998).

A schematic representation of acto-myosin crossbridge cycle may give an insight in how the  $P_i$  and  $AlF_4^-$  might affect the series of steps in a cycle



Scheme 5.1

### Cross-bridge Model

In this model, M.ATP, M.ADP. $P_i$  are the detached crossbridge states (non force generating), AM.ADP. $P_i$  is a weakly attached non force exerting cross-bridge state, whereas AM.ADP (force generating) and AM are strongly attached states. As  $P_i$  is unlikely to affect the behaviour of detached states only weakly or strongly attached states should be affected. Increase in the forward reaction rate constants of steps 2 & 3 significantly increase isometric tension but have little or no effect on unloaded shortening velocity. Increase in the forward rate constants of steps 3, 4 or 5 increases shortening velocity. Increasing the forward rate of step 5 markedly increase the shortening velocity (Pate and Cooke 1989). Thus to affect the gliding velocity, the step 4 or 5 should be affected, which are the strongly bound force exerting steps in the cycle or there should be an intermediate step between step 3 and 4 with bound ligand that is still a strong binding state.

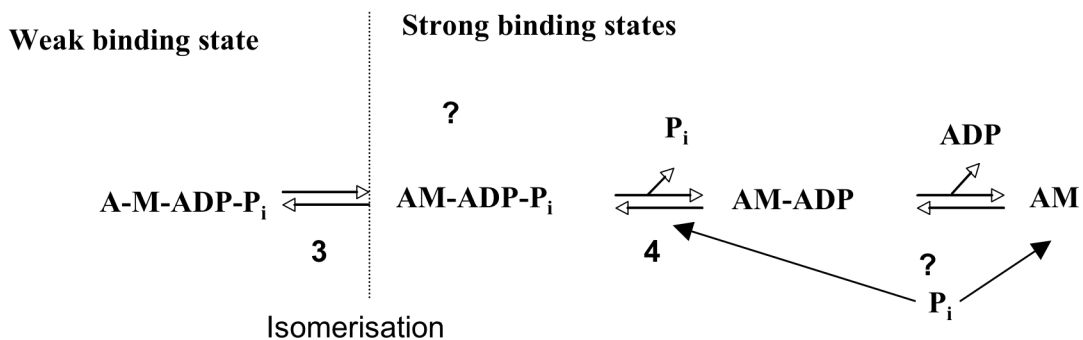
Unlike the groups, who have studied effect of  $P_i$  in muscle fibers where there are many factors that could interfere and contribute to the effect, we have studied the cross-bridge cycle for the effect of  $P_i$  and its analogue,  $AlF_4^-$  on the isolated proteins in ensemble and also at a single molecule level.

With the above proposed model for  $P_i$  binding to AM.ADP state and reversal of strong binding, force exerting state to a non-force generating state, we should expect:

a) No inhibitory effect on actin filament gliding velocity. b) The dwell time should increase in the presence of  $P_i$  and also, the number of fluorescent events should increase in proportion to increase in dwell time.

However, we observed that: a) Actin filament gliding velocity decreased at low  $[MgATP]$  in the presence of  $P_i$ , whereas with increase in  $[MgATP]$  the inhibitory effect was nullified. Additionally, fragmentation of actin filaments occurred at low  $[MgATP]$ . b) Dwell time was unaffected in the presence of  $P_i$ , however decrease in number of fluorescent signals occurred. Our observations were better fitted to the model where  $P_i$  could also bind to the empty nucleotide-binding pocket of myosin II, and compete with ATP.

With the introduction of AM.ADP. $P_i$  strong binding, force exerting state (scheme 5.2) in the above proposed model, from fiber studies. There are two possibilities by which  $P_i$  can inhibit the gliding velocity: 1) by binding to the AM.ADP state resulting in an 'AM.ADP. $P_i$ ' state with a strong binding properties and long lifetime. 2) By binding to the 'AM' state at the end of 'powerstroke', resulting in an 'AM. $P_i$ ' state, probably with strong binding properties.



**Scheme 5.2**

In this scheme the bar (-) between A and M represents weak binding.

If  $P_i$  binds to the AM.ADP state, forming a strong binding, force exerting AM.ADP. $P_i$  state, it should decrease the gliding velocity independent of the ATP concentration. And also it should prolong the average dwell time, but we have not observed significant increase in dwell time. Our hypothesis is strengthened by the fact that, the frequency of event appearance decreased significantly in single molecule dwell time measurements in the presence of  $P_i$ .

Therefore we propose that  $P_i$  can also bind to the empty nucleotide-binding pocket resulting in an AM. $P_i$  state. This is consistent with our motility and dwell time results.

If the resulting AM.P<sub>i</sub> state is a strong binding state, in this case P<sub>i</sub> binding to the AM state will extend the period over which the myosin head is in a strong binding state and thus would result in a decrease in a gliding velocity, secondly compete with ATP. This could explain our results, as the motility would be affected only when the cross-bridge remains in the strong binding state for a longer time. Our results are in agreement with a previous study where P<sub>i</sub> was shown to be a weak competitive inhibitor for MgATP with a K<sub>i</sub> of 80 mM, (Pate, Cooke 1989) where K<sub>i</sub> is an inhibition constant.

The actin filament gliding velocity is ATP dependent at low substrate concentration until it reaches the saturating conditions where it becomes independent of substrate concentration. As the ATP is not available immediately at low ATP concentration the velocity is limited. When the gliding velocity is measured at 30 μM MgATP, it is approximately 4 times slower than at the saturating [ATP]. That means a considerable fraction of nucleotide free acto-myosin state should be available for P<sub>i</sub> binding at low [ATP]. The same applies at other concentrations of ATP where inhibition of gliding velocity is observed. That gliding velocity is reduced by P<sub>i</sub> at low [ATP] can therefore be explained by binding of P<sub>i</sub> to the empty nucleotide-binding pocket of myosin resulting in a strong binding AM.P<sub>i</sub> state, i.e., increasing a period over which a myosin head is 'stuck' in a strong binding state that impedes filament sliding velocity.

A weak binding state (AM.ADP.P<sub>i</sub>) would not slow down the motility, but formation of such a weak binding AM.ADP.P<sub>i</sub> state seems to be the predominant result of P<sub>i</sub> binding at saturating ATP concentrations, as isometric tension is reduced by P<sub>i</sub> at saturating ATP concentration. Under these experimental conditions the possibility of P<sub>i</sub> binding to the nucleotide-binding pocket is unlikely as the binding affinity of MgATP is much higher than that of P<sub>i</sub>. Thus, P<sub>i</sub> binding to the empty nucleotide-binding pocket should be irrelevant at saturating ATP concentration and become evident only at low ATP concentrations.

One might argue that in the presence of P<sub>i</sub>, the increased formation of weakly bound (non-force generating) crossbridge states (AM.ADP.P<sub>i</sub>) reduces the total number of force generating crossbridges. Thus if actin sliding occurs against an applied load, the reduction of the number of force producing states will decrease the gliding velocity. However, in this case gliding velocity should be reduced under conditions where active force is reduced in fibers i.e., also at saturating ATP

concentrations. This, however, is not seen. Secondly, with fewer force producing interactions acting on a gliding filament, fragmentation of actin filaments should be less in the presence of  $P_i$ . Instead we observed increased fragmentation of actin filaments. This is more consistent with  $P_i$  binding to the empty nucleotide binding pocket results in a strong binding  $AM.P_i$  state that impedes filament gliding and then increases fragmentation of actin filaments.

Since  $P_i$  bound AM seems to be relatively strong binding state we assume that  $P_i$  must bind to the nucleotide binding pocket to the site other than  $\gamma$  phosphate binding site. It is believed that if  $P_i$  binds to  $\gamma$  phosphate site, the formation of hydrogen bond between  $\gamma$   $P_i$  and switch-II, switch-I loops (conserved loops in active site), thereby weakening the actomyosin interaction. (Takagi et al., 2004)

In the dwell time assays we have observed different populations having different time constant ( $\tau$ ), from actin-activated myosin. This will be discussed in detail, in second part of the thesis.

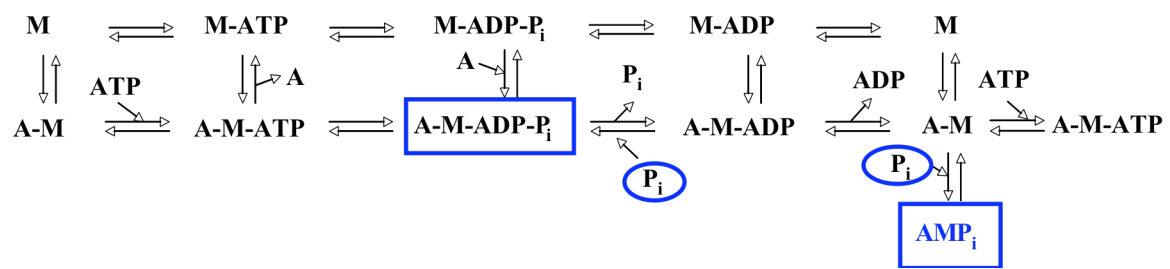
$P_i$  and  $AlF_4^-$  affected the gliding velocities to different extents.  $P_i$  seems to be stronger inhibitor than  $AlF_4^-$ . The number of fluorescent signals appearing at any given time corresponds to the occupied myosin heads by Cy3-EDA-ATP or Cy3-EDA-ADP. We counted the number of fluorescent signals over 10 consecutive frames (Fig 4.10) in the presence and absence of  $P_i$  and  $AlF_4^-$ . The number of myosin molecules within the field of view was kept constant by comparing data from the same field of view. We assumed that the number of signals within the field of view reflects the number of myosin molecules with Cy3-EDA-ATP and the comparison of density of events would provide the possible number of binding sites available for  $P_i$  or  $AlF_4^-$  binding.

In the presence of  $AlF_4^-$ , the average dwell time for both the major population and the second population has increased  $\approx 2$  folds. In addition, the observed number of signals has increased about 2 fold. We assume that if the dwell time has increased by certain period that should correspond to the number of signals in the defined area. Probably higher concentration of  $AlF_4^-$  would be needed to see the same inhibitory effect on the gliding velocity as inorganic phosphate for the binding to AM state.

In the presence of inorganic phosphate, the number of myosin heads that should have bound Cy3ATP decreased by 50%. So we assume that 50% heads are occupied by  $P_i$  at the given concentration of Cy3-EDA-ATP and  $P_i$  at given time. This could

also explain the difference in the extent by which gliding velocity is reduced by  $P_i$  or  $AlF_4^-$ . Inorganic phosphate appeared to be a stronger inhibitor than  $AlF_4^-$  i.e., the binding of  $AlF_4^-$  to the empty nucleotide-binding pocket is weaker than seen with  $P_i$  while binding of  $AlF_4^-$  to the active site in the presence of ADP seems to be much stronger (slower dissociation) as suggested by the extended lifetime of the fluorescent events.

Our proposed model for  $P_i$  binding to different states:



According to this model,  $P_i$  can either bind to AM.ADP state forming AM.ADP. $P_i$  or at low ATP concentrations  $P_i$  can also bind to the empty nucleotide binding pocket producing AM. $P_i$  strong binding intermediate.

Previous studies from stiffness measurements in fibers have shown that pyrophosphate can bind to AM state and AM. $PP_i$  is a strong binding state (Brenner, B. & Schoenberg, M. 1986). One might assume similar effects on gliding velocity and dwell times if there are contaminants  $PP_i$  in phosphate buffer. But we have taken care of  $PP_i$  by treating the phosphate buffer for  $PP_i$  contamination. Secondly, we checked the effect of  $PP_i$  on the number of fluorescent signals arising from Cy3ATP binding to myosin molecules. We did not observe significant decrease in density of events at low  $PP_i$  concentration, which may remain in phosphate buffer as contaminant. We assume that the observed effects are genuinely from  $P_i$  itself. And this is also evident from structural analogue of  $P_i$ ,  $AlF_4^-$  that showed similar effects as that to  $P_i$ .

In our studies we have used unregulated actin filaments, so the regulatory proteins (tropomyosin & troponin) might contribute to the effect of  $AlF_4^-$  and  $P_i$  in intact muscle fibers as it is considered to be fasten the ADP release step (Homsher and Tobacman, 2003).

We have discarded the signals that were shorter than 300 millisecond as our analysis program may not include all the very short signals with low fluorescence

intensities. Some of the longer time events may be cut due to the limitation of recording period, as we could not measure the dwell times of the events that already started before the recording and those started late and could not be covered by the whole rerecorded period. So these events could not be counted. This could be the reason for the sharp fall in the number of signals at the end in the dwell time plots. This is evident in the plots where the total numbers of events were plotted on logarithmic scale.

---

## Part II

In previous dwell time analysis, ATP dwell times from actomyosin system could not be defined by single exponential function, but rather by multiple exponentials, suggesting the presence of different hydrolysis rate bearing myosin populations. So the deviation from expected single reaction rate in the presence of homogeneous population of myosin molecules drew the attention to this behavior of the actomyosin system. This led me to investigate the factors that are responsible for producing different reaction rates. Although, earlier there have been several speculations about this peculiar behavior, the details were not investigated.

The second part of my thesis focuses on the myosin ATPase cycle using the same approach as in part I by measuring dwell time. In this study, myosin alone was used instead of the actomyosin system to sort out if the actin brings the additional population due to the strain exerted by actin filaments on myosin, which affects the release of ATP hydrolysis products ADP and  $P_i$ .

## 6 Introduction

The knowledge of the biochemical processes is usually derived from ensemble measurements of molecules. The ensemble-averaged experiments have either the limitations that they can barely distinguish dynamical fluctuations (single molecule changes with time) and static heterogeneity (molecules are statically different); also they could not extract the interconversion dynamics (switching between the different conformations). Single molecule studies have provided the solution to overcome these difficulties. Recent developments in single molecule detection (SMD) techniques allowed researchers to study the molecular dynamics of motor proteins (Sowa 2005), protein conformations (Yang et. al., 2003), enzymatic rates (Oijen et.al., 2003), RNA catalysis (Zhuang et al., 2000) and DNA/protein interactions, etc. By using SMD technique distributions and temporal fluctuations in the molecular properties were characterized from the time trajectories over wide ranges of time scales.

We used single molecule detection technique to study the dwell time distribution of rabbit skeletal muscle myosin II, by monitoring individual ATP binding upto the ADP release. Motor protein myosin II has been studied extensively for the enzymatic turnover at both ensemble and single molecule level. In the past, most of the information about the myosin kinetics was extracted from the solution studies (ensemble measurements). Recently, individual ATP hydrolysis for single myosin molecules was determined using fluorescently labeled ATP (Owia et. al., 2000, Funatsu et. al., 1995, Conibear et.al., 1998, Iwane et. al., 1997). The dwell time measurements determined the rate constant for ATP hydrolysis (step from ATP binding to the ADP release from myosin active site), however the data fitting showed that the process was not absolutely monophasic, rather it was a mixture of slow and fast components. This deviation from the expected single rate constant was interpreted as some impurities in the reaction mixture and artifacts from various external factors (Conibear et. al., 1998).

We then studied the myosin II molecules for dwell time distributions at ensemble and individual molecule level, to determine the responsible factors that cause this deviation from expected single reaction rate.



## 7 Results

We studied the distribution of dwell times obtained from binding of fluorescently labeled ATP (Cy3-EDA-ATP) to myosin II molecules, in an aqueous environment on a BSA coated surface. 'Dwell time' was measured i.e., the time that nucleotide remain in myosin nucleotide binding pocket. As mentioned in the earlier part, TIRF microscopy was used to measure dwell times.

### 7.1 Ensemble dwell time measurements from skeletal muscle myosin II

We wanted to determine whether the multiple (3) exponentials observed in dwell time measurements in the presence of myosin decorated actin filaments in previous section was due to the different strain exerted by actin filaments on the myosin heads. Therefore, here we used only myosin II for dwell time measurements.

Muscle myosin II was extracted from single muscle fiber. The diluted myosin II in AB buffer was introduced in the flow cell coated with 0.5 mg/ml BSA. 5 nM Cy3-EDA-ATP (2' & 3' isomers) was applied along with the antibleach system. The individual interactions of the Cy3-EDA-ATP with myosin appeared as fluorescent signals, were detected and recorded. The events were collected from the large number of molecules in the flow cell. The dwell time distribution was characterized by fitting to exponential functions. But, distribution of the dwell time events did not fit to a single exponential function in dwell time histogram or in a plot where numbers of events over time were plotted (Fig. 7.1A & B, respectively). Satisfactory fit was obtained only with the data fitting to double exponential function. Single and double exponential fit on the logarithmic scale (Fig. 7.1C) gives a clearer picture of poor single exponential fit on linear scale. We had expected a dwell time distribution fit to a single exponential function; instead we observed 2 distinct populations of dwell time events. The fast component had time constant of 1s and the slower one with 5 s. The 2 populations were significantly different from each other, evident from the time constants that showed nearly 5 folds difference.

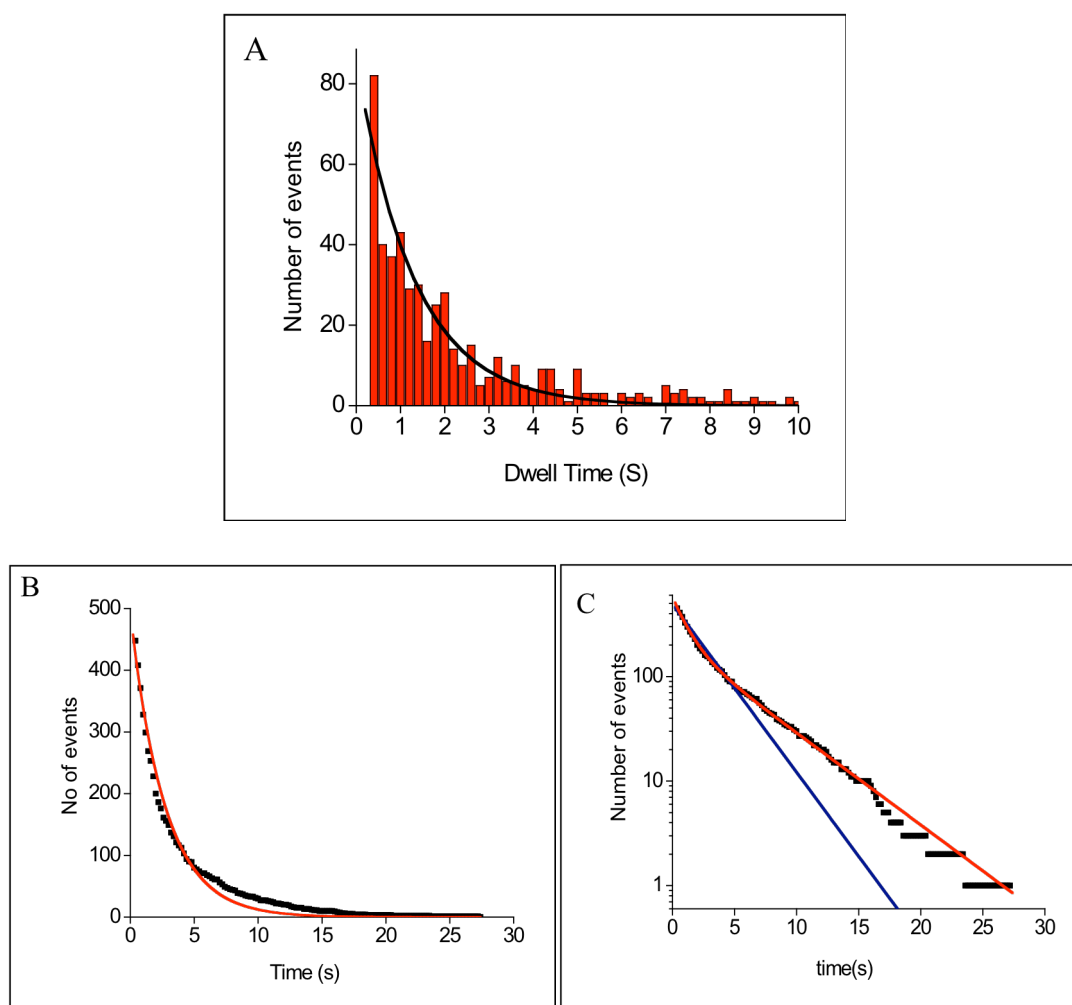


**Fig 7.1** The on time distribution derived from large number of myosin molecules on BSA coated surface with 5 nM Cy3-EDA-ATP (mixed Cy3-EDA-ATP isoforms).

A) Dwell time histogram plotted for the distribution of dwell time events fitted to a single exponential term.  $N = N_0 e^{-t/\tau}$

B) Number of events was plotted vs time. Data could not be fitted to a single exponential function. The solid line is a single exponential fit.

C) Same data plotted on the logarithmic scale. Blue line shows single exponential fit whereas red line is double exponential fit that gave satisfactory fit with the time constants 1 s and 5 s.

$$N = N_1 e^{-t/\tau_1} + N_2 e^{-t/\tau_2}$$

$N$  = total number of events,  $N_1$  and  $N_2$  fraction of events having two different time constants.  $\tau_1$  &  $\tau_2$  = time constants for 2 populations.

In previous dwell time measurements (Oiwa, 2000; Bagshaw & Conibear, 1999) this behavior was observed but not studied in detail. We wanted to investigate the cause of this deviation from expected single exponential distribution, e.g.:

- 1) mixed Cy3-EDA-ATP (2' & 3') isoforms, which was shown to have different hydrolysis rate and fluorescent intensity (Owia et al., 2000);
- 2) different light chain or heavy chain isoforms of myosin II even in single muscle fibers;
- 3) contribution of nonspecific signals, for example from binding of Cy3 nucleotide to the BSA coated surface;
- 4) different orientation of the myosin molecules on BSA coated surface;
- 5) co-operation between the 2 myosin head domains.

First we investigated whether the deviation from single exponential distribution of dwell time histogram may be caused by 2 isoforms of Cy3-EDA-ATP, since we had used a mixture of the two isoforms. We therefore used the purified 2' and 3' Cy3-EDA-ATP isoforms. Also to minimize the contribution of fluorescent signals from nonspecific binding of fluorescent nucleotide to the BSA coated surface, we collected data from individual myosin of interest just of the size of a fluorescent spot. The idea was i) to collect a sufficient number of dwell time events from an individual myosin of interest such that a dwell time histogram could be generated. We hypothesized that only specific binding of Cy3-EDA-ATP to a myosin could yield several dwell time signals while nonspecific binding to the BSA within the small area would be unlikely, as only 2-3 events appeared as nonspecific binding of 3'Cy3-EDA-ATP to the BSA coated surface without myosin at 30 nM 3'Cy3-EDA-ATP concentration at any given recording time. Additionally, no fluorescent events were observed for several minutes from the area where initial nonspecific event occurred. 2) We reduced the density of myosin molecules such that within the field of view only few regions of interest could be found where multiple fluorescent events could be detected. This means we attempted to collect fluorescent events arising from individual myosin molecules. Apart from minimizing chances to include nonspecific binding events into our analysis, this approach also allowed to test for heterogeneity (e.g. different heavy chain or light chain isoforms) among different individual molecules.

## 7.2 Individual molecule dwell time measurements

The individual molecule dwell time measurements required the highest possible concentration of pure Cy3-EDA-ATP and low concentration of myosin molecules to collect as many dwell time events as possible from one individual molecule over extended recording period.

### 7.2.1 Dwell time measurements from individual muscle Myosin II

The lifetime of the events from individual myosin molecules were measured over an extended period of time (2000 sec), on a surface coated with 0.5 mg/ml of BSA. Records of events was started immediately after infusion of 30 nM pure 3' Cy3-EDA-ATP. The dwell times for fluorescent spots were recorded over 20,000 frames (10 frames/s). Fig 7.2 shows the time trajectory of fluorescence within one region of interest, i.e., the time trajectory reflects signals from just one individual myosin molecule. Over 50-100 dwell time events could be collected from an individual molecule at this concentration of Cy3-EDA-ATP. Cy3-EDA-ATP concentration was limited to the concentration of only 30 nM, because with increasing the concentration of fluorescently labeled nucleotide, the background fluorescence was too high to detect single fluorescent spots. Each individual region of interest, i.e., each individual myosin molecule was analysed for dwell time events. Fitting to exponential functions was used to determine the time constant of the dwell time distribution of each individual molecule. This was done for 30 individual molecules. Most of those individual molecules showed a double exponential with 2 distinct populations having time constants of 0.12 - 0.54 s for fast and 1.1- 8.7 s for slow components respectively. Fig. 7.3 shows plots for individual molecules fitted with single and double exponential functions. 7 molecules could be fitted with single exponential function yielding time a constant of 0.3 - 0.6 s, one example is shown in fig 7.3 b. Note that variability in reaction rates was seen among individual molecules. Some molecules seemed to be faster than others, but most molecules still have two populations of dwell times and the difference between the time constants for the fast and slow component was always 5 fold or higher. In figure 7.4 the time constants from 30 individual molecules are plotted for fast and slow components separately, showing the large variability.

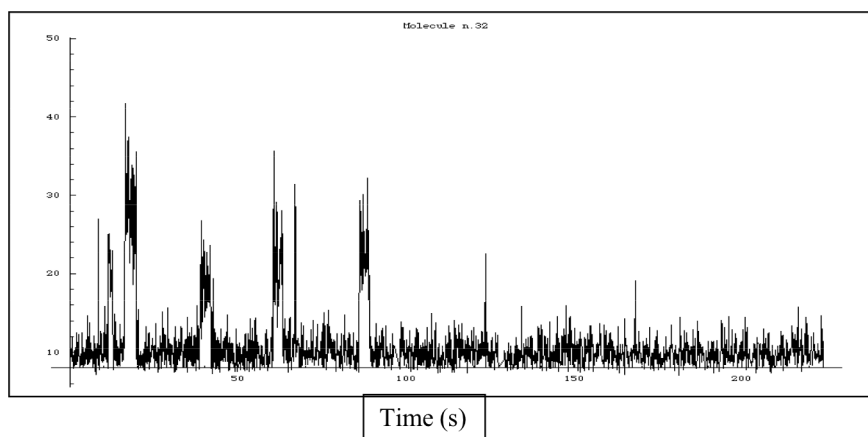


**Fig. 7.2 Real time observation** of the occurrence of dwell time events from individual myosin molecule. Events detected over only a period of 200 sec are shown here. Over 20,000 frames (2000 sec), 50-100 dwell time events were detected in such time trajectories for individual myosin molecules. Myosin concentration was 30 pM and pure 30 nM 3'Cy3-EDA-ATP isoform was used.

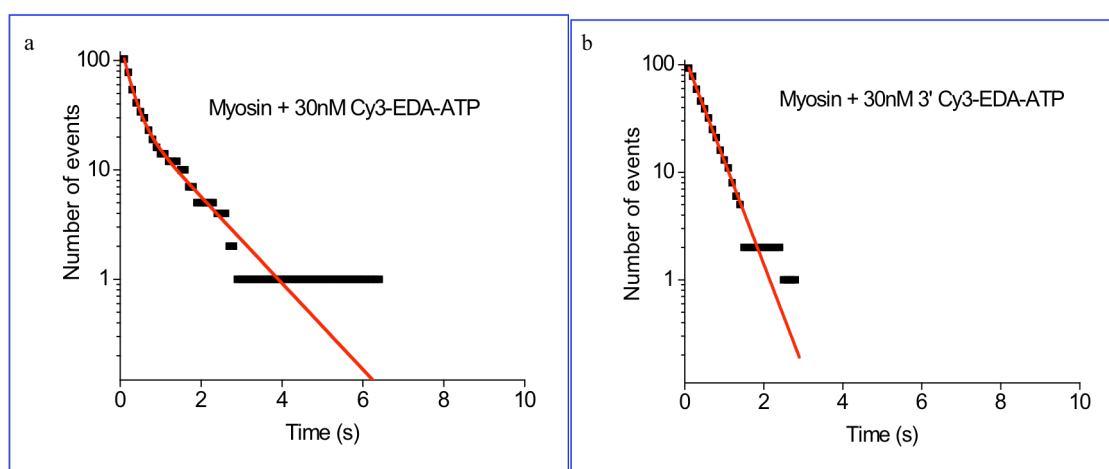


**Fig. 7.3** Number of events obtained from individual skeletal muscle myosin II molecules with pure 30 nM 3'Cy3-EDA-ATP isoform is plotted on logarithmic scale a) Molecule that could be fitted with a double exponential function yielding 2 time constants of 0.22 s and 1.1 s, respectively. b) Molecule for which single exponential gave satisfactory fit with time constant of 0.45 sec. Ionic strength = 55 mM, T = 22°C

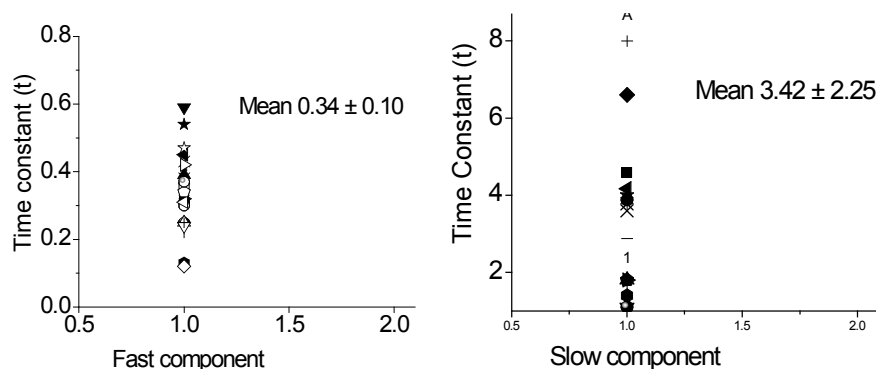


**Fig. 7.4 Time constants (s) from 30 individual molecules** for fast and slow components.

This experimental arrangement and specific conditions (low myosin density, signals only from the region of interest) made it highly unlikely that it is nonspecific binding of Cy3-EDA-ATP to the BSA coated surface that generates the two populations of dwell times. Instead, it appeared that 2 populations are also seen when dwell times were analysed for individual myosin molecules.

Next, we asked whether the two populations of dwell times seen even with individual molecules might come from the co-operation between the 2 heads of the myosin II molecule or from different light chain isoforms associated with the two heads of one individual myosin II molecule, as it has been reported that myosin II extracted from even single muscle fiber can have different light chain isoforms (Botinelli & Reggiani, 1994). Therefore, we determined dwell time of single headed myosin II construct expressed in Dictyostelium cells.

### **7.3 Actin sliding on a surface coated with single headed Dictyostelium myosin II**

The expressed single headed Dictyostelium myosin II was tested for the functionality. First, it was checked whether single headed Dictyostelium myosin II can bind to a BSA coated surface. It was found that rhodamine-phalloidin labeled actin filaments could attach to a BSA coated surface to which single headed Dictyostelium myosin had been added. However, testing for the gliding upon infusion of 2 mM MgATP caused actin filaments to detach from the surface and no gliding was observed. This indicated that the number of Dictyostelium myosin II molecule on the BSA coated surface was too low to support the actin gliding. Only when the Dictyostelium myosin II was immobilized on nitrocellulose-coated surface, Rh-phalloidin labeled F-actin showed smooth movement upon infusion of 2 mM MgATP with a gliding velocity of  $\approx 1 \mu\text{m}/\text{sec}$ .

#### **7.3.1 Dwell time measurements with Pure Cy3-EDA-ATP isoform (Ensemble measurement)**

Dwell times were measured from a large number of single headed Dictyostelium myosin molecules using the purified 3'Cy3-EDA-ATP isoform. The single headed Dictyostelium myosin molecules were immobilized on a surface coated with 0.5 mg/ml BSA in AB buffer. Infusion of 1 nM Dictyostelium myosin into the BSA coated flow cell was followed by addition of 5 nM of purified 3'Cy3-EDA-ATP. We also measured the dwell times in the presence of 2'Cy3-EDA-ATP. The events were collected from large number of molecules. The dwell time events again did not fit to the single exponential function but rather required 2 exponential terms. This demonstrates that still two components can be detected. The time constants of the two terms were 0.6 s and 3.4 s for 3' Cy3-EDA-ATP for the fast and slow component, respectively. The time constants did not differ much from the 2' Cy3-EDA-ATP with 0.5 s and 3.5 s, respectively.

Although we had a homogeneous population of single headed Dictyostelium myosin molecules and purified Cy3-EDA-ATP isoforms, the question remained unanswered where the 2 populations of dwell time come from. Next, we therefore

investigate whether the two dwell time can also be seen when individual molecule are analysed. Thus, we switched to measurements on individual Dictyostelium myosin II molecules.

### 7.3.2 Dwell time measurements on individual Dictyostelium myosin molecule immobilized on a BSA coated surface

The Dictyostelium myosin concentration was decreased to 100 pM whereas 30 nM  $3'$ Cy3-EDA-ATP concentration was used. Same approach was used to collect the large number events from individual myosin molecule, as used for measuring dwell time events from individual muscle myosin II molecules. The multiple numbers of events arising from individual molecules were collected and plotted for the number of events. 50-100 events were collected from an individual molecule. Data of 33 individual myosin molecules were analysed. Most of the molecules still required a double exponential function for satisfactory fitting. (Figure 7.5 upper panel). The time constant ranged from 0.4 - 1 s for the fast component and 5 - 10 s for the slow component. Again some variability was observed among the individual molecules. In the lower panel of fig 7.5, the time constants of the 33 individual molecules are plotted.

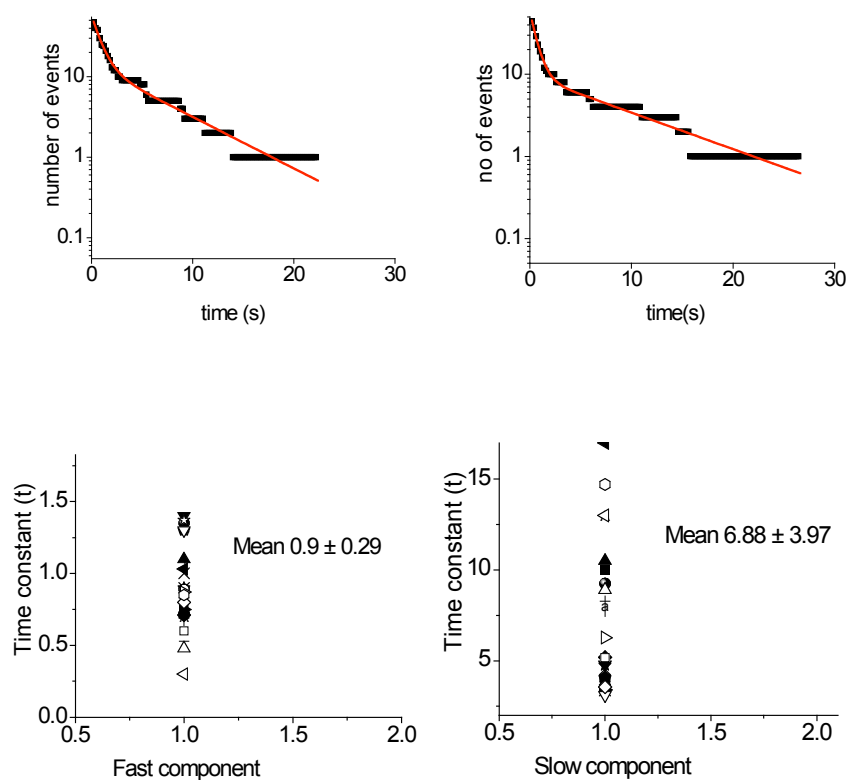




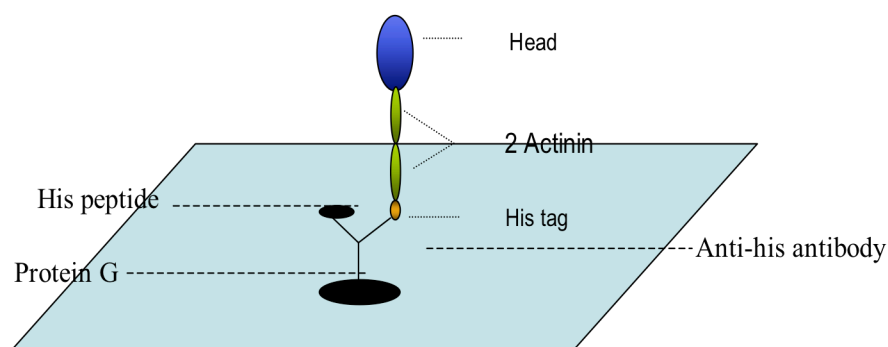
**Fig.7.5 Top Panels, distribution of events** of 2 individual Dictyostelium myosin molecules immobilized on BSA coated surface. Bottom panels, time constants of 33 individual molecules obtained by fitting of double exponential function to the number of events vs time. Ionic strength 55 mM; temperature 22-25°C.

As shown in fig 7.5, even single headed Dictyostelium myosin with the light chain domain replaced by 2 actinin subunits i.e., without light chains, yielded two population of dwell times even from an individual molecule.

However, the orientation of the myosin molecules on the surface was a matter of concern since it was possible that some of the molecules did not maintain the proper orientation throughout the recording period. Thus, to ensure proper orientation of the myosin molecules throughout the observation period, we used protein G/ anti His antibody-coated surface to make sure that molecules maintain a ‘head up’ position. We checked the motility of actin filaments supported by single headed Dictyostelium myosin II on the Protein G/ anti His antibody-coated surface to make sure that myosin molecules were in a proper orientation and the actin and ATP binding sites were properly accessible. The observed actin filament gliding velocity was 1.5  $\mu\text{m}/\text{sec}$  under our experimental conditions of 55 mM ionic strength and 22-25°C temperature.

### 7.3.4 Measurement on Protein G coated surface

Single headed Dictyostelium myosin was immobilized on a protein G coated surface with fluorescently labeled (Alexa488) Anti-His antibody-coated surface (Figure 7.6). Since we infused a mixture of 1 nM His peptide and 100 pM Dictyostelium myosin (molar ratio of 10:1) in a flow cell, we assumed that on average every antibody should carry single myosin molecule and the second antigen binding site of an antibody was blocked by His-peptide. 30 nM 3’Cy3-EDA-ATP was added



to the flow cell.

**Fig. 7.6. Schematic representation of the** experimental arrangement for individual molecule dwell time measurements. Dictyostelium myosin II is bound to the protein G coated surface of a coverslip through anti-His tag antibody.

22 molecules were analysed for the distribution of dwell time events and plotted individually. Many molecules fitted to the double exponential function with clear distinction between the 2 components (fast and slow). Figure 7.7 shows plots from 2 molecules clearly showing double exponential fit, but one seems to be faster (molecule a) than the other (molecule b). The time constant for the fast and slow components ranged from 0.5 - 1s and 4 - 15 s respectively. The lower panels demonstrate the large variability among individual molecules.

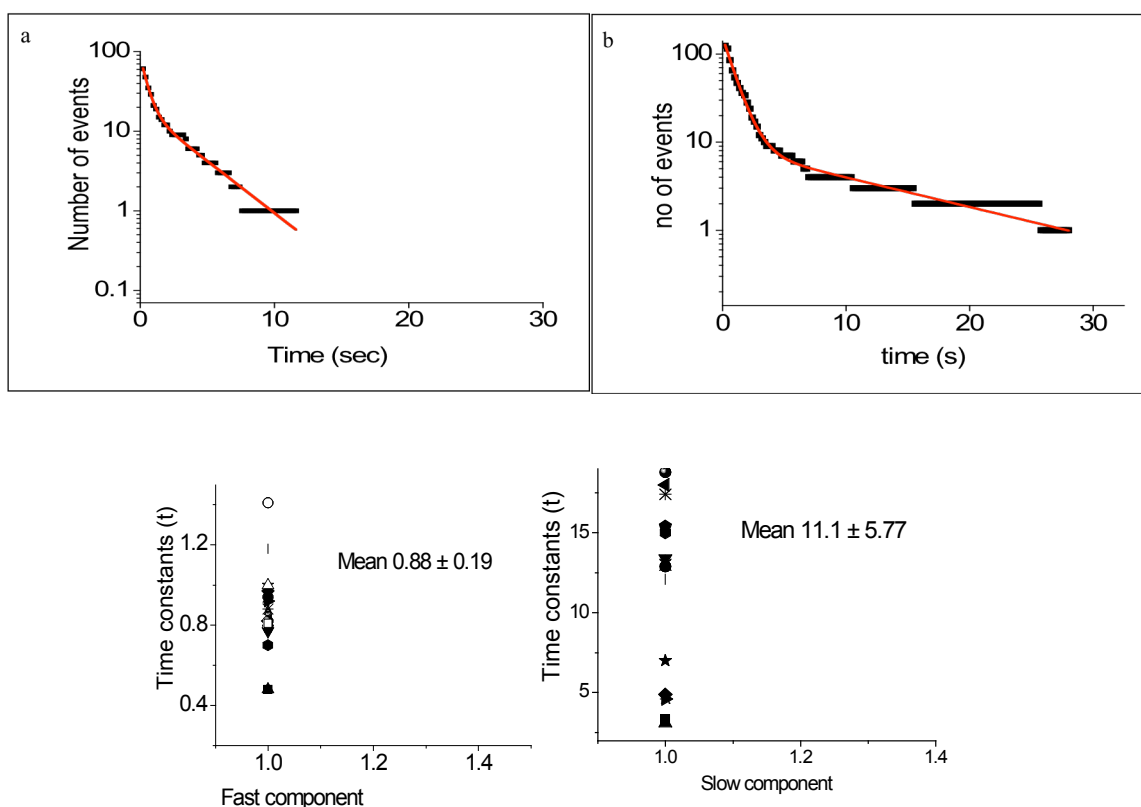


**Fig. 7.7 Number of events vs time**, events derived from time trajectories of individual myosin molecules on protein G coated surface. Upper panel shows plots from two individual molecules. Data fitted to double exponential functions with time constant 0.48 s and 3.3 s (for molecule a) and 1s and 12 s (for molecule b) respectively. A total of 22 molecules were analysed individually. 18 molecules required double exponential function for fitting of

number of events. The time constants for the fast and slow components are shown in the lower panels. Note that the time constants of all the molecules, including those derived from single exponential fits to the number of events are plotted here. Ionic strength = 55 mM, T= 22°C.

Four molecules could be fitted with the single exponential decay function (Fig. 7.8) with a time constant of 0.8 - 1s. This is in the range of the fast component of the other molecules that required two exponential functions for better fitting.

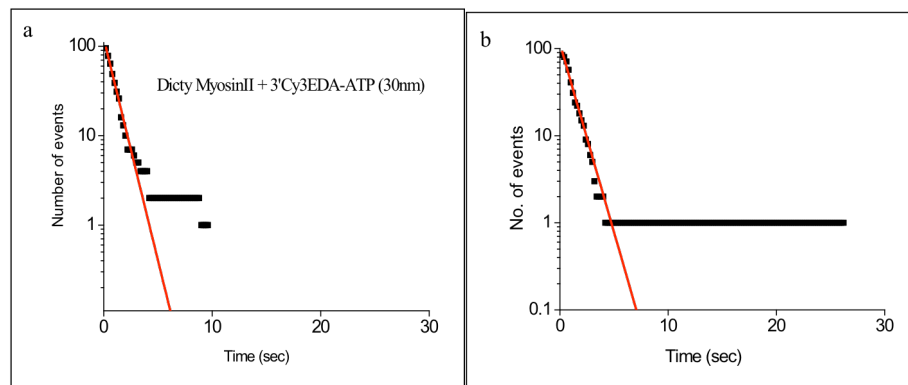
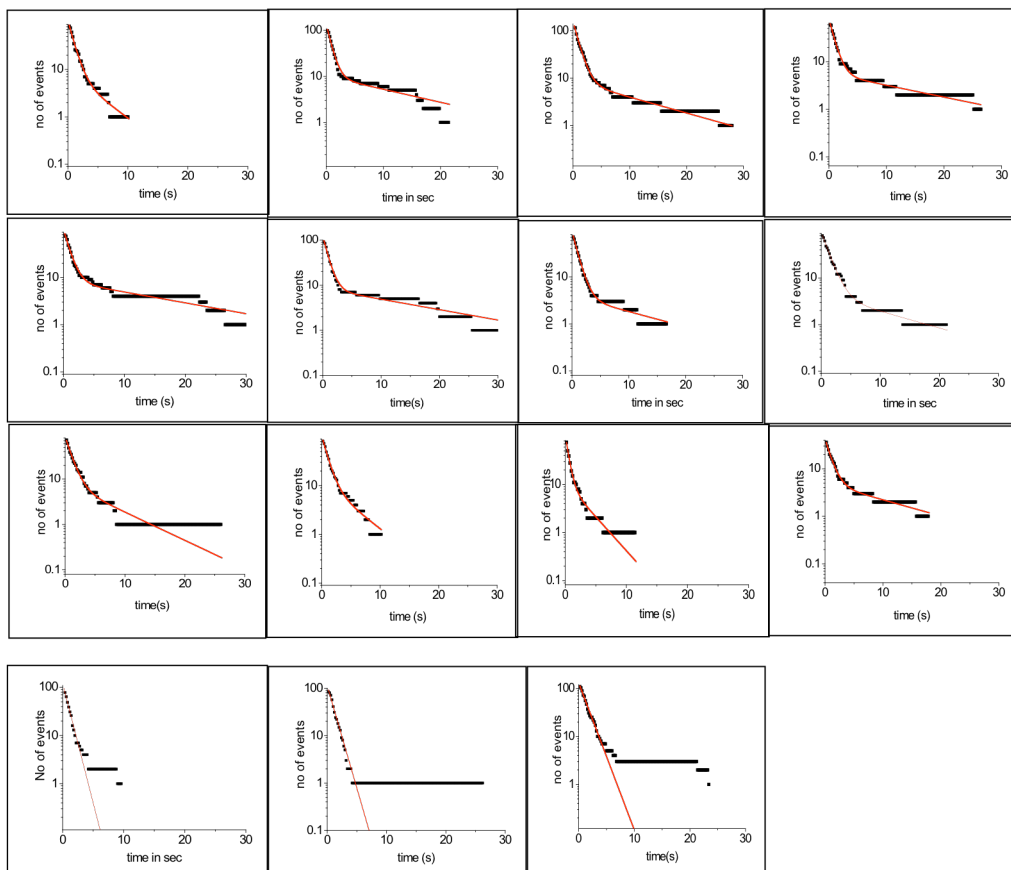


**Fig. 7.8 Dwell time events** from individual myosin molecule. 2 molecules are shown here, fitted well to single exponential with the time constant of 0.87 s (molecule a) and 1s (molecule b).

Fig. 7.9 shows the dwell time distributions from several individual Dictyostelium



myosin II molecules.

**Fig. 7.9 Number of events vs time** plotted for 15 individual molecules shows the variability among the molecules even though they were measured under identical experimental conditions. 12 molecules required double exponential function for satisfactory fitting, the lower panels show 3 molecules with single exponential fit.

These plots present a large range of molecules with fast, slow and intermediate time constants, required for fitting the number of events. This large diversity came as a surprise as all molecules were treated the same way and should be elements of a homogeneous population of molecules. The only difference was the spatial distribution on the surface.

### 7.3.5 'Off time' measurement

The time that the myosin molecule has to wait for another Cy3-EDA-ATP molecule to bind, i.e., for the new start of event is termed 'off time' or 'waiting time'. This off time should depend on the concentration of fluorescently labeled ATP. Fig 7.10 shows the 'off time' distribution between the events from a myosin molecule individually analysed for 'on times' (dwell times). Off times could be fitted to single exponential with the time constant of 26 s for this molecule. Thus ATP binding rate should be  $1.26 \times 10^6 \text{ M}^{-1}\text{s}^{-1}$ . Though few molecules could be fitted to double exponential function yielding 2 different binding rates for ATP.

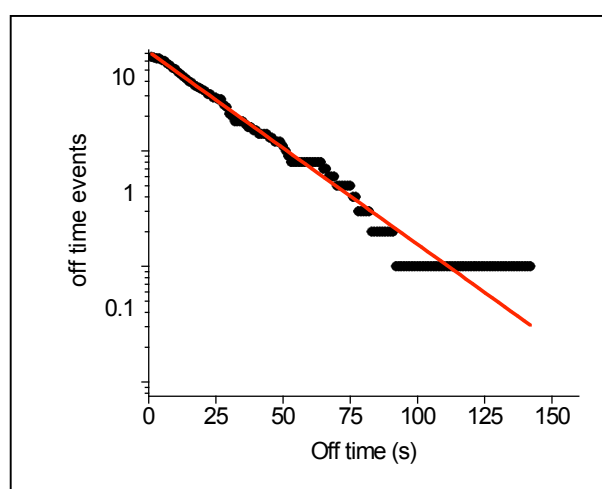
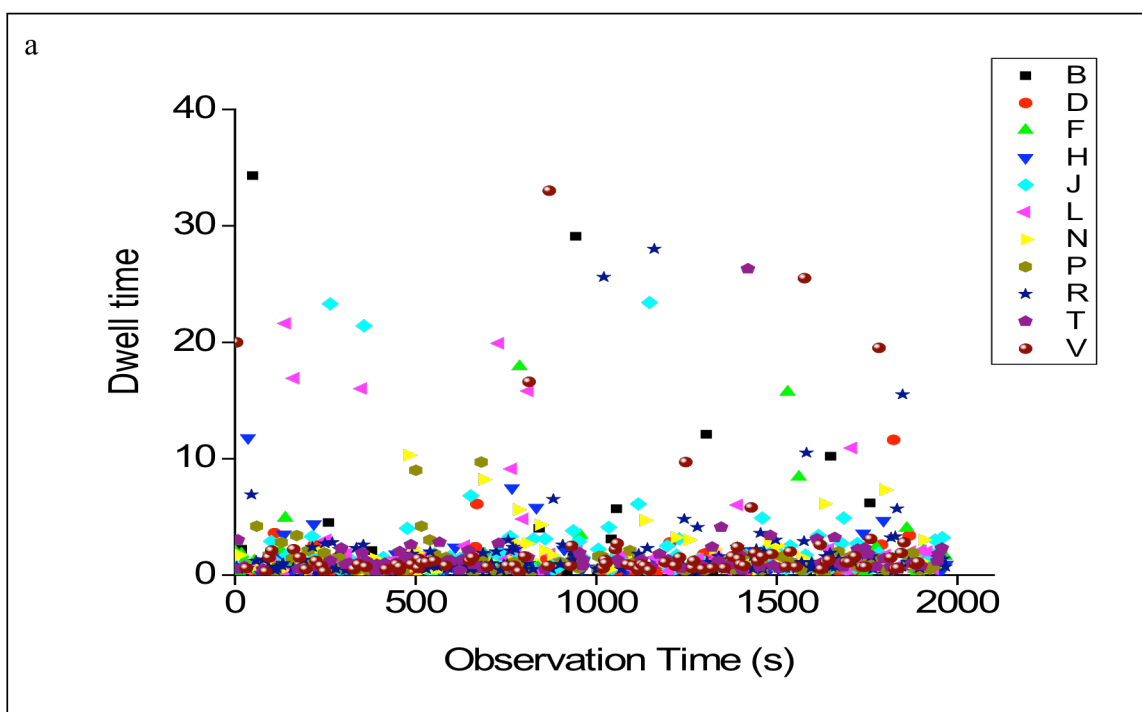


**Fig 7.10** The number of off time events derived from single myosin molecule plotted over time, events were obtained at 30 nM 3'Cy3-EDA-ATP. The solid line is a single exponential fit with time constant 26 s.

### 7.3.6 Distribution of events throughout the recorded period

To rule out that the two populations of dwell times seen even with individual molecules are the result of damage of the myosin molecules during the observation period, or result from accumulation of Cy3-EDA-ADP, dwell time duration of each event was plotted against time for event occurrence during the observation period of 2000 seconds.

Fig 7.11a shows that fast or slow events are not clustered during a particular range of the observation period i.e., we did not observe any regular pattern of event appearance. Long and short events occurred randomly throughout the recording period. The time trace of an individual molecule (Fig 7.11b) shows no evident regular pattern of fast event followed by fast event and slow event followed by a slow event, i.e., the lifetimes of the events appeared random throughout the entire time trace.



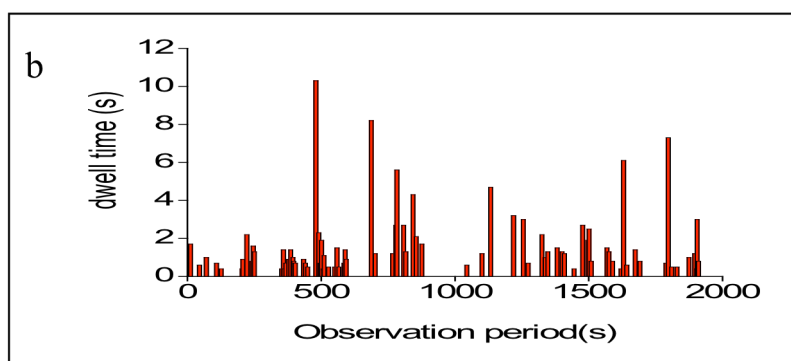


**Fig. 7.11 Distribution of dwell time duration** throughout the observation period (2000 sec). **a)** The events from 12 individual molecules are plotted together. **b)** Events from an individual molecule. Note that in the time trajectories events with long or short dwell times appeared evenly distributed throughout the entire observation period of 2000 sec.

## 8 Discussion

Two dwell time populations were observed in the ensemble measurements from myosin II molecules. To our surprise, the two dwell time populations were also seen even from individual molecules, where homogeneous population of single headed *Dictyostelium* myosin II and purified 3' Cy3-EDA-ATP were used in the measurements, on protein G/ anti-His antibody coated surface. This was unexpected, as single population was expected from a homogeneous population. We propose here that the two consistent dwell time populations correspond to the existence of 2 conformations of individual myosin molecule.

Time resolved individual molecule dwell time measurements allowed us to follow the stochastic nature of ATP binding, followed by cleavage up to the ADP release. Within the stochastic nature of the observed events, two populations of dwell times were found, although from known kinetic studies only (one step) a single exponential distribution had been expected. One possible explanation is that the myosin molecules exist in two stable conformations, one with slow kinetics for ATP binding upto the ADP release, and other with about 5 fold faster kinetics. We found most of the individual myosin with 2 distinct time constants, and only few molecules with a single exponential distribution of dwell times. This could mean that these few molecules remained in one of the two conformations over the recorded period. These molecules had the same time constant as the fast population seen in the molecules with both fast and slow components. But even these few molecules that could be fit with a single exponential function showed one or few long events that were outside the distribution, described by a single exponential (Fig 7.8). This means that these molecules very likely had also yielded 2 populations of dwell times if they had been observed over extended time period or at a higher substrate (ATP) concentration. The long events did not appear predominantly at the beginning or at the end of recording period but were homogeneously distributed throughout the total observation period. Also, long dwell times were not predominantly followed by another long dwell time. This suggests that the conformation with long dwell time very likely does not prevail for long time. Instead, it appears that switching between the two conformations is fast compared to the waiting period between the events. However, since we always obtained a large number of shorter events compared to the longer ones, it appears that

the conformation responsible for shorter dwell times may be preferred over the other conformation.

The time constants of individual molecules showed substantial variability among different myosin molecules despite using homogeneous population (Dictyostelium myosin II). Expressed single headed Dictyostelium myosin II was used where, light chain binding domains were replaced by artificial lever arm to exclude the possibilities from different heavy or light chain isoforms or cooperativity between 2 heads. In addition, Protein G/ anti-His antibody-coated surface was used to provide proper binding orientation. Nevertheless, the interesting fact is that the two populations with fast and slow time constants for dwell time distribution were consistent in all the experimental conditions.

Collection of a large number of events at low substrate concentration required long recording periods. Thus, the stability of the myosin molecules was a main concern. We therefore examined the lifetime of the events at the beginning of recording time and towards the end. Long events were distributed evenly throughout the time trajectory as evident from Fig.7.11 where 12 trajectories from individual molecules were combined. From this we conclude that myosin was stable over the recorded period at least concerning the duration of dwell times.

The possibility that Cy3-EDA-ADP formed by the ATP hydrolysis is responsible for a second population is also unlikely since both long and short dwell times appeared evenly throughout the observation period. In addition, the number of myosin molecules on the surface was much smaller (300 times) than the number of Cy3ATP molecules in the solution.

We could not determine how often an individual molecule switches between the two dwell time population. i.e., we did not see duration of short vs long dwell times. This is most likely due to the fact that the off times were quite long (time constant 26 seconds). This is due to the limited concentration of fluorescently labeled substrate (30 nM), which prevented more frequent occurrence of events. High substrate concentration, however, were not possible because at high substrate concentration the signals of individual Cy3-EDA-ATP molecules bound to myosin molecules disappeared in the higher fluorescent background. We noticed however, that short events occurred quite frequently compared to long lifetime events, thus implies that molecules switch quite quickly from long lifetime event to short event lifetimes. This



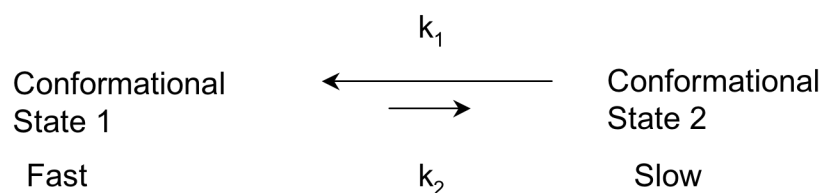
implies that the conformations yielding short dwell time event is preferred over the conformation yielding long dwell times.

Our experiments could not determine what triggers the postulated transition between 2 conformations that lead to long and short dwell times, whether it is stimulated by ATP binding or occurs during ATP cleavage or release of products. Although the myosin molecule exhibit different conformation is known, we provide additional new information about the interconverting conformations responsible different reaction rates.

The off time corresponds to the waiting time for the binding of ATP to the myosin molecule. The off time distribution shows that Cy3-EDA-ATP binds to myosin with a single rate constant (single exponential off time distribution). In some cases however, a second population of off times was found i.e., off time distributions followed a double exponential function. Whether the postulated two conformations responsible for the two dwell time distributions are also associated with 2 off time distributions is unclear from our experiments.

Single molecule measurements for the enzymatic turnover on cholesterol oxidase (Xie, S. 2000) also yielded different reaction rates. In this case switching between two conformations could be demonstrated by fluorescence spectroscopy. Conclusion of two different conformations for myosin may be supported by the FRET measurements (Ishijima, Yanagida 1997) on myosin S1. Cy3 (donor) and Cy5 (acceptor) dyes attached to the SH1 and SH2 groups of myosin subfragment 1 (S1) showed fluctuations in the FRET efficiency. This was attributed to the two different stable conformations of the S1 molecules. Such two different conformations were considered to be the cause of ‘memory’ of the S1 molecule. In fluorescence spectroscopic measurement, with TMR (tetra methyl rhodamine) bound to the SH1 of S1, the existence of slow conformational transition was observed slow changes in the emission spectra of single flurophore.

To account for our data we proposed a model of 2 conformational states of a myosin II motor molecule.



In state 1 the dwell times are short, i.e., the overall reaction from ATP binding to ADP release are fast while in state 2 dwell time is approximately 5 folds slower, i.e., overall reaction from ATP binding to ADP release is 5 times slower. We refer state 1 as fast dwell time population bearing state and state 2 as slow dwell time population yielding state. Our observation further suggest that the switching between these 2 states is fast compared to the ‘waiting periods’, but that state 1 is favored over state 2.  $k_1$  and  $k_2$  are the reaction rates for interconversion between state 1 and 2. It seemed that the conversion from state 2 to state 1 is faster than conversion of state 1 to state 2. However, we could not determine the actual values of the interconversion rates as our waiting period were too long.

Single-molecule fluorescence detection technique provides ample opportunity to study biomolecules and their complex processes that might have important implications to the cellular functions. Labelling the molecule at the active site might provide a clearer picture of the conformations, but care must be taken that the activity of the molecule is not affected. Increase in substrate concentration would help in depicting different catalytic rates influenced by conformations, in more details.

## 9 Conclusions

My research goal was to resolve a situation where all the effects of  $P_i$  were not explained by the previous hypothesis of  $P_i$  binding to M.ADP or AM.ADP state.

The major discovery was the inhibitory effect of  $P_i$  on actin filament gliding velocity at only low ATP concentrations. Of special interest was the observation that the fragmentation of actin filament occurs in the presence of  $P_i$ . This finding led to the hypothesis that a strong binding AM. $P_i$  intermediate is formed in the presence of  $P_i$  by binding of  $P_i$  to the empty nucleotide-binding pocket. To test this hypothesis, effects of  $P_i$  on ATP hydrolysis cycle were studied at the single molecule level. Measurements of the dwell time of fluorescently labeled nucleotide on the myosin molecules and of the density of fluorescent signal in the presence of  $P_i$  further strengthened our hypothesis that a **strong binding AM. $P_i$  intermediate** might exist.

In this study, dwell time measurements raised a question about the different populations in the seemingly homogeneous population of myosin molecule. Detailed study at the individual molecule level revealed that **two conformations of active site** of myosin might exist that are responsible for fast and slow ATP hydrolysis rate, which was consistent in all the measurements.

## 10 Future Prospects

### 10.1 Effects of $P_i$ in the presence of regulatory proteins.

It is necessary to check the effects of  $P_i$  and its structural analog  $AlF_4^-$  in the presence of actin filaments with regulatory proteins, troponin and tropomyosin (regulated actin filaments) which also calls for the use of  $Ca^{2+}$  to check whether these regulatory proteins have some other effects. It would be also interesting to check these effects at individual molecule level, but it is difficult to immobilize actin-myosin complex with low concentrations of myosin that would be required for individual molecule studies. A large number of myosin heads are required to keep an actin filament immobilized on the surface. Alternatively, actin filaments with the shorter lengths could be tested if a single myosin can hold it, but then the additional problem is with the addition of MgATP, whereby, the actin might dissociate and it may not be possible to collect a large number of events from one molecule. It should be possible when the actin filament is tethered at both ends and the individual myosin molecule is brought in its close contact allowing actomyosin interaction, and then large number of ATPase events could be obtained under preferred conditions, without loss of actin or myosin molecule. This would require a combination of optical trap (that can trap the actin filament) and evanescent field microscopy (to measure dwell time events). This would also allow the estimation of the length of powerstroke, the time of actomyosin interaction and the simultaneous dwell time from individual myosin molecule.

## 10.2 Individual molecule studies to check the conformations of the active site

Because of the limitation of use of fluorescently labeled nucleotide, the dynamic fluctuation (or interconversion) between the 2 different conformations of active site could not be estimated, which we believed to occur from our results.

This could be achieved in two ways:

1. By labeling myosin molecule at active site and monitor the conformational change directly, using FRET (Fluorescence Resonance Energy Transfer) or using Fluorescence Spectroscopy for emission spectra.
2. By increasing the substrate concentration and accumulate all subsequent dwell time events.

The appropriate labeling of amino acid residue in active site might help to monitor the conformational change during active ATP hydrolysis. But the care must be taken that the labeling does not affect the property of the molecule. One can also label the myosin in 50 kDa cleft that lies between the upper and lower 50 kDa domains and is linked to the active site. The emission spectra from the labelled residues might provide the information about the conformations.

The possibility to increase fluorescently labelled ATP concentration without affecting the quality of signal (good signal to noise ratio) would be useful to gather large amount of dwell time events, attainable by adjusting the depth of the evanescent field.

---

## Reference List

- Baker, J.E., Brosseau, C., Joel, P.B. and Warshaw, D.M. 2002. The Biochemical kinetics Underlying Actin Movement Generated by One and Many Skeletal Muscle Myosin Molecules. *Biophys. J.* 82: 2134-2147.
- Bagshaw CR, Eccleston JF, Eckstein F, Goody RS, Gutfreund H, Trentham DR. 1974. The magnesium ion-dependent adenosine triphosphatase of myosin. Two-step processes of adenosine triphosphate association and adenosine diphosphate dissociation. *Biochem J.* 141(2):351-64.
- Bagshaw CR, Trentham DR. 1974. The characterization of myosin-product complexes and of product-release steps during the magnesium ion-dependent adenosine triphosphatase reaction. *Biochem J.* 141(2):331-49.
- Brenner B., Yu LC, Greene LE, Eisenberg E, Schoenberg M. 1986. Ca<sup>2+</sup>-sensitive cross-bridge dissociation in the presence of magnesium pyrophosphate in skinned rabbit psoas fibers. *Biophys J.* 50(6): 1101-8.
- Brenner B. 1990. Transient detachment of force-generating cross-bridges in Ca(2+)-activated skinned psoas fibres of the rabbit. *Journ of Physiol* 426:40P.
- Brenner B, Schoenberg M, Chalovich JM, Greene LE, Eisenberg E. 1982. Evidence for cross-bridge attachment in relaxed muscle at low ionic strength. *Proc Natl Acad Sci U S A* 79(23):7288-91.
- Brenner B, 1993. Dynamic actin interaction of cross-bridges during force generation: implications for cross-bridge action in muscle. *Adv exp med biol.* 332, 531-543
- Brenner B, Yu LC.1993. Evidence for structural changes in crossbridges during force generation. *Adv exp med biol.* 332, 461-469.
- Chalovich JM, Eisenberg E. 1982. Inhibition of actomyosin ATPase activity by troponin-tropomyosin without blocking the binding of myosin to actin. *J Biol Chem* 257(5):2432-7.

- Chase PB, Martyn DA, Kushmerick MJ, Gordon AM. 1993. Effects of inorganic phosphate analogues on stiffness and unloaded shortening of skinned fibres from rabbit. *J Physiol*. 460, 231-246
- Cooke R, Pate E. 1985. The effects of ADP and phosphate on the contraction of muscle fibers. *Biophys J* 48(5):789-98.
- Cope MJT, Whisstock J, Rayment I, Kendrick-Jones J. 1996. Conservation within the myosin motor domain: implications for structure and function. *Structure* 4(8):969-87.
- Conibear PB, Kuhlman PA, Bagshaw CR. (1998) *Adv. Exp. Med. Biol.* 453, 15-26
- Dantzig JA, Goldman YE, Millar NC, Lackett J, Homsher E. 1992. Reversal of the cross-bridge force-generating transition by photogeneration of phosphate in rabbit psoas muscle fibres. *J Physiol (Lond)* 451:247-78.
- Eisenberg E, Greene LE. 1980. The relation of muscle biochemistry to muscle physiology. *Annu Rev Physiol* 42:293-309.
- Eisenberg E, Hill TL, Chen Y. 1980. Cross-bridge model of muscle contraction. Quantitative analysis. *Biophys J* 29(2):195-227.
- Eisenberg, E., & Hill, T.L. (1985). Muscle contraction and free energy transduction in biological systems. *Science* 227: 999-1006.
- Fisher AJ, Smith SA, Thoden, Smith R, Sotoh K, Holden HM, Rayment I, 1995. X-ray structures of the myosin motor domain of *Dictyostelium discoideum* complexed with Mg.ADP.BeFx and MgADP.AIF<sub>4</sub><sup>-</sup>. *Biochemistry*, 34, 8960-8972.
- Funatsu T, Harada Y, Tokunaga M, Saito K, Yanagida T. 1995. Imaging of single fluorescent molecules and individual ATP turnovers by single myosin molecules in aqueous solution. *Nature* 374(6522):555-9.
- Geeves MH, Holmes KC. 1999. Structural Mechanism of Muscle Contraction. *Annu Rev Biochem* 68:687-728.

- Goldman YE, Brenner B. 1987. Special topic: molecular mechanism of muscle contraction. General introduction. *Annu Rev Physiol* 49:629-36.
- Goldman YE, 1987. Kinetics of the actomyosin ATPase in muscle fibers. *Ann. Rev. Physiol.* 49,637-654
- Gyimesi, M., Bagshaw, C.R., Malnasi-Csizmadia, A. 2005. Traces of pyrophosphate in phosphate buffer affect myosin kinetics. *Biophys. J.* 88
- Harada Y, Sakurada K, Aoki T, Thomas DD, Yanagida T. 1990. Mechanochemical coupling in actomyosin energy transduction studied by in vitro movement assay. *J Mol Biol* 216(1):49-68.
- Hibberd MG, Dantzig JA, Trentham DR, Goldman YE. 1985. Phosphate release and force generation in skeletal muscle fibers. *Science* 228(4705):1317-9.
- Hibberd MG, Trentham DR. 1986. Relationships between chemical and mechanical events during muscular contraction. *Annu Rev Biophys Biophys Chem* 15:119-61.
- Hodge T, Cope MJ. 2000. A myosin family tree. *J Cell Sci.* 113(Pt 19):3353-4.
- Holmes KC, Popp D, Gebhard W, Kabsch W. 1990a. Atomic model of the actin filament. *Nature.* 347(6288):44-9.
- Holmes KC, Popp D, Gebhard W, Kabsch W. 1990b. Atomic model of the actin filament [see comments]. *Nature* 347(6288):44-9.
- Homsher, E., Nili, M., Chen, I.Y. and Tobacman, L.S. 2003. Regulatory Proteins Alter Nucleotide Binding to Acto-Myosin of Sliding Filaments in Motility Assays. *Biophys. J.* 85; 1046-1052.
- Houdusse A, Szent-Gyorgyi AG, Cohen C. 2000. Three conformational states of scallop myosin S1. *Proc Natl Acad Sci U S A* 97(21):11238-43.
- Huxley AF, Niedergerke R. 1954. Structural changes in muscle during contraction; interference microscopy of living muscle fibres. *Nature.* 173(4412):971-3.



- Huxley H, Hanson J. 1954. Changes in the cross-striations of muscle during contraction and stretch and their structural interpretation. *Nature*. 173(4412):973-6.
- Huxley HE. 1963. Electron microscope studies on the structure of natural and synthetic protein filaments from striated muscle. *J Mol Biol* 7:281-308.
- Huxley HE. 1969. The mechanism of muscular contraction. *Science* 164(886):1356-65.
- Huxley AF, and Simmons RM. 1971. Proposed mechanism of force generation in striated muscle. *Nature* 233, 533-538.
- Iwamoto, H. 1995. Strain sensitivity and Turnover Rate of Low Force Cross-bridges in Contracting Skeletal Muscle fibres in the Presence of Phosphate. *Biophys. J.* 68; 243-250
- Ishii, Yoshiharu., Kimura, Yuji., Kitamura, Kazuo., Tanaka, Hiroto., Wazawa, Tetsuichi and Yanagida, Toshio. (2000) *Clinical and Experimental pharmacology and Physiology* 27, 229-237
- Iwane AH, Funatsu T, Harada Y, Tokunaga M, Ohara O, Morimoto S, Yanagida T. (1997) *FEBS Lett.* 407, 235-238
- Kabsch W, Mannherz HG, Suck D, Pai EF, Holmes KC. 1990. Atomic structure of the actin:DNase I complex. *Nature* 347(6288):37-44.
- Kraft T, Mahlmann E, Mattei T, Brenner B. 2005. Initiation of the power stroke in muscle: insights from the phosphate analog AIF<sub>4</sub>. *Proc Natl Acad Sci U S A.* 102(39):13861-6. Epub 2005 Sep 20.
- Kron SJ, Spudich JA. 1986. Fluorescent actin filaments move on myosin fixed to a glass surface. *Proc Natl Acad Sci U S A* 83(17):6272-6.
- Kron SJ, Toyoshima YY, Uyeda TQ, Spudich JA. 1991. Assays for actin sliding movement over myosin-coated surfaces. *Methods Enzymol* 196:399-416.

Lehman W, Vibert P, Uman P, Craig R. 1995. Steric-blocking by tropomyosin visualized in relaxed vertebrate muscle thin filaments. *J Mol Biol* 251(2):191-6.

Lorenz M, Popp D, Holmes KC. 1993. Refinement of the F-actin model against X-ray fiber diffraction data by the use of a directed mutation algorithm. *J Mol Biol* 234(3):826-36.

Lu, H. Peter., Xun, Luying., Xie, X. Sunney. (1998) *Science* 282, 1877-1882.

Lymn RW, Taylor EW. 1971. Mechanism of adenosine triphosphate hydrolysis by actomyosin. *Biochemistry*. 10(25):4617-24.

Werber MM, Peyser YM, Muhlrud A. 1992. Characterization of stable beryllium fluoride, aluminum fluoride, and vanadate containing myosin subfragment 1-nucleotide complexes. *Biochemistry*.11(31):7190-7.

Maruta S, Henry GD, Sykes BD, Ikebe M. 1993. Formation of the stable Myosin-ADP- $\text{AlF}_4^-$  and Myosin-ADP-Beryllium fluoride complexes and their analysis using  $^{19}\text{F}$  NMR. *The Journal of Biological Chemistry*. 268,10,7093-7100.

Mermall V, Post PL, Mooseker MS. 1998. Unconventional myosins in cell movement, membrane traffic, and signal transduction. *Science* 279(5350):527-33.

Millar NC, Homsher E. 1990. The effect of phosphate and calcium on force generation in glycerinated rabbit skeletal muscle fibers. A steady-state and transient kinetic study. *J Biol Chem* 265(33):20234-40.

Milligan RA, Flicker PF. 1987. Structural relationships of actin, myosin, and tropomyosin revealed by cryo-electron microscopy. *J Cell Biol* 105(1):29-39.

Milligan RA, Whittaker M, Safer D. 1990. Molecular structure of F-actin and location of surface binding sites. *Nature* 348(6298):217-21.

Onishi H, Mochizuki N, Morales MF. 2004. On the myosin catalysis of ATP hydrolysis. *Biochemistry*. 43(13):3757-63.

Owia, K., Eccleston, J.F., Anson, M., Kikumoto, M., Davis, C.T., Reid, G.P., Ferenczi, M.A., Corrie, J.E.T., Yamada, A., Nakayama, H., Trentham, D.R. 2000.

Comparative Single-Molecule and ensemble Myosin Enzymology: Sulfoindocyanine ATP and ADP Derivatives. *Biophys. J.* 78: 3048-3071.

Pardee JD, Spudich JA. 1982. Purification of muscle actin. *Methods Enzymol* 85 Pt B:164-81.

Pate, E. and Cooke, R. 1985. The Inhibition of Muscle Contraction By Adenosin 5' ( $\beta$ ,  $\gamma$ -Imido) Triphosphate And By Pyrophosphate. *Biophys. J.* 47: 773-780.

Pate E, Cooke R. 1989. A model of crossbridge action: the effects of ATP, ADP and Pi. *J Muscle Res Cell Motil* 10(3):181-96.

Pate, E., Franks-Skiba, K. and Cooke, R. 1998. Depletion of Phosphate in Active Mucle Fibres Probes Actomyosin States Within the Powerstroke. *Biophys. J.* 74: 369-380.

Rayment I, Rypniewski WR, Schmidt-Base K, Smith R, Tomchick DR, Benning MM, Winkelmann DA, Wesenberg G, Holden HM. 1993. Three-dimensional structure of myosin subfragment-1: a molecular motor. *Science.* 261(5117):50-8.

Rayment I. 1996, The structural basis of the myosin ATPase activity. *The Journal of Biological Chemistry.* 271, 15850-15853.

Reedy MK, Holmes KC, Tregear RT. 1965. Induced changes in orientation of the cross-bridges of glycerinated insect flight muscle. *Nature.* 207(3):1276-80.

Schroder RR, Manstein DJ, Jahn W, Holden H, Rayment I, Holmes KC, Spudich JA. 1993. Three-dimensional atomic model of F-actin decorated with Dictyostelium myosin S1. *Nature.* 364(6433):171-4.

Sowa, Y., Rowe, D. A., Leake, C.M., Yakushi, T., Homma, M., Ishijima, A., Berry, M.R. (2005) *Nature* 437, 916-919

Sellers JR. 2000. Myosins: a diverse superfamily. *Biochim Biophys Acta* 1496(1):3-22.

- Siemankowski RF, Wiseman MO, White HD. 1985. ADP dissociation from actomyosin subfragment 1 is sufficiently slow to limit the unloaded shortening velocity in vertebrate muscle. *Biochemistry* 82:658-662.
- Sleep JA, Hutton RL. 1980. Exchange between inorganic phosphate and adenosine 5'-triphosphate in the medium by actomyosin subfragment 1. *Biochemistry* 19(7):1276-83.
- Stein LA, Schwarz RP, Jr., Chock PB, Eisenberg E. 1979. Mechanism of actomyosin adenosine triphosphatase. Evidence that adenosine 5'-triphosphate hydrolysis can occur without dissociation of the actomyosin complex. *Biochemistry* 18(18):3895-909.
- Szent-Gyorgyi AG. 1968. The role of actin-myosin interaction in contraction. *Symp Soc Exp Biol.* 22:17-42.
- Taylor EW. 1979. Mechanism of actomyosin ATPase and the problem of muscle contraction. *CRC Crit Rev Biochem* 6(2):103-64.
- Tesi, C., Colomo F., Nencini, S., Pirrodi, N. and Poggesi C. 2000. The Effect of Inorganic Phosphate on Force Generation in Single Myofibrils from Rabbit Skeletal Muscle. *Biophys. J.* 78: 3081-3092.
- Tesi, C., Colomo F., Pirrodi, N. and Poggesi C. 2002. Characterization of the cross-bridge force generating step using inorganic phosphate and BDM in myofibrils from rabbit skeletal muscles. *J. Phys.* 15;541.1: 187-199.
- Thedinga E, Karim N, Kraft T, Brenner B. 1999. A single-fiber in vitro motility assay. In vitro sliding velocity of F-actin vs. unloaded shortening velocity in skinned muscle fibers [In Process Citation]. *J Muscle Res Cell Motil* 20(8):785-96.
- Toyoshima YY, Toyoshima C, Spudich JA. 1989. Bidirectional movement of actin filaments along tracks of myosin heads. *Nature* 341(6238):154-6.
- Tokunaga M, Kitamura K, Saito K, Iwane AH, Yanagida T. (1997) *Biochem Biophys Res Commun.* 235, 47-53.

- Trentham DR, Eccleston JF, Bagshaw CR. 1976. Kinetic analysis of ATPase mechanisms. *Q Rev Biophys* 9(2):217-81.
- Van Oijen AM, Blainey PC, Crampton DJ, Richardson CC, Ellenberger T, Xie XS. (2003) *Science* 301, 1235-1238
- Webb MR, Hibberd MG, Goldman YE, Trentham DR. 1986. Oxygen exchange between Pi in the medium and water during ATP hydrolysis mediated by skinned fibers from rabbit skeletal muscle. Evidence for Pi binding to a force-generating state. *J Biol Chem* 261(33):15557-64.
- White HD, Taylor EW. 1976. Energetics and mechanism of actomyosin adenosine triphosphatase. *Biochemistry* 15(26):5818-26.
- Woledge, R.C., Curtin, N.A., Homsher, E. 1985. Energetic aspects of muscle contraction. *Monogr Physiol Soc.* 41:1-357.
- Xue Q, Yeung ES. 1995. Difference in the chemical reactivity of individual molecules of an enzyme. *Nature.* 373. 681-683.
- Yount RG, Lawson D, Rayment I. 1995. Is myosin a "back door" enzyme? *Biophys J* 68(4 Suppl):44S-47S; discussion 47S-49S.
- Yang, H., Luo, G., Karnchanaphanurach, P., Louie, T., Rech, I., Cova, S., Xun, L., Xie, S. (2003) *Science* 302, 262-266
- Yu LC, Brenner B. 1989. Structures of actomyosin crossbridges in relaxed and rigor muscle fibers. *Biophys J* 55(3):441-53.
- Zhuang X, Bartley LE, Babcock HP, Russell R, Ha T, Herschlag D, Chu S. (2000) *Science* 288, 2048-2051

## Own Publications

**Amrute, M.** and Brenner, B. 2006. Inorganic phosphate binds to the empty nucleotide-binding pocket of myosin II. Biophys Meeting. Poster presentation.

**Amrute-Nayak, M.** Antognozzi, M. and Brenner B. Inorganic phosphate binds to the empty nucleotide-binding pocket. Manuscript in preparation for the Journal of Cell Biology (JCB).

**Amrute-Nayak, M.** and Brenner B. Single Molecule Studies Revealed Two Different Conformational States with Different Catalytic Rate in Myosin II. Manuscript in preparation for the journal, Proceedings of the National Academy of Sciences (PNAS).

---

## Erklärung zur Dissertation

Hierdurch erkläre ich, dass die Dissertation \_\_

### **Studies on the ATP-Hydrolysis Cycle of Myosin II at the Ensemble and Single Molecule Level using Total Internal Reflection Fluorescence Microscopy**

selbstständig verfasst und alle benutzten Hilfsmittel sowie evtl. zur Hilfeleistung herangezogene Institutionen vollständig angegeben wurden.

Die Dissertation wurde nicht schon als Diplom- oder ähnliche Prüfungsarbeit verwendet.

Hannover, den

---

(Unterschrift)

Name: Mamta Amrute-Nayak

---

## CURRICULUM VITAE

### **PERSONAL PROFILE:**

Mrs. Mamta Amrute-Nayak

**Date of Birth** : 10<sup>th</sup> Jan 1979

**Sex:** Female

**Nationality:** Indian

### **Address For Correspondence:**

Medizinische Hochschule Hannover

Molekular- und Zellphysiologie

OE 4210

Carl-Neuberg-Straße 1

30625 Hannover, Germany.

Telefon: +49-511-532-2759

+49-17624046047

Fax: +49-511-532-4296

**Email:** [mamtaamrute@yahoo.com](mailto:mamtaamrute@yahoo.com)

[Amrute.Mamta@mh-hannover.de](mailto:Amrute.Mamta@mh-hannover.de)

### **QUALIFICATIONS:**

**1998-2000 : Master of Science** in Biochemistry from University of Pune, Maharashtra, INDIA. (First class with 60% Marks)

**1995-1998 : B.Sc. (Bachelor of Science)** in Zoology, Chemistry and Microbiology from Amaravati University, Amaravati, Maharashtra, INDIA (First class with distinction, 74.74% Marks)

**1995: 10+2 (Higher secondary)** from Amaravati Board, Amaravati, Maharashtra, INDIA. (First Class with 69.33% Marks)

**1993: 10<sup>th</sup> (Secondary)** from Amaravati Board, Maharashtra, INDIA (First class with distinction 80.33% Marks)



---

**REFERENCE:**

**Prof. Bernhard Brenner:**

Medizinische Hochschule Hannover,

Molekular- und Zellphysiologie,

OE 4210, Carl-Neuberg-Straße 1

30625 Hannover

Telefon: 0511-532-6396

Fax: 0511-532-4296

E-Mail: [Brenner.Bernhard@MH-Hannover.de](mailto:Brenner.Bernhard@MH-Hannover.de)